UNIVERSITY OF WEST ATTICA
SCHOOL OF ENGINEERING
DEPARTMENT OF NAVAL ARCHITECTURE
DIVISION OF MARINE ENGINEERING

Diploma Thesis

Supercritical CO_2 Cycle and Applications – Potential Use in Ships

Georgios I. Litsakis

18393072

Supervisor

Dimitrios Koubogiannis

Athens, November 2023

ΠΑΝΕΠΙΣΤΗΜΙΟ ΔΥΤΙΚΗΣ ΑΤΤΙΚΗΣ
ΣΧΟΛΗ ΜΗΧΑΝΙΚΩΝ
ΤΜΗΜΑ ΝΑΥΠΗΓΩΝ ΜΗΧΑΝΙΚΩΝ

«Υπερκρίσιμος Κύκλος CO_2 και Εφαρμογές του – Δυνατότητες Χρήσης του σε Πλοία»

Μέλη Εξεταστικής Επιτροπής συμπεριλαμβανομένου και του Εισηγητή

Η διπλωματική εργασία εξετάστηκε επιτυχώς από την κάτωθι Εξεταστική Επιτροπή:

Α/α	ΟΝΟΜΑΤΕΠΩΝΥΜΟ	ΒΑΘΜΙΔΑ/ΙΔΙΟΤΗΤΑ	ΨΗΦΙΑΚΗ ΥΠΟΓΡΑΦΗ
1	Κουμπογιάννης Δημήτριος	Αναπληρωτής Καθηγητής	Dimitrios Koumpogiannis Digitally signed by Dimitrios Koumpogiannis Date: 2023.10.31 21:55:41 +02'00'
2	Λιβανός Γεώργιος	Αναπληρωτής Καθηγητής	Georgios Livanos Digitally signed by Georgios Livanos Date: 2023.11.01 18:31:28 +02'00'
3	Χατζηαποστόλου Αντώνιος	Αναπληρωτής Καθηγητής	Antonios Hatziapostolou Digitally signed by Antonios Hatziapostolou Date: 2023.11.01 14:38:02 +02'00'

ΔΗΛΩΣΗ ΣΥΓΓΡΑΦΕΑ ΔΙΠΛΩΜΑΤΙΚΗΣ ΕΡΓΑΣΙΑΣ

Ο κάτωθι υπογεγραμμένος Γεώργιος Λιτσάκης του Ιωάννη, με αριθμό μητρώου 18393072, φοιτητής του Πανεπιστημίου Δυτικής Αττικής της Σχολής Μηχανικών του Τμήματος Ναυπηγών Μηχανικών, δηλώνω υπεύθυνα ότι:

«Είμαι συγγραφέας αυτής της διπλωματικής εργασίας και ότι κάθε βοήθεια την οποία είχα για την προετοιμασία της είναι πλήρως αναγνωρισμένη και αναφέρεται στην εργασία. Επίσης, οι όποιες πηγές από τις οποίες έκανα χρήση δεδομένων, ιδεών ή λέξεων, είτε ακριβώς είτε παραφρασμένες, αναφέρονται στο σύνολό τους, με πλήρη αναφορά στους συγγραφείς, τον εκδοτικό οίκο ή το περιοδικό, συμπεριλαμβανομένων και των πηγών που ενδεχομένως χρησιμοποιήθηκαν από το διαδίκτυο. Επίσης, βεβαιώνω ότι αυτή η εργασία έχει συγγραφεί από μένα αποκλειστικά και αποτελεί προϊόν πνευματικής ιδιοκτησίας τόσο δικής μου, όσο και του Ιδρύματος.

Παράβαση της ανωτέρω ακαδημαϊκής μου ευθύνης αποτελεί ουσιώδη λόγο για την ανάκληση του διπλώματός μου».

Ο Δηλών

Γεώργιος Λιτσάκης

Acknowledgements

I would like to express my sincere gratitude to my supervisor, Dimitrios Koubogiannis, whose guidance and feedback have been critical for the writing of this thesis. I will be forever thankful for the personal time he has dedicated to helping me with the completion of this work.

I am also grateful for the immense amount of support I have received from my friends and especially my family all these years. Without them, my academic journey and everything else I have achieved so far would simply not be possible. Furthermore, their belief in me has kept me highly motivated all these years.

This piece of work marks the end of a five-year academic journey at the University of West Attica, arguably the greatest chapter of my life so far. The skills and knowledge I have acquired through all these years will be a valuable asset throughout my professional career. For this, I would also like to express my gratitude to the whole academic staff of the Department of Naval Engineering at the University of West Attica for being a great source of inspiration and knowledge throughout my educational path.

Περίληψη

Με την κλιματική αλλαγή να αποτελεί ένα από τα μεγαλύτερα προβλήματα της σύγχρονης εποχής, η απανθρακοποίηση της ναυτιλίας έχει γίνει η νούμερο ένα προτεραιότητα για τη διεθνή ναυτιλιακή κοινότητα. Στα πλαίσια αυτής της προσπάθειας, μια πληθώρα τεχνολογικών λύσεων εξετάζεται με σκοπό τη μείωση των εκπεμπόμενων ρύπων από τα πλοία. Η παρούσα εργασία επικεντρώνεται στην ανάκτηση της απορριπτόμενης θερμότητας ενός ναυτικού κινητήρα με τη χρήση υπερκρίσιμου κύκλου διοξειδίου του άνθρακα. Ο κλειστός κύκλος Brayton με υπερκρίσιμο διοξείδιο του άνθρακα ως εργαζόμενο μέσο, είναι μία νέα τεχνολογία που υπόσχεται παραγωγή ισχύος με υψηλό βαθμό απόδοσης και μικρό μέγεθος εγκατάστασης, χάρη στις ιδιότητες των υπερκρίσιμων ρευστών. Σκοπός της παρούσας εργασίας είναι να γίνει μία βιβλιογραφική επισκόπηση των ιδιοτήτων αυτών, καθώς και της διαθέσιμης έρευνας γύρω από τον υπερκρίσιμο κύκλο Brayton, ενώ παράλληλα, θα αναπτυχθεί και ένα σχετικό θερμοδυναμικό μοντέλο για ανάκτηση απορριπτόμενης θερμότητας. Πιο συγκεκριμένα, μέσω της συγγραφής κώδικα στο περιβάλλον του MATLAB και με τη χρήση της βιβλιοθήκης COOLPROP, θα γίνει ο υπολογισμός και η βελτιστοποίηση των επιδόσεων ενός αναγεννητικού υπερκρίσιμου κύκλου Brayton με σκοπό την ανάκτηση της θερμότητας που απορρίπτεται από έναν κινητήρα MAN 6G70ME-C10.5-GA-EGRBP. Η ανάλυση των επιδόσεων του συνδυασμένου κύκλου καθώς και του κύκλου Brayton ως μεμονωμένο σύστημα έγινε τόσο στο ονομαστικό όσο και στα μερικά φορτία της μηχανής. Τα αποτελέσματα έδειξαν ότι με βελτιστοποίηση του λόγου πίεσης του κύκλου Brayton, ο βαθμός απόδοσης του συνδυασμένου συστήματος μπορεί να αυξηθεί κατά 2.9% και η ειδική κατανάλωση καυσίμου μπορεί να μειωθεί κατά 2.8%, ενώ σημαντική είναι και η βελτίωση των επιδόσεων ακόμα και σε χαμηλότερα φορτία. Επιπλέον, μελετήθηκε η επίδραση της ισχύος της κύριας μηχανής στις επιδόσεις του υπερκρίσιμου κύκλου Brayton, όπου 7 μηχανές ίδιας τεχνολογίας και διαφορετικής ισχύος συγκρίθηκαν και τα αποτελέσματα έδειξαν πιθανή σύνδεση του βέλτιστου λόγου πίεσης με τη θερμοκρασία των καυσαερίων. Τέλος, έγινε σύγκριση του μοντέλου μας με παρόμοιο μοντέλο οργανικού κύκλου Rankine και τα αποτελέσματα έδειξαν πως ο υπερκρίσιμος κύκλος Brayton έχει παρόμοιες επιδόσεις με τον οργανικό κύκλο Rankine, μία τεχνολογία που χρησιμοποιείται εδώ και πολλά χρόνια για την ανάκτηση της απορριπτόμενης θερμότητας.

Λέξεις Κλειδιά: Υπερκρίσιμος Κύκλος Διοξειδίου του Άνθρακα, Υπερκρίσιμα Ρευστά Ανάκτηση Απορριπτόμενης Θερμότητας σε Πλοίο, Αναγεννητικός Κύκλος Brayton

Abstract

With climate change being the defining issue of our generation, decarbonization of the shipping industry has become the top priority of the maritime community. In an effort to reduce emissions from shipping, numerous technological and design solutions are being investigated. This thesis focuses on the recovery of the heat wasted by marine engines using a supercritical carbon dioxide Brayton cycle. The supercritical carbon dioxide Brayton cycle is an innovative technology that promises power generation with unprecedented performance and a small form factor, due to the properties of supercritical fluids. The objective of this thesis is to provide important insight on this new technology as well as the current stage of research. Furthermore, a thermodynamic model will be developed in MATLAB with the use of the COOLPROP library, aiming to analyze and optimize the performance of a recuperated supercritical carbon dioxide Brayton cycle used for waste heat recovery of a MAN 6G70ME-C10.5-GA-EGRBP marine engine. The performance analysis was conducted at the engine's specified maximum continuous rating as well as at partial loads. The results showed that with the use of this technology, the combined system's thermal efficiency can be increased by 2.9% and its specific fuel oil consumption can be reduced by 2.8%, while there are also significant performance benefits even at lower loads. Moreover, the effect of the main engine's power on the supercritical Brayton cycle's performance was studied, where 7 marine engines of the same injection technology and different power outputs were compared, and the results revealed a possible relationship between the optimal pressure ratio and the engine's exhaust gas temperature. Finally, our model was compared to a similar organic Rankine cycle model, an already field proven technology in the waste heat recovery sector. The results showed that both systems have similar performance.

Keywords: Supercritical Carbon Dioxide Cycle, Supercritical Fluids, Waste Heat Recovery Onboard Vessels, Recuperated Brayton Cycle

Table of Contents

Nomenclature

ANL:	Argonne National Laboratory
ASME:	American Society of Mechanical Engineers
CC:	Combined Cycle
CCGT:	Closed Cycle Gas Turbine
CEAS:	Computerized Engine Application System
CFD:	Computational Fluid Dynamics
CO_2:	Carbon Dioxide
CSP:	Concentrated Solar Power
DOE:	Department of Energy
EGR:	Exhaust Gas Recirculation
EGS:	Enhanced Geothermal System
EPRI:	Electric Power Institute
GE:	General Electric
GHG:	Green House Gasses
HRSG:	Heat Recovery Steam Generator
HTR:	High Temperature Recuperator
IMO:	International Maritime Organization
INL:	Idaho National Laboratory
LCOE:	Levelized Cost of Electricity
LNG:	Liquified Natural Gas
LTR:	Low Temperature Recuperator
MDO:	Marine Diesel Oil
ME:	Main Engine
MEPC:	Marine Environment Protection Committee
MGO:	Marine Gas Oil
MIT:	Massachusetts Institute of Technology
NREL:	National Renewable Energy Laboratory
ORC:	Organic Rankine Cycle
PCHE:	Printed Circuit Heat Exchanger
R&D:	Research and Development
RBC:	Recuperated Brayton Cycle
RCBC:	Recompression Brayton Cycle
SBC:	Simple Brayton Cycle
SCBC:	Supercritical Carbon Dioxide Brayton Cycle
SCF:	Supercritical Fluid
sCO_2:	Supercritical Carbon Dioxide
SFOC:	Specific Fuel Oil Consumption
SMCR:	Specified Maximum Continuous Rating
SNL:	Sandia National Laboratory
STEP:	Supercritical Transformational Power
TAC:	Turbine- Alternator-Compressor
WHR:	Waste Heat Recovery

1. Introduction

1.1. Motivation

Climate change has been the center of attention during the 21st century and decarbonization of the industry seems to be the only real solution. The maritime transportation plays a very important role in the worldwide economy and despite being one of the most efficient means of transportation, it still has a large and continuously growing share in worldwide emissions. With shipping being responsible for around 2.9% of global emmissions caused by human activities, and these emissions being suspected to grow anywhere from 90% to 130% of 2008 emissions by 2050 [1], it is mandatory for immediate action to be taken in order to reduce them.

In 2018, the Intenational Maritime Organization (IMO) announced a new policy framework with the ambition of cutting down greenhouse gasses (GHG) emissions at least in half by 2050 compared to their level in 2008, with the ultimate goal to phase out GHG emissions from shipping as soon as possible. Moreover, this policy framework aims to reduce the carbon intensity of international shipping by at least 40% by 2030, with efforts to reduce it by 70% by 2050 compared to 2008 [2].

With shipping being a multi-trillion dollar industry, projected to grow even more in the upcoming years, it is clear that its decarbonization will be a huge economic and logistic challenge. The presently available technology is simply not capable of achieving IMO's goals for decarbonization [3], thus new ways of improving the ship's energy efficiency are desperately in need.

Even though there is a wide variety of potential design and operational solutions to improve a vessel's energy efficiency, altering the propulsion and power systems seem to be the most promising ones. Modern ships, mainly rely on diesel engines for both propulsion and electric power generation, so naturally, changing the fuel used in shipping seems to be the best solution for achieving IMO's long term goals for decarbonization. Fuels like ammonia could in theory be used to achieve zero CO_2 emissions, however, each one of these fuels poses new technical challenges that make their implementation difficult. For example, ammonia is a very toxic and difficult to store substance, not to mention its very limited availability and high cost [4]. These challenges, although not insurmountable, make the successful implementation of a new fuel uncertain. Thus, no potential candidate for improving the ship's energy efficiency shall be ruled out, as it could end up helping with the decarbonization of the industry in the mid or long term.

The use of turbines (e.g. steam or gas turbines) has failed to dominate the shipping industry. Steam turbines, despite being the main mean of propulsion in the early days of steam ships, have quickly become obsolete due to the use of diesel engines. Another prime example of this phenomenon is Liquifed Natural Gas Carriers, a relatively modern ship type, initially

using steam turbines as their main propulsion system, in order to take advantage of the boil off gas. Yet again, dual fuel marine diesel engines have quickly replaced those systems, proving once again that diesel engines are more suitable for the propulsion and power generation onboard a ship. There are in fact many reasons why diesel engines are the main mean of ship propulsion today, the most important ones being efficiency, weight and space. The factors of weight and space are pretty self-explanatory. The more spacious and heavy a propulsion system is, the less ammount of cargo can be carried by a ship of given displacement. In terms of efficiency, modern day diesel engines are more efficient in partial loads than steam and gas turbines, thus making them a more attractive solution for ship owners [5].

The supercritical carbon dioxide (sCO_2) Brayton cycle, is a state-of-the-art technology utilizing the properties of CO_2 in its supercritical state, in order to increase the thermal efficiency of the conventional Brayton cycle. As we are going to explain later, the use of supercritical CO_2 as the working fluid also allows for a very compact installation. The sCO_2 Brayton cycle (SCBC) has been proven to be a very promising solution to increase the energy efficiency of onshore power plants, where steam and gas turbines are still the dominant means of power generation. Despite the promise it has shown in this scenario, very little research has been done so far in terms of its potential use on ships. During this thesis, we are going to analyze the main working principles of a closed loop, inderectly fired supercritical carbon dioxide Brayton cycle, as well as describe how it could be potentially used onboard ships for waste heat recovery.

1.2. Objective

The main objective of this thesis is to analyze a zero dimensional thermodynamic model of a closed loop, indirectly fired SCBC within MATLAB's environment and assess its performance. The term zero dimensional model is used to describe a model utilizing exclusively energy equations to predict the performance of an engine, in contrary to a multi dimensional model, that also allows for visualization of gas flow and combustion products [6]. Furthermore, the results of this analysis shall be used to validate whether the SCBC has the potential to be used onboard ships. Throughout this thesis, a detailed description of the working principles, as well as the advantages, disadvantages and main components of the SCBC, shall also be given.

1.3. Thesis Outline

This thesis is devided into 5 chapters, each one tackling a different side of the subject. In this section, the contents of each chapter are provided.

- The first chapter is an introduction to this thesis. First, the motivation behind the current research is described, then the main objectives are briefly presented and the rest of the thesis is outlined.
- The second chapter is a recap of the theoretical background of gas turbines. It is very important that the reader is provided with such a recap of the basic working and thermodynamic principles behind gas turbines, in order to completely understand the contents of the next chapters. This chapter begins with an introduction to gas turbines. While this introduction includes information about basic open loop cycle components and industrial gas turbines, a specific reference to closed loop systems is also made. The chapter then continues with a brief description of the basic thermodynamic principles that lead to the expressions that will be used in the modeling process. Having introduced those principles, the Brayton cycle is then explained in the next section. The performance equations are expressed, while ways to improve the cycle's efficiency are also described. Finally, in order to use those equations in real world conditions, the real gas turbine cycle needs to be introduced. This last section is about the way that pressure losses and irreversibilities of the components are mathematically expressed with the use of coefficients.
- The third chapter is a summary of the properties of supercritical fluids with an emphasis on supercritical carbon dioxide and the properties that make it a suitable working fluid for a closed Brayton cycle. The main advantages of SCBC will also be presented in this chapter and the main cycle configurations will be described. Finally, the theory behind the thermodynamic behaviour of real gasses will be summarized in order to set the ground for the modeling of the cycle in the fifth chapter.
- The fourth chapter is a review of the literature related to SCBC. First, a summary of the historical development of closed loop gas turbines is presented. Then, the current research related to SCBC is reviewed. This research is split in four fields, namely SCBC applications, cycle component development, working fluid mixtures and experiments. Some of the most noteworthy publications are also referenced in this chapter.
- The fifth chapter is a detailed presentation of our model and its development process. In this chapter, the mathematical expressions as well as the main engine data used in our model will be provided and the performance of the supercritical carbon dioxide Brayton cycle as a waste heat recovery system for a marine engine will be calculated. Finally, our results will be compared to similar studies regarding the supercritical Brayton cycle, as well as an organic Rankine cycle, in order to decide how this state-of-the-art system compares to an already proven technology.

2. Theoretical Background

In this chapter, the theory behind gas turbines will be presented. Starting with a brief description of gas turbines, all of their major components will be analyzed. Despite the first section mainly focusing on open loop systems, a specific reference to industrial and closed loop gas turbines will also be made. After all, closed loop systems share a lot of the same components and principles with open loop systems. The chapter then continues with an explanation of some basic thermodynamic principles and the expression of the equations that will be used in the modeling process later in this thesis. Continuing, the Brayton cycle will be introduced and some of the most common performance improvement methods will be described. Finally, the chapter closes with an introduction to the real gas turbine cycle. During this last section, the ways that real world conditions affect the cycle's performance will be explained and the real processes' equations will be mathematically expressed. This chapter along with the next one will set the ground for the modeling of the cycle in the fifth chapter.

2.1. Gas Turbines

A gas turbine is a rotary internal combustion engine that extracts energy from a gas' continuous flow. Its operation is essentially a Brayton cycle, and its main working principle relies on a hot pressurized gas flowing through a turbine and spinning the turbine's rotating blades while it gradually slows down. Gas turbines are most commonly used to power aircraft, fluid compressors and electrical generators, as well as ships. Despite the main working principles of all gas turbines being the same, there are many different configurations, depending on the intended use. For example, there are turbojet and turbofan engines, producing thrust to power an aircraft utilizing the high-speed jet of the fluid exiting the turbine (either exhaust gas or a mixture of exhaust gas and compressed air respectively), while turboprops are also used to power aircraft by moving a propeller which in turn produces the necessary thrust. Outside of aviation, gas turbines are also used for power generation. This type of engine is called a turboshaft engine as the power is extracted via a shaft rotation, not a high-velocity jet of a fluid. The main parts of a gas turbine, are the following:

- Compressor
- Combustor
- Turbine

These three parts are common to all open loop gas turbines and form the power producing part of the engine, also known as the core or gas generator [7]. The most common types of gas turbines are illustrated below [8].

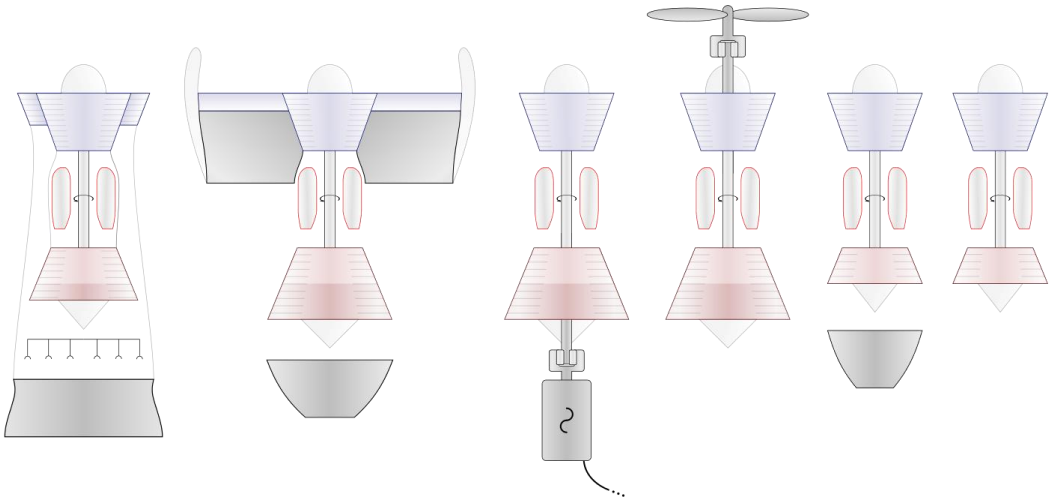

Figure 2.1: Six Different Configurations of a Gas Turbine. From left to right, a low-bypass afterburning turbofan; high-bypass turbofan; turboshaft connected to an electric generator; turboprop; turbojet; gas generator (core) with no inherent use [8]

Figure 2.2: The GE9X, the world's most powerful aircraft engine yet, mounted on General Electric's 747 test platform. The GE9X was exclusively developed to power Boeing's latest aircraft, the Boeing 777X [9].

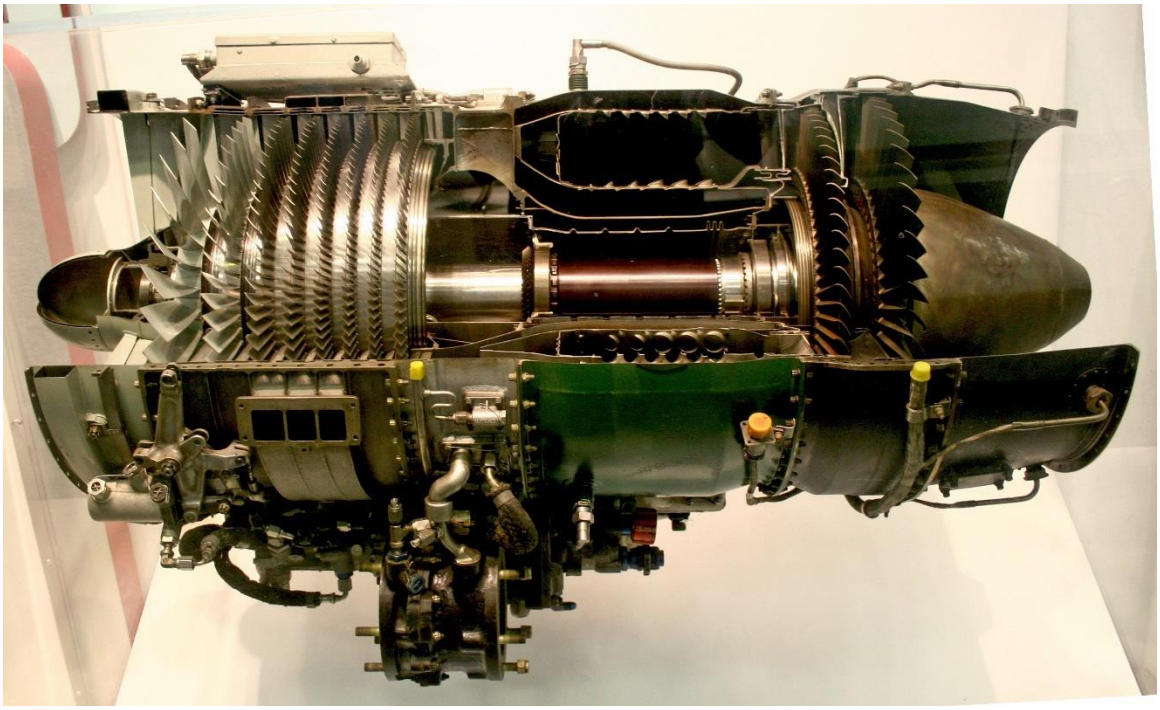

Figure 2.3: An axial-flow gas turbine, the GE J85, sectioned for display [7].

2.1.1. Compressor

A compressor is a mechanical device and a vital part of a gas turbine used to increase a gas' pressure. Compressors fall into two major categories, depending on the direction of the flow, centrifugal and axial compressors. Centrifugal compressors accelerate the flow by flinging it outwards. They are easy to manufacture and are recommended for small increases in pressure and small engines [10].

Axial compressors on the other hand, can accommodate more air flow than centrifugal compressors [10]. Depending on the desired pressure increase, axial flow compressors can consist of more than one stage and in this case are called multistage compressors. Every stage consists of two rows of blades, a moving row in the front of the direction of the flow squeezing the fluid and increasing its velocity, called the rotor, and a stationary one converting this velocity to pressure increase and bringing the flow parallel to the axis, called the stator [11]. The stator's blades are mounted directly on the compressor's shell, while the rotor's blades are mounted on the compressor's axle so that they can rotate when the engine is running. Depending on the compressor, there are also some other rows of stationary blades that are not part of a stage. These rows are the inlet and exit guide vanes and their role is to alter the flow's angle so that the flow properly enters or exits the stages. A multistage compressor is shown in the image below [11].

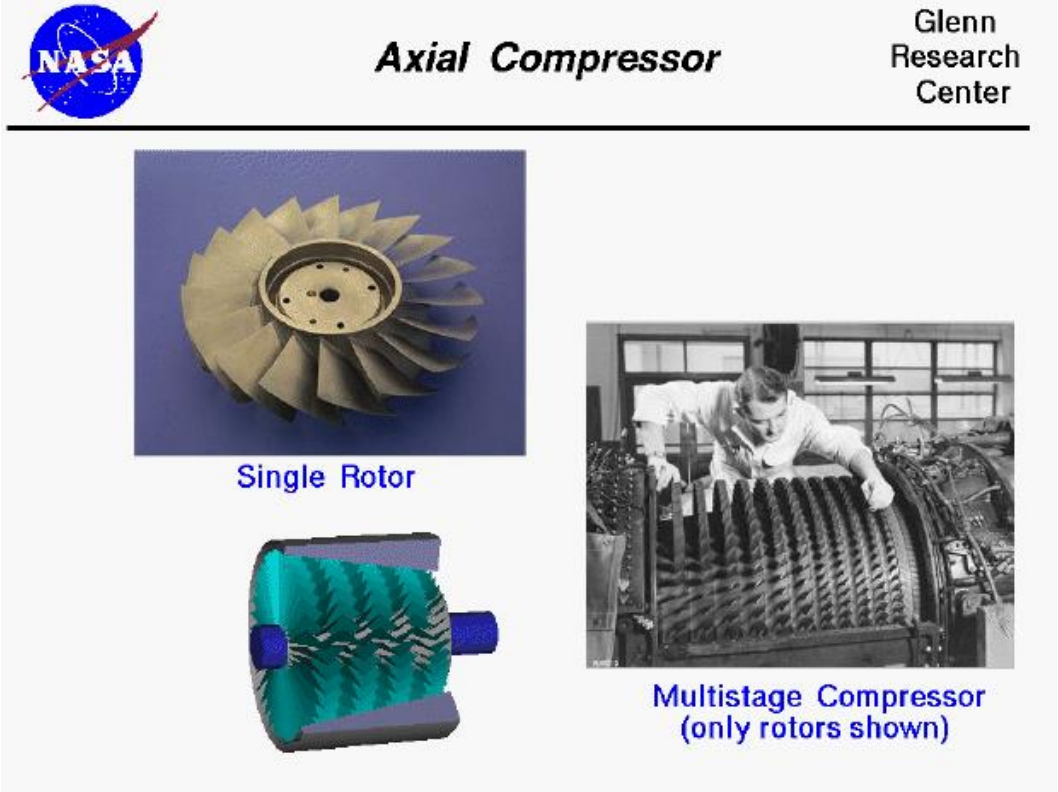

Figure 2.4: A Multistage Axial Compressor [11]

2.1.2. Combustor

The combustor or combustion chamber is the part of the gas turbine where the air gets mixed with fuel and the mixture is burnt. Before the air gets mixed with the fuel, it must pass through the diffuser. The diffuser slows down the high velocity stream that exits the compressor to a velocity optimal for the combustor. The slowing down of the flow inevitably causes a drop in pressure, thus, the ultimate design goal for a diffuser is to minimize the pressure loss as much as possible [12].

After the diffuser, the air splits into 4 main parts, the primary; the intermediate; the dilution and the cooling air. The primary air is the main combustion air that enters the combustion zone through the main channels in the dome and the first set of liner holes [12]. The liner is the component that contains the whole combustion process and introduces the various air flow paths to the combustion zone. It is built to withstand high temperature cycles and is cooled by air with methods of film cooling or transpiration. The dome, in collaboration with the swirlers, generates turbulence in the flow, so that the air can rapidly mix with the fuel which is introduced to the system via the fuel injector. Older designs incorporated bluff bodies instead of swirlers to create wake turbulence as the main mixing mechanism. The created turbulence, however, introduces losses in pressure. The design goal for a swirler is to create only as much turbulence as needed to sufficiently mix the fuel and air, thus

minimizing the pressure loss. When the air and fuel streams are sufficiently mixed, combustion begins. The combustion is initiated with the help of an igniter and is self-sustained afterwards, thus the igniter is no longer used under normal operation. In some systems, there are also ignition- assisting technologies in place. A prime example of such a technology is direct oxygen injection to the ignition area, a system that helps the fuel combust easier. This is a particularly useful safety measure for aircraft engines that may have to restart at high altitudes [12].

The intermediate air enters the combustion zone via the second set of liner holes. Its role is to cool down the air inside the combustion zone and dilute the high concentrations of carbon monoxide and hydrogen [12].

Dilution air is injected to the combustion zone via holes at the end of the chamber and helps to cool down and create a uniform temperature for the working fluid before it enters the turbine. As the maximum cycle temperature of a gas turbine is dictated by the temperature that the turbine blades can withstand, the dilution air is there to regulate the temperature of the exhaust gas that exits the chamber and protect the turbine's blades. Improvements in turbine technology allow the blades to withstand greater temperatures, thus dilution air tends to get used less these days, allowing for an increase of primary air [12].

Finally, cooling air is the air in charge of cooling and protecting the liner. The most common method of cooling is film cooling, where air gets injected through small holes in the liner creating a film of air to protect it from the combustion temperatures. In some cases, up to 50% of the inlet air is used as cooling air and it is crucial that the cooling air does not interact with the combustion process [12].

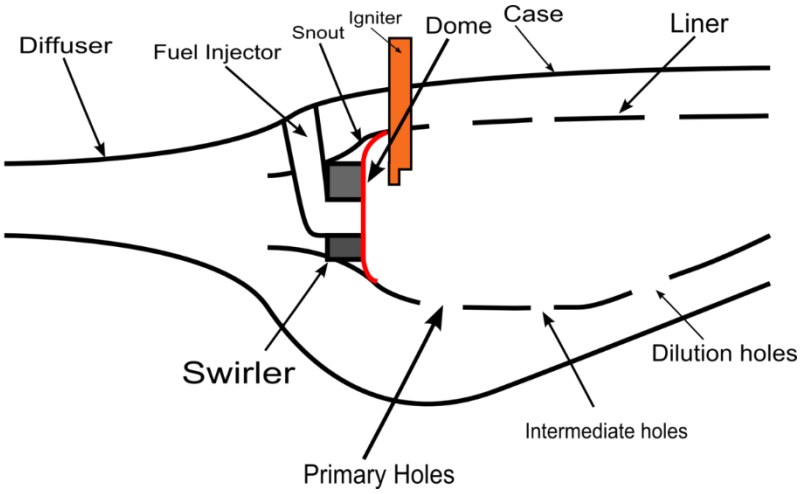

Figure 2.5: A Components Diagram of a Combustor [12].

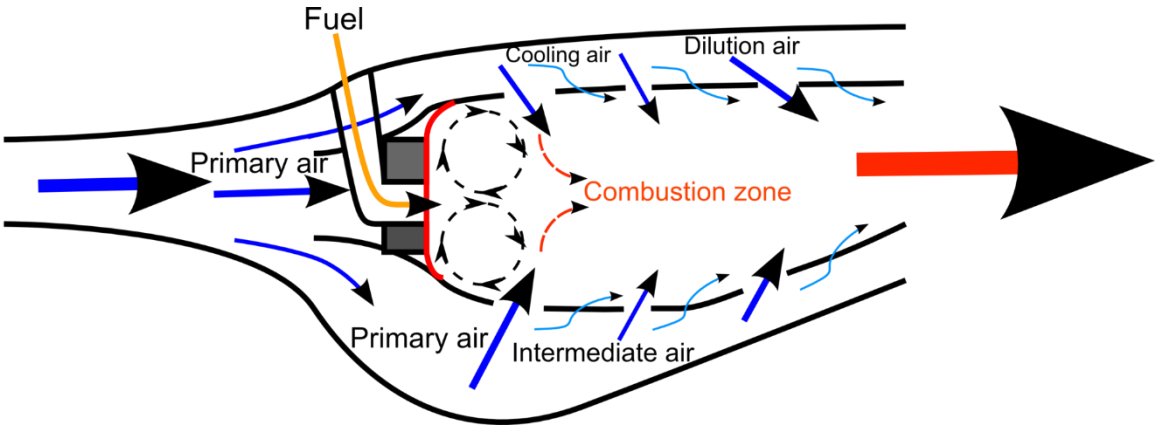

Figure 2.6: Diagram of air flow paths in a gas turbine combustor [12].

There are three types of combustors:

- Can Type Combustor: can type combustors are self-contained cylindrical combustion chambers with each one of them having its own casing, liner, igniter and injector [13]. Depending on the engine size, multiple "cans" are arranged around the engine's axis and their shared exhaust is fed to the turbine [13]. Can type combustors were quite common in the early days of gas turbines due to their simple design. They are easy to repair, as it is possible to maintain each can individually. Due to their increased weight, volume, and pressure losses, most modern gas turbines do not use can type combustors. However, can type combustors are a great fit for centrifugal compressors, as the flow can be divided into separate streams at the exit of the compressor [13].

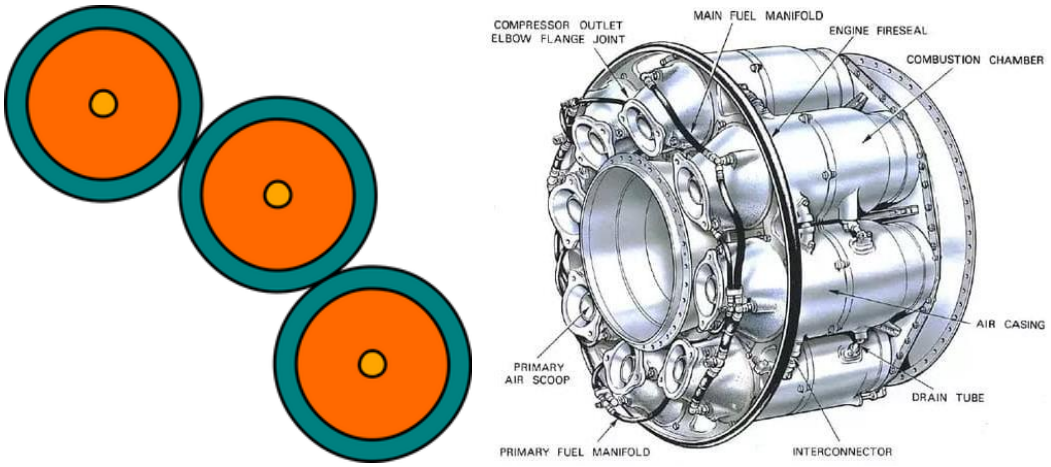

Figure 2.7: Can Type Combustor [13]

- Cannular Type Combustor: also known as can- annular type combustor, this type consists of discrete combustion zones with separate liners and fuel injectors, all encased by a common ring casing, called the annulus. The combustion zones communicate with each other via liner holes or tubes, allowing some intermediate and dilution air to flow circumferentially. The cannular type combustors eliminate the need for separate igniters and provide a more uniform gas temperature at the outlet of the combustor. They are more complex to maintain than can type combustors, however, they have lower pressure drop. This type of combustor is used by many modern engines, Rolls- Royce Tay turbofans being a prime example [13].

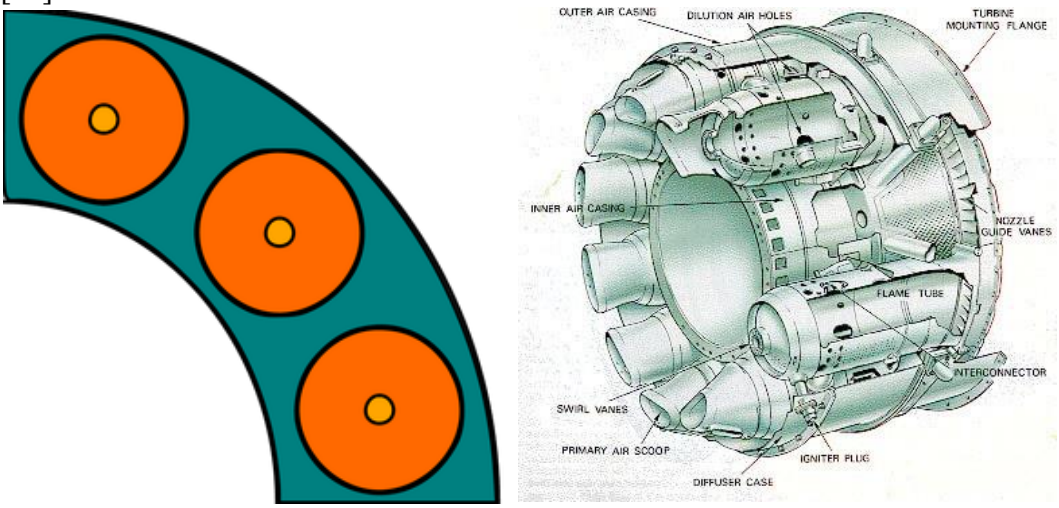

Figure 2.8: Cannular Type Combustor [13]

- Annular Type Combustor: annular type combustors have separate combustion zones contained in a shared liner and casing. They offer a more uniform combustion temperature compared to the other types while also minimizing the combustor's size and weight. They also have the lowest pressure drop out of all the combustor types and host a simple, yet difficult to maintain design. The primary air directly enters the combustion zone, while the intermediate and dilution air flow circumferentially and enter via liner holes. Annular combustors are used by most modern engines. The most advanced variant of annular combustors is one that features two combustion zones around the ring and is called the double annular-type combustor. This technology segregates the combustor into two zones, a pilot zone used at low power levels and a main zone used in combination with the pilot zone at high power levels. Double annular combustors designed by GE focus on cutting down NO_X and CO_2 emissions [13].

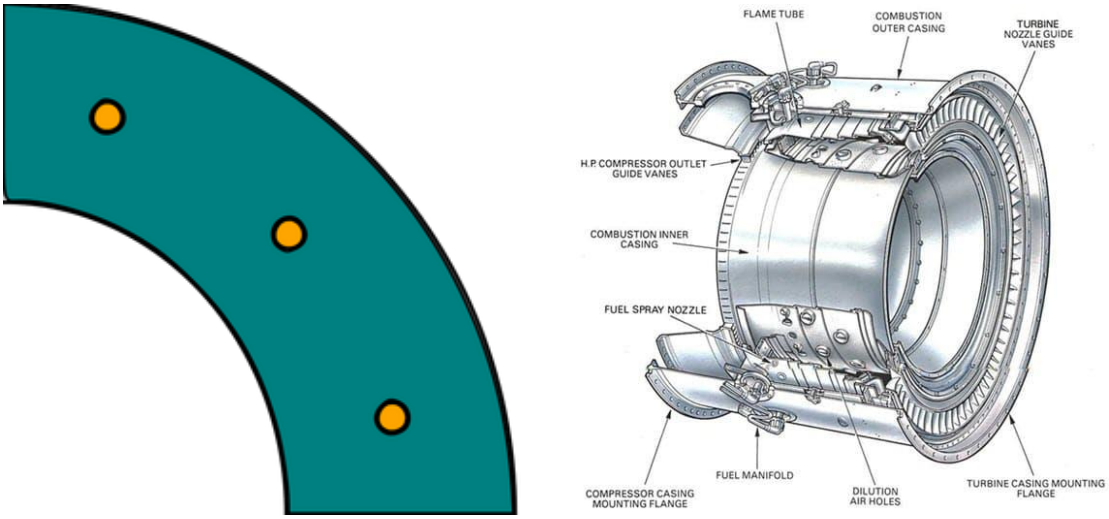

Figure 2.9: Annular Type Combustor [13]

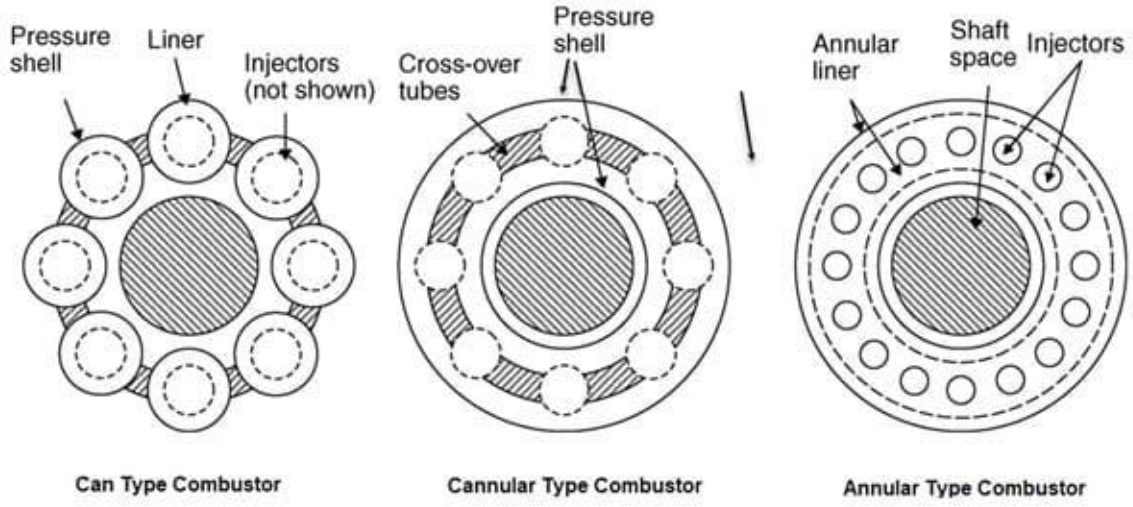

Figure 2.10: Comparison between the different combustor types [13]

2.1.3. Turbine

A turbine is a rotary mechanical device capable of converting a flow's energy into useful work. The use of turbines is not limited to gas turbines, as turbines can be used to extract energy from any flow, from wind (wind turbines) to ocean currents (tidal turbines). Depending on the physical principle they use to extract energy, turbines can be split into two main categories.

- Impulse turbines work by changing the direction of the flow hitting the turbine's blades. The resulting impulse then rotates the turbine's rotor (moving blades),

thus producing useful work, leaving the flow with diminished energy [14]. Before reaching the rotor, the flow must first pass through the stator (stationary blades) which converts the flow's pressure into velocity.

- Reaction turbines produce work by their blades reacting to the flow. As with impulse turbines, the flow must first pass through a stator which converts part of the pressure to velocity. Contrary to impulse turbines, a pressure drop is observed in both the stator and the rotor, as a result of the fluid's interaction with the blades [14]. A direct comparison between impulse and reaction turbines is shown in *Figure 2.11*.

Modern turbines use both impulse and reaction concepts to varying degrees [14]. For compressible flows, the use of multiple stages is usually required. As explained in *Chapter 2.1.1*, a stage consists of one stationary set of blades called the stator and one moving set of blades called the rotor. In contrast to compressors, the stator is the first one to be found in the direction of the flow, as it converts part of the pressure to velocity, which is then used by the rotor. The work produced by the turbine can be utilized in many ways, depending on the application. For example, in a turbojet engine, the turbine produces only as much work as needed to power the compressor and auxiliary systems, while rejecting a high velocity stream of exhaust gas through a nozzle which in turn provides the necessary thrust to power an aircraft. In turboshaft engines on the other hand, the turbine extracts as much energy as possible from the fluid to power both the compressor and provide shaft work as well.

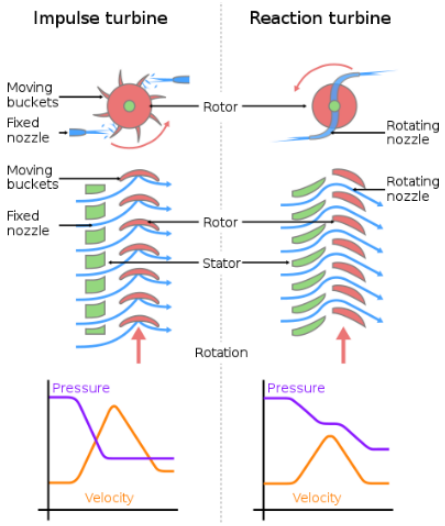

Figure 2.11: Schematic of Impulse and Reaction Turbines (left) [14]

2.1.4. Industrial Gas Turbines

Industrial gas turbines are essentially turboshaft engines used for onshore and offshore power production. Depending on the power requirements, sometimes the core of an aircraft

engine (aeroderivative) is paired with a power turbine to produce power. As mentioned in the previous chapter, aircraft engines such as turbojets and turbofans have turbines that produce enough work only to power the compressor and auxiliary systems of the aircraft. The fluid then gets rejected in the form of a high velocity jet which provides enough thrust to power the aircraft. Instead of rejecting the gas in the form of a jet, a power turbine that produces power from the flow's leftover energy can be used. This allows for the use of lightweight aircraft engines in order to produce electricity onshore or offshore, where the use of a large industrial gas turbine is not a viable option. Another advantage of aeroderivative engines is their ability to manage load changes quicker than industrial gas turbines, meaning that they can also be used as a backup power generation method. For larger power plants, larger industrial gas turbines are used. For comparison, GE's most powerful gas turbine, the 9HA.02 has a net output of 571 MW [15] compared to their most powerful aeroderivative gas turbine, the LMS100 PA+ with a net output of 113 MW [16]. Industrial gas turbines differ from aeronautical designs in that the engine weight is no longer a concern. This allows for the use of standard materials instead of the exotic ones sometimes found in aircraft engines in order to save weight. The absence of weight limitation also allows for the use of heat exchangers in order to improve the efficiency of the power plant. One common practice is that of regeneration, where the high temperature exhaust gas is used to preheat the air before it enters the combustion chamber. This method significantly increases the engine's efficiency and cuts down on fuel costs. Another common method of improving the efficiency is the use of a steam turbine in combination with a gas turbine. These power plants are called combined cycle power plants and the gas turbine only produces part of the power, while its exhaust gas heat is captured by a heat recovery steam generator (HRSG). The HRSG is an energy recovery heat exchanger that produces steam by utilizing the exhaust gas of an engine. Then, a steam turbine is used to increase the powerplant's power output. A combined cycle power plant can produce up to 50% more electricity from the same fuel than a traditional simple cycle power plant [17].

2.1.5. Closed Loop Gas Turbines

A closed loop gas turbine, also known as a closed cycle gas turbine, is an external combustion engine that operates on the Brayton cycle. Since it is an external combustion engine, there is no direct combustion taking place and the heat is supplied externally, usually via a heat exchanger. This makes closed loop systems a great candidate for heat recovery applications. Another big difference of a closed loop system compared to an open loop one is that the working fluid must be cooled after the turbine's outlet, before it repeats the cycle. In an open loop gas turbine, the cycle is repeated by introducing fresh air into the system, but this is not an option for closed loop systems.

A closed cycle gas turbine allows for a variety of gases (helium, carbon dioxide, nitrogen, argon etc.) to be used as the working fluid. The main advantage of using different working fluids is that every fluid has its own properties. For example, fluids like CO_2 in their

supercritical state have larger density than air. This in turn allows for a much smaller engine size, since the necessary volume flow to achieve the same mass flow as air is much less. Fluids like helium can also be used due to their lower viscosity and higher heat capacity which allows for more generated power per mass unit. Another important technical advantage is the absence of corrosion in the turbine blades since the exhaust gas no longer comes in contact with them.

Despite their many advantages, closed loop gas turbines are still in experimental state. The high cost, yet to be proven performance in real world conditions and remaining research and development on crucial cycle components are big obstacles in the implementation of such systems. Today, small scale experimental closed cycle gas turbines are operated by Sandia Laboratories, Bettis Atomic Power Laboratories and other research institutes.

2.1.6. Heat Exchangers

Since heat exchangers are the main heat input method for closed loop systems as well as a vital part of improving a gas turbine's efficiency, it is important to understand their main working principles. A heat exchanger is a device used to transfer heat from a hot stream of fluid to a colder one. Heat exchangers are split into three main categories depending on the direction of the flow.

- In parallel flow heat exchangers, the cold and warm streams enter at the same end of the exchanger and flow parallel to each other, until they exit the exchanger [18]. The cold fluid's temperature can never exceed the minimum temperature of the hot fluid.
- In counter flow heat exchangers, the two streams enter from opposite ends of the heat exchanger and flow in opposite directions. This means that the hot stream's maximum temperature is met at the same point as the maximum temperature of the cold stream. The temperature of the cold fluid can exceed the minimum temperature of the hot fluid. Counter flow heat exchangers are the most efficient ones [18].
- In cross flow heat exchangers the fluids travel perpendicular to one another [18].

Due to the various applications of heat exchangers, many different types have been developed over the years. Some of the most common ones are described below.

- Double pipe heat exchangers consist of a small tube inside a larger one. One fluid flows inside the small tube while the other flows in the annular gap between the two tubes. Double pipe heat exchangers can be used as both counter and parallel flow heat exchangers. They are cheap to design and maintain and are recommended for smaller industries. On the other hand, they offer the lowest efficiencies out of all the exchangers [18].

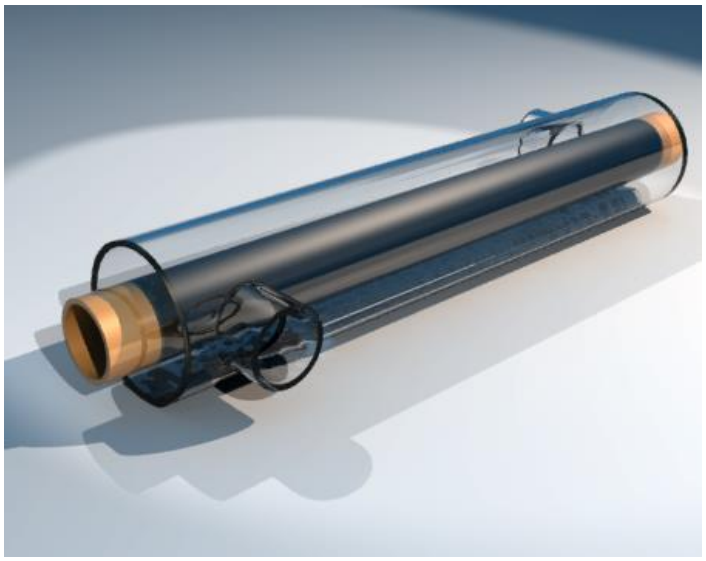

Figure 2.12: A model of a double pipe heat exchanger rendered in Blender [18].

- Shell and tube heat exchangers consist of numerous tubes encased in a shell. One fluid flows inside the tubes while the other flows inside the shell. Baffles are attached to the shell in order to properly support the tubes and create the necessary turbulence to maximize the heat transfer between the two fluids. Since the design goal for a heat exchanger is to maximize the contact area between the fluids, shell and tube heat exchangers have better heat transfer efficiency than double pipe heat exchangers. In the case of air-cooling shell and tube heat exchangers, fins are added on the tubes to increase the heat transfer area [18].

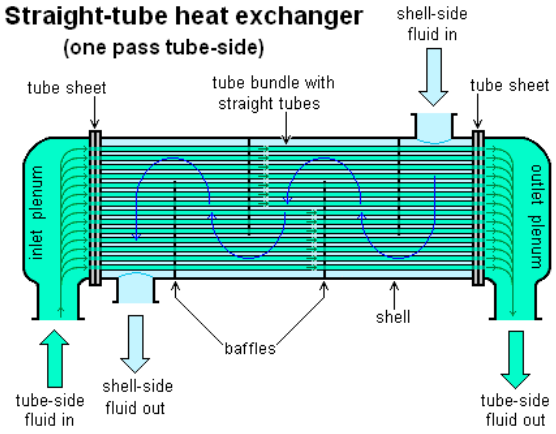

Figure 2.13: A shell and tube heat exchanger [18].

- Plate heat exchangers (PHE) consist of thin metal plates with large surface area stacked together to create a multi-layer heat exchanger. The plates are usually corrugated to provide strength to the plates, generate turbulence and maximize the heat transfer surface area. Each pair of plates forms a channel sealed by gaskets to prevent leaks and allow or prevent the flow of a fluid between the two plates. Plate heat exchangers are counter flow heat exchangers where the type of fluid (warm or cold) is alternated between two consecutive channels. The big surface area provides excellent heat transfer efficiency and greatly increases the temperature change speed. Smaller plate heat exchangers can also be used for domestic applications, while these exchangers tend to exclude the use of gaskets and have their plates brazed together [19].

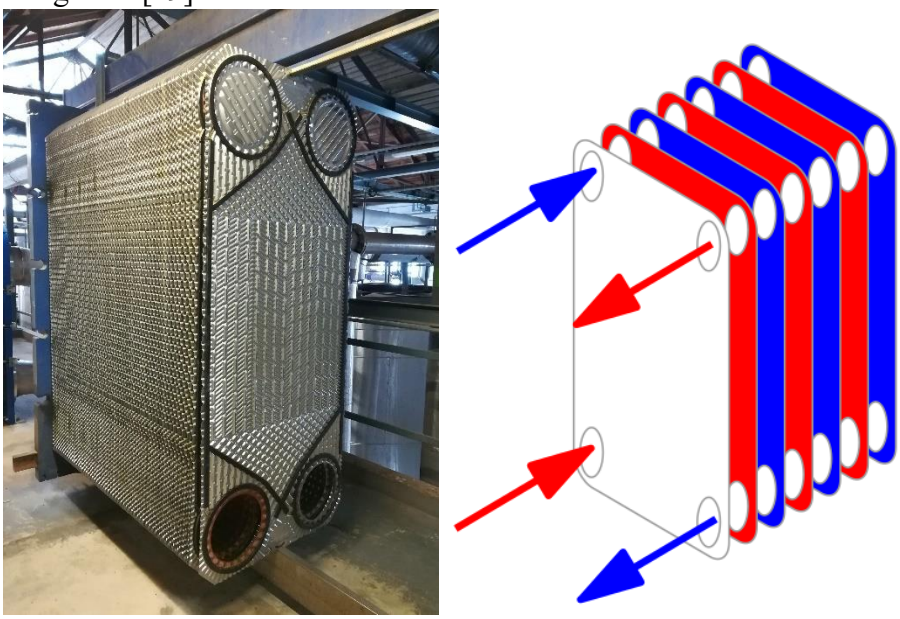

Figure 2.14: A dismantled plate heat exchanger (left); A plate heat exchanger diagram [19] (right).

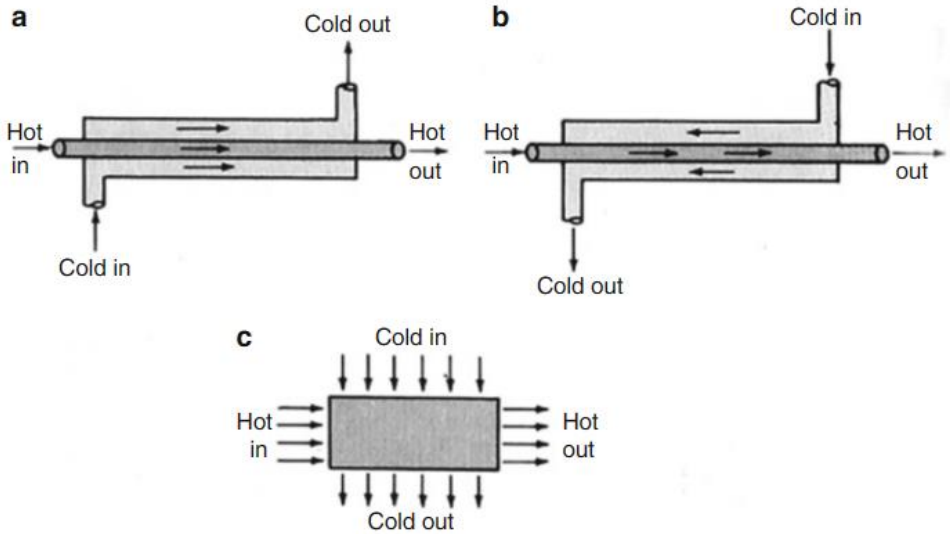

Figure 2.15: Parallel flow Heat Exchanger (a); Counter flow Heat Exchanger (b); Cross flow Heat Exchanger (c) [20].

2.2. Basic Thermodynamic Principles

In this section, a brief description of the basic thermodynamic principles used in our modeling process will be given.

2.2.1. Ideal Gas Law

The ideal gas law is the equation of state of a hypothetical ideal gas [21] and is expressed as following:

$$pv = RT \quad (2.1),$$

Where p is pressure, v is specific volume, T is temperature and R is the ideal gas constant.

2.2.2. Specific Enthalpy and Specific Internal Energy

Specific internal energy is a property of a thermodynamic system and expresses the amount of energy required to bring a system from its standard internal state to the present internal state of interest [22]. It is associated with the random motions of molecules [23].

Specific enthalpy is also a property of a thermodynamic system and it is defined as the sum of the specific internal energy of the system and the product of its pressure and specific volume [24]. Mathematically, it is expressed by the following formula:

$$h = u + pv \quad (2.2)$$

For an ideal gas, both the specific internal energy and specific enthalpy are solely a function of temperature. From the definitions of specific heat capacities at constant pressure, $C_P = \left(\frac{\partial h}{\partial T}\right)_{P=ct}$, and constant volume, $C_v = \left(\frac{\partial u}{\partial T}\right)_{v=ct}$, it can be concluded that both C_P and C_V are also solely a function of temperature. Thus, for an ideal gas, the changes in specific internal energy and specific enthalpy can be calculated by the following formulas:

$$\Delta u_{12} = C_v(T_2 - T_1) \quad (2.3)$$

$$\Delta h_{12} = C_p(T_2 - T_1) \quad (2.4)$$

The above formulas are valid provided that C_P and C_V remain constant. Finally, C_P and C_V can be associated with the ideal gas constant by the following expressions:

$$R = C_p - C_v \quad (2.5)$$

$$C_p = \frac{\gamma R}{\gamma - 1} \quad (2.6)$$

$$C_v = \frac{R}{\gamma - 1} \quad (2.7),$$

where γ is the adiabatic coefficient.

2.2.3. First Law of Thermodynamics

The first law of thermodynamics is the expression of the energy conservation law in the language of thermodynamics. According to this law, in a closed system, "energy cannot be created or destroyed", or in other words, "the total energy in a closed system remains constant, although, it can be converted from one form to another" [25]. The two main forms of energy used to describe a thermodynamic system are heat Q and thermodynamic work W. Moreover, the internal energy of the system U is used to take into account the balance of energy in the system [25]. The first law of thermodynamics can be mathematically expressed by the following equation:

$$\Delta U = Q - W \quad (2.8)$$

This means that if we provide heat Q and extract work W from a closed system, a change in its internal energy U equal to Q-W will be measured. The first law of thermodynamics adequately expresses the balance of energy in a system; however, it does not describe the possibility of the conversion between thermodynamic work and heat.

2.2.4. Second Law of Thermodynamics

The second law of thermodynamics describes the possibility of an energy interconversion process happening within a system. A simple definition of this law is that "not all heat can be converted into work in a cyclic process" [26]. The second law of thermodynamics can be expressed through many statements, with the most famous ones being those from Kelvin, Planck and Clausius. The statements by Kelvin and Planck are equivalent and are both used for heat engines, in contrary to the Clausius statement which is used for cooling engines. Since the topic of this thesis is relative to heat engines, we are only interested in the Kelvin- Planck statement of the law:

"It is impossible for any device that works in a cycle to completely convert heat received from a high temperature reservoir into work, without rejecting any amount of heat to a low temperature reservoir. On the other hand, a system completely converting work into heat is possible" [27].

The upper statement is the fundamental working principle of any heat engine and the meaning behind it is that no heat engine with 100% thermal efficiency can be constructed. The statement is further illustrated in the following figure [28].

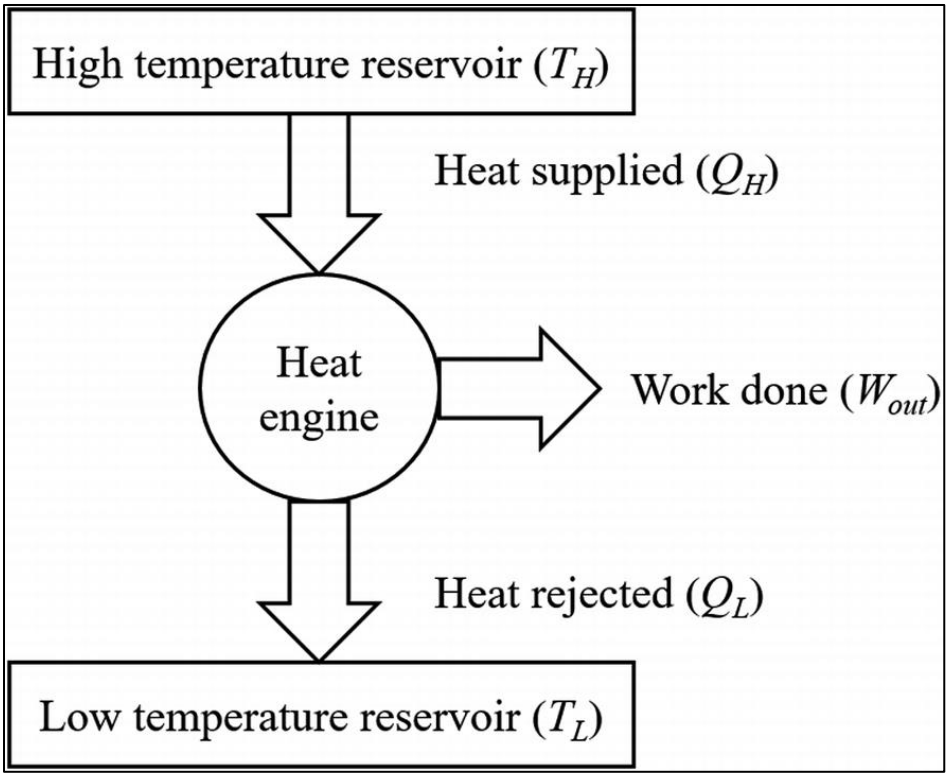

Figure 2.16: Working Principle of a Heat Engine [28].

According to the second law of thermodynamics, the thermal efficiency of a heat engine is given by the following mathematical expression:

$$\eta_{th} = \frac{W_{out}}{Q_H} \quad (2.9),$$

where W_{out} is the net work produced by the heat engine and Q_H is the heat provided by the high temperature reservoir. Considering the heat engine as a closed system and using the first law of thermodynamics, we can express the produced net work as the difference between the provided and rejected heat, thus further simplifying the expression 2.9:

$$\eta_{th} = 1 - \frac{Q_L}{Q_H} \quad (2.10)$$

Given that a rejected heat (Q_L) value equal to zero is a violation of the second law of thermodynamics, the equation 2.10 clearly shows that the thermal efficiency of a heat engine is always lower than one.

Some versions of the second law of thermodynamics introduce entropy as a property of a thermodynamic system. Entropy can be used to predict whether or not a thermodynamic process is possible, even if it's in agreement with the first law of thermodynamics [26]. Entropy for an idealized and reversible process in a closed system can be mathematically expressed as following:

$$ds = \frac{\delta Q}{T} \quad (2.11)$$

Applying the equation 2.11 to a thermodynamic process changing the system from an initial state (1) to another (2), the change of entropy during the process can be measured by integrating the equation as following:

$$\Delta s_{12} = \int_1^2 \frac{\delta Q}{T} \quad (2.12)$$

In the case of a reversible cyclic process, the change of entropy is equal to zero, because it only depends on the initial and final states of the process. From the definition of entropy, it can be easily seen that an adiabatic (meaning no heat is exchanged) and reversible process is an isentropic process (meaning $\Delta s=0$). However, the opposite is not necessarily true, due to the fact that the exchange of proper amounts of heat during an irreversible process can lead to no change in entropy [29].

2.2.5. Clausius Inequality and Increase in Entropy Principle

The Clausius inequality, also known as Clausius theorem, states that for any thermodynamic cycle, regardless of whether it is reversible or not, the following inequality is true:

$$\oint \frac{\delta Q}{T} \leq 0 \quad (2.13),$$

where the equality is only true for a reversible thermodynamic cycle.

Let's now consider an irreversible cycle consisting of an irreversible process $(1) \rightarrow (2)$ followed by a reversible process $(2) \rightarrow (1)$ as illustrated in the following figure [30]:

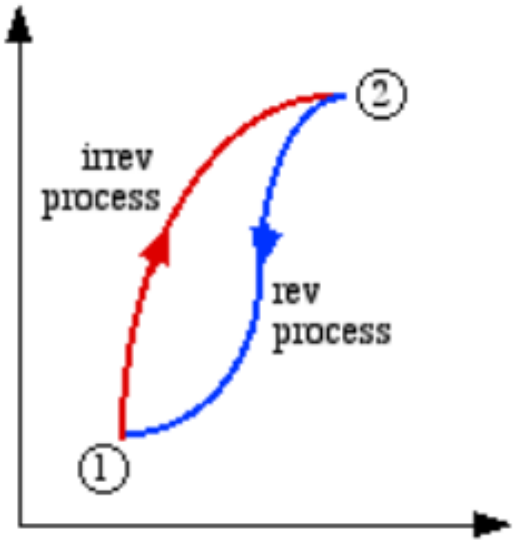

Figure 2.17: Example of an Irreversible Cycle [30]

According to the Clausius inequality, for an irreversible cycle:

$$\oint \frac{\delta Q}{T} < 0 \Leftrightarrow \int_{1_{irrev}}^{2} \frac{\delta Q}{T} + \int_{2_{rev}}^{1} \frac{\delta Q}{T} < 0 \overset{eq\ 1.11}{\Longleftrightarrow} \int_{1_{irrev}}^{2} \frac{\delta Q}{T} + \int_{2_{rev}}^{1} ds < 0 \Leftrightarrow$$

$$\int_{1_{irrev}}^{2} \frac{\delta Q}{T} + (s_1 - s_2) < 0 \Leftrightarrow s_2 - s_1 > \int_{1_{irrev}}^{2} \frac{\delta Q}{T}$$

For irreversible adiabatic processes, like the real processes taking place in turbines and compressors, we know that $\delta Q=0$, so the above inequality takes the following form:

$$s_2 - s_1 > 0 \Leftrightarrow s_2 > s_1 \quad (2.14)$$

This inequality is known as the increase in entropy principle and it states that for any irreversible adiabatic process, there is an increase in entropy. This principle will be very useful in the following chapters when we are going to explain that the real world conditions (e.g. friction and turbulance) introduce irreversibilities in the processes of the turbines and compressors, processes that would otherwise be reversible. These irreversibilities cause an increase in entropy at the outlet of the compressor or turbine, compared to the inlet.

2.2.6. Gibbs Equation and Idiabatic Processes

The Gibbs equation is a particularly useful tool for measuring the change of entropy during an ideal gas process. The Gibbs equation has the following expression:

$$Tds = du + pdv \quad (2.15)$$

The above equation is also known as the first Gibbs equation or T-ds relation. Knowing that $h=u+pv$, the expression 2.15 takes the following form:

$$Tds = dh - vdp \quad (2.16)$$

According to the ideal gas law, $v = \frac{RT}{p}$, whereas from the definition of heat capacity we can write $dh = C_P dT$. The equation 2.16 now takes the following form:

$$ds = C_P \frac{dT}{T} - R\frac{dp}{p} \quad (2.17)$$

Finally, by integrating the equation 2.17, we get that the change of entropy during a process, regardless of if it is reversible or not [29], is equal to:

$$\Delta s_{12} = C_P \ln\left(\frac{T_2}{T_1}\right) - Rln\left(\frac{p_2}{p_1}\right) \quad (2.18)$$

This equation is very important, as it allows us to calculate the change of entropy, something that otherwise could not be directly measured. As we said earlier, isentropic processes are of great importance in turbomachinery, because they are the ideal processes

taking place in compressors and turbines. Using the ideal gas law and the definition of specific heat capacity at constant pressure, for an isentropic process, the following equation is true:

$$\frac{p_2}{p_1} = \left(\frac{T_2}{T_1}\right)^{\frac{\gamma}{\gamma-1}} \quad (2.19)$$

This expression provides a relation between the properties of an ideal gas during an adiabatic process. For example, if we are given the compression ratio of a compressor and the temperature at the inlet, using the expression 2.19 we can calculate the temperature at the outlet.

2.2.7. Stagnation Properties

Once we try to apply the first law of thermodynamics in a turbine or a compressor, we will quickly figure that the kinetic energy of the fluid plays a significant role in the energy balance of our system. More specifically, the first law of thermodynamics for adiabatic processes, like the ones taking place in compressors and turbines, can be expressed as following:

$$-W_{12} = \Delta U \quad (2.20),$$

Where W_{12} is the thermodynamic work produced and ΔU is the change of the internal energy, equal to the sum of the change of enthalpy, kinetic and potential energy of the fluid. From the definition of kinetic energy and given that the potential energy is the same at the inlet and the outlet, we can write the expression 2.20 as following:

$$-W_{12} = \Delta H_{12} + \Delta K_{12} = m\left[\left(h_2 + \frac{V_2^2}{2}\right) - \left(h_1 + \frac{V_1^2}{2}\right)\right] \quad (2.21)$$

The specific stagnation enthalpy of the fluid is defined as:

$$h_t = h + \frac{V^2}{2} \quad (2.22),$$

and it includes both the static enthalpy and kinetic energy of the fluid. The stagnation enthalpy is used to express the total level of intenal energy of a fluid flowing through a compressor or a turbine [29], and it corresponds to the static enthalpy of the fluid brought to rest isentropically from a velocity V (stagnation point) [31].

Using the expression 2.4, the stagnation temperature of an ideal gas is defined as:

$$T_t = T + \frac{V^2}{2C_P} \quad (2.23)$$

The definition of the stagnation pressure is a bit more complicated than the stagnation temperature and enthalpy, and it requires the introduction of the Mach number:

$$M = \frac{V}{c} \quad (2.24),$$

where V is the local flow velocity and c is the speed of sound in the medium [32]. For compressible flows, the speed of sound is calculated as:

$$c = \sqrt{\gamma RT} = \sqrt{\gamma \frac{P}{R}} \quad (2.25),$$

Using the above equation, we can express the local flow velocity as:

$$V^2 = M^2 c^2 = \gamma RT M^2 \quad (2.26),$$

Combining the expressions 2.6, 2.23 and 2.26, we have that $\frac{T_t}{T} = 1 + \frac{\gamma-1}{2} M^2$. Using the expression 2.19, for an isentropic process:

$$\frac{p_t}{p} = \left(\frac{T_t}{T}\right)^{\frac{\gamma}{\gamma-1}} = \left(1 + \frac{\gamma-1}{2} M^2\right)^{\frac{\gamma}{\gamma-1}} \quad (2.27),$$

where p_t is the stagnation pressure.

2.3. Brayton Cycle

The Brayton cycle is an ideal thermodynamic cycle that describes the operation of gas turbines and other heat engines that use air or another gas as their working fluid. The Brayton cycle was first proposed by Englishman John Barber in 1971, but it took its name from George Brayton who was the one to initially develop it for use in piston engines [33]. The ideal cycle consists of the following thermodynamic processes, also shown in the figure below [33]:

- $1 \rightarrow 2$ Isentropic compression. The working fluid is drawn into a compressor, and its pressure is increased.
- $2 \rightarrow 3$ Isobaric heat addition. The working fluid gets heated at constant pressure by passing through a heat exchanger or a combustion chamber.
- $3 \rightarrow 4$ Isentropic expansion. The working fluid passes through a turbine, giving up its energy while moving the turbine's rotors, thus producing useful work.
- $4 \rightarrow 1$ Isobaric heat rejection. The working fluid gets cooled to its initial temperature at constant pressure in order to repeat the cycle. This heat rejection is accomplished using a cooler in closed loop systems, or by introducing fresh air to the system in open loop gas turbines.

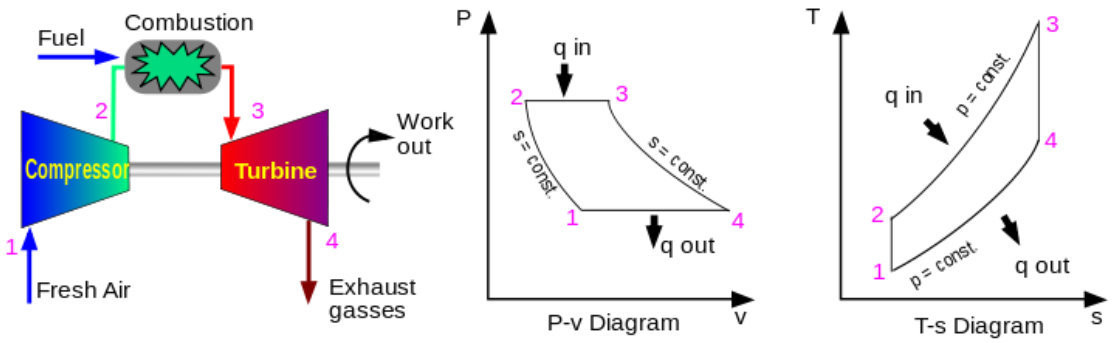

Figure 2.18: Components diagram of an open loop gas turbine (left), P-v Diagram of a Brayton Cycle (middle), T-s Diagram of a Brayton Cycle (right) [33]

The net work produced by the Brayton cycle can be calculated by subtracting the thermodynamic work provided during the compression process from the total work produced during the expansion process:

$$W_{out} = |W_{34}| - |W_{12}| \overset{eq.\ 2.21}{\Longleftrightarrow} W_{out} = m \times (|\Delta h_{t34}| - |\Delta h_{t12}|) \overset{eq.\ 2.4}{\Longleftrightarrow}$$

$$W_{out} = m \times C_P \times \big((T_3 - T_4) - (T_2 - T_1)\big) \quad (2.28)$$

Using the first law of thermodynamics and since no thermodynamic work is produced or consumed in the heat exchangers and combustion chamber, the heat provided to the working fluid during the isobaric heat addition is equal to:

$$Q_{in} = m \times (h_{t3} - h_{t2}) \overset{eq.\ 2.4}{\Longleftrightarrow} Q_{23} = m \times C_P \times (T_3 - T_2) \quad (2.29)$$

Using the expression 2.9, the thermal efficiency of the Brayton cycle can be calculated:

$$\eta_{BC} = \frac{W_{net}}{Q_{in}} = \frac{T_3 - T_4 - T_2 + T_1}{T_3 - T_2} = 1 - \frac{T_4 - T_1}{T_3 - T_2} \Leftrightarrow \eta_{BC} = 1 - \left(\frac{T_1}{T_2}\right)\frac{\left(\frac{T_4}{T_1} - 1\right)}{\left(\frac{T_3}{T_2} - 1\right)} \quad (2.30)$$

Given that the compression and expansion processes are isentropic and that the heat addition and rejection processes are isobaric, we can use the equation 2.19 to create a relation between the minimum and maximum pressure and the temperatures of the cycle:

$$r = \frac{p_{max}}{p_{min}} = \left(\frac{T_2}{T_1}\right)^{\frac{\gamma}{\gamma-1}} = \left(\frac{T_3}{T_4}\right)^{\frac{\gamma}{\gamma-1}} \quad (2.31)$$

From the above equation it can be concluded that $\frac{T_2}{T_1} = \frac{T_3}{T_4}$ or $\frac{T_3}{T_2} = \frac{T_4}{T_1}$. Thus, the expression 2.30 can be further simplified:

$$\eta_{BC} = 1 - \left(\frac{T_1}{T_2}\right) = 1 - \left(\frac{T_4}{T_3}\right) = 1 - \frac{1}{r^{\left(\frac{\gamma-1}{\gamma}\right)}} \quad (2.32),$$

where r is the compression ratio. From the expression above we can see that the thermal efficiency increases with the increase of the compression ratio. Let's now examine the

cycle's behaviour in relation to the maximum and minimum temperature, but first we need to introduce the term of non- dimensional net work output [34]:

$$\widetilde{w}_{out} = \frac{w_{out}}{C_P T_1} \overset{eq.\ 2.28}{\Longleftrightarrow} \widetilde{w}_{out} = \frac{T_3 - T_4 + T_1 - T_2}{T_1} = \left(\frac{T_3}{T_1}\right)\left(1 - \frac{T_4}{T_3}\right) - \left(\frac{T_2}{T_1} - 1\right) \overset{eq.\ 2.31}{\Longleftrightarrow}$$

$$\widetilde{w}_{out} = t\left(1 - \frac{1}{r^{\left(\frac{\gamma-1}{\gamma}\right)}}\right) - \left(r^{\left(\frac{\gamma-1}{\gamma}\right)} - 1\right) \quad (2.33),$$

where $t = \frac{T_3}{T_1}$ is the ratio between the maximum and minimum temperature of the cycle. It is proven [34] that the non- dimensional net work output maximizes when:

$$r^{\left(\frac{\gamma-1}{\gamma}\right)} = \sqrt{t} \overset{eq.\ 2.33}{\Longleftrightarrow} \frac{T_2}{T_1} = \frac{T_3}{T_4} = \sqrt{\frac{T_3}{T_1}} \Leftrightarrow \frac{T_3}{T_1} = \left(\frac{T_2}{T_1}\right)^2 = \left(\frac{T_3}{T_4}\right)^2 \Leftrightarrow \frac{T_3}{T_1} = \frac{T_2}{T_1}\frac{T_3}{T_4} \Leftrightarrow$$

$$T_2 = T_4 \quad (2.34)$$

While the thermal efficiency shows no dependency on the temperature ratio of the cycle, an increase in the compression ratio results in higher efficiencies but in some cases lower work production. The work produced from the cycle shows a strong dependency on the temperature ratio. This is further illustrated below:

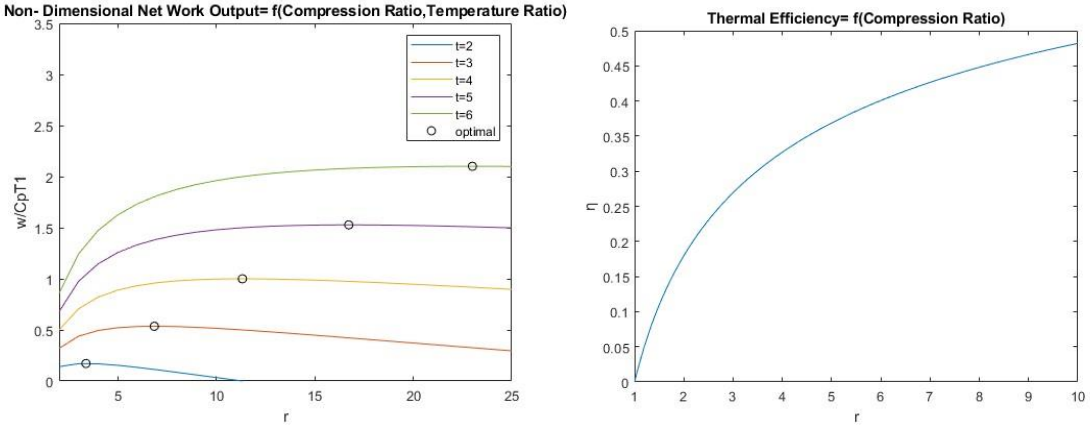

Figure 2.19: Non- Dimensional Net Work Output as a Function of Compression and Temperature Ratio. The black markers correspond to the optimal compression ratio for each temperature ratio, γ=1.4. (left). Thermal Efficiency as a function of Compression Ratio, γ=1.4 (right).

In gas turbines, the maximum temperature of the cycle is dictated by the turbine blades material properties and the maximum temperature they can withstand. The lowest temperature of the cycle is dictated by the ambient temperature for open loop systems or by the capabilities of the cooling solution in closed loop systems. This means that during the design process, given the amount of work needed for the installation, only the compression ratio needs to be dictated. The optimal point corresponds to the pressure ratio that produces the most net work for a given temperature ratio. If we were to choose a compression ratio lower than the optimal, according to the expression 2.31, the temperature at the outlet of the turbine will be higher than the temperature at the outlet of the

compressor, meaning that the flue gas can be utilized to heat up the working fluid before it enters the combustion chamber (thermal regeneration), in order to further increase the cycle's thermal efficiency.

2.3.1. Brayton Cycle Efficiency Improvement

In the previous section, the thermodynamic efficiency of the Brayton cycle was expressed as a function of the cycle's compression ratio and temperatures. We concluded that an increase of the cycle's compression ratio results in an increase of the cycle's efficiency. Since there are limitations on how much the pressure can be increased, many Brayton cycle modifications aiming to improve its performance have been developed over the years, the most common ones being regeneration, multiple stage compression with intercooling and multiple stage expansion with reheating [35].

Regeneration is the simplest and thus the most common modification to the Brayton cycle and it involves the use of a heat exchanger to preheat the working fluid before it enters the combustor. The heat exchanger utilizes the hot exhaust gases exiting the turbine to heat up the working fluid. This modification results in lower fuel consumption and thus lower emissions, due to the fact that part of the cycle's required heat is given by the exhaust gases that would otherwise be discharged to the environment.

Multistage compression with intercooling relies on the basic thermodynamic principle of isothermal compression. As shown in the image below, compression under constant temperature requires less work than an isentropic compression. Compressing a gas in two or more stages while cooling it with an intercooler in between the stages requires less work than a simple compression, thus more net work is produced by the cycle.

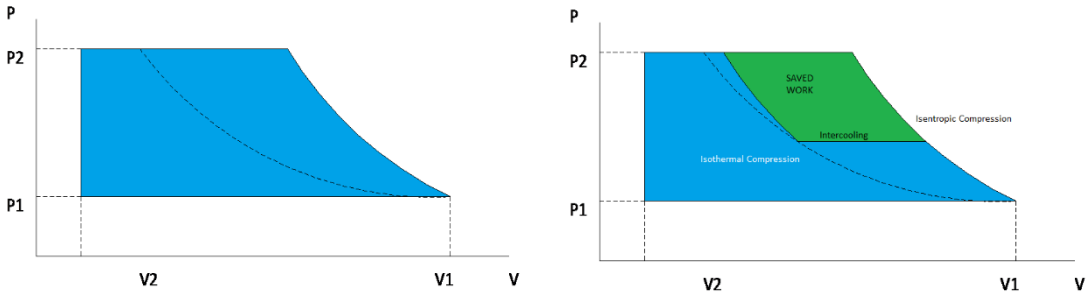

Figure 2.20: Comparison between single stage isentropic compression [left] and multi stage compression with intercooling [right]. The work required for compression is illustrated by the blue area [36]

Multi- stage expansion with reheating is based on the same idea as multistage compression with intercooling, but in reverse. The gas expands in two or more stages while being heated in between the stages. Reheating the gas allows for more work to be produced as illustrated in the image below [37]. The surface area between the states 4-5-6-4' in the P-V diagram represents the extra work produced during the expansion when reheating is used.

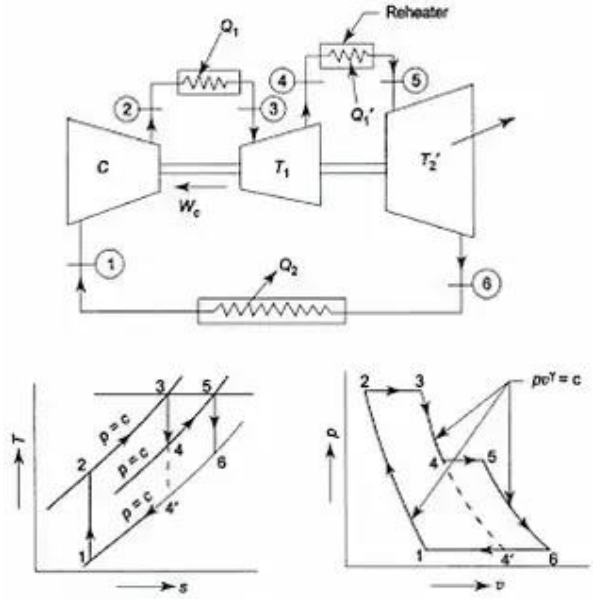

Figure 2.21: Brayton cycle with multiple stage expansion and reheating [37]

It is important to note that both intercooling and reheating do not necessarily result in an increase of the cycle's efficiency. Despite both methods increasing the net work output of the cycle, in many cases the extra heat provided outweighs the net work increase, resulting in lower efficiencies. Usually, for those modifications to be beneficial, many compression and expansion stages must be used. This is also the reason reheating and intercooling are only used in large industrial gas turbines.

2.4. Actual Gas Turbine Cycle

The real-world conditions, such as turbulence, friction, and the differences in the working fluid's properties during the cycle, differentiate the actual cycle that the turbine is running on from the ideal Brayton cycle. For example, the processes taking place in turbines and compressors are actually irreversible, and thus, no longer isentropic. This results in more thermodynamic work needed for the compressor and less work produced by the turbine compared to the ideal cycle. Moreover, the friction inside ducts can lead to pressure drops. This applies to both the inlet and outlet ducts of an open loop gas turbine, as well as the combustion chamber and heat exchangers. Finally, in most modern heat exchangers of reasonable size, the temperature of the hot fluid at the inlet, is still higher than the temperature of the cold fluid at the outlet, meaning that more heat could be exchanged [38].

Due to the aforementioned phenomena, the actual gas turbine cycle needs to be compared with the Brayton cycle through coefficients. An actual gas turbine cycle T-s diagram is illustrated [39] below:

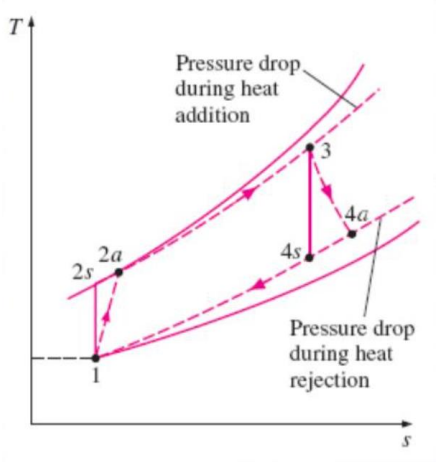

Figure 2.22: Ideal Brayton Cycle (Continuous line) vs Actual Gas Turbine Cycle (Dashed line) [39]

2.4.1. Compressor

As mentioned in *Chapter 2.2.5*, the ideal process taking place inside a compressor is isentropic. In real world conditions, factors like friction and turbulence introduce irreversibility in this process, thus making it no longer isentropic. In order to approach the actual process with the help of the ideal one, the term of isentropic efficiency must be introduced. The isentropic efficiency is a parameter used to describe how efficient a device is at approximating a corresponding isentropic device [40]. For example, we expect that a compressor needs to be provided with more work than what is ideally needed. Thus, with the help of the expressions 2.21 and 2.22, the isentropic efficiency of a compressor is given by the following expression:

$$\eta_{is,C} = \frac{W_i}{W_a} = \frac{h_{t,2i} - h_{t,1}}{h_{t,2a} - h_{t,1}} \quad (2.35),$$

where W_i is the ideal work required by the compressor, W_a is the actual work required by the compressor, $h_{t,1}$ represents the specific stagnation enthalpy of the fluid at the inlet of the compressor, $h_{t,2i}$ represents the specific stagnation enthalpy of the fluid at the outlet of the ideal compressor and $h_{t,2a}$ represents the specific stagnation enthalpy of the fluid at the outlet of the actual compressor.

For well-designed compressors, the isentropic efficiency ranges from 75 to 85% [41]. A comparison between the actual and the ideal processes is illustrated in the figure below [38]. The increase in entropy at the outlet due to the increase in entropy principle is also worth noting.

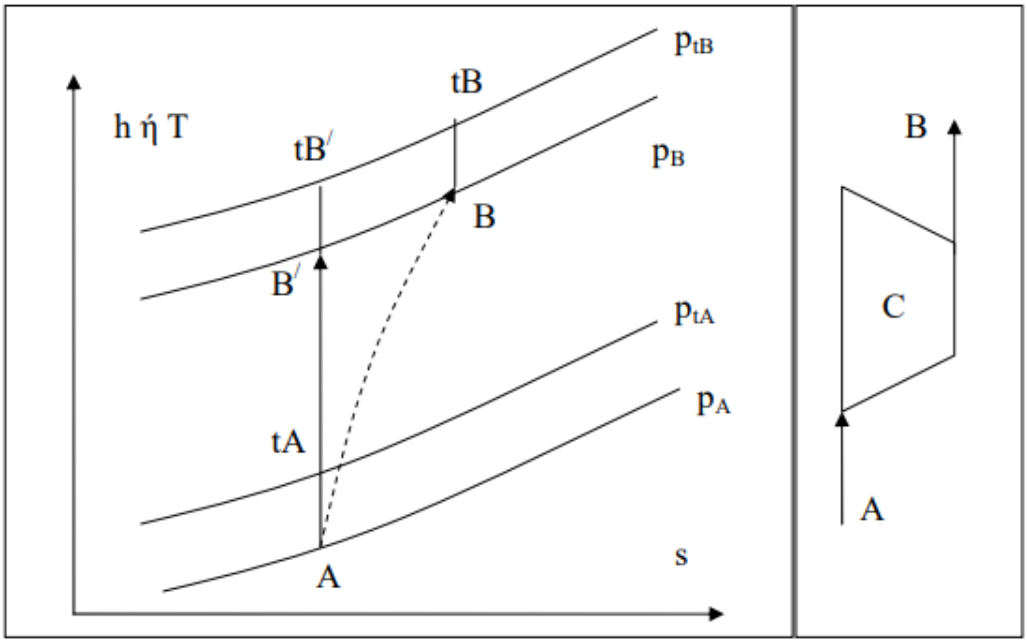

Figure 2.23: Comparison between the actual (dashed line) and ideal process (continuous line) of a compressor [38].

2.4.2. Turbine

For a turbine, the isentropic efficiency is calculated accordingly, however, we expect to receive more work from an ideal turbine than the actual one. Thus, the isentropic efficiency of a turbine is defined as:

$$\eta_{is,T} = \frac{W_a}{W_i} = \frac{h_{t,1} - h_{t,2a}}{h_{t,1} - h_{t,2i}} \quad (2.36),$$

where W_a is the actual work received from the turbine, W_i is the ideal work received from the turbine, $h_{t,1}$ represents the specific stagnation enthalpy of the fluid at the inlet of the turbine, $h_{t,2a}$ represents the specific stagnation enthalpy of the fluid at the outlet of the actual turbine and $h_{t,2i}$ represents the specific stagnation enthalpy of the fluid at the outlet of the ideal turbine.

For turbines, the isentropic efficiency ranges from 70 to 90% [42]. A comparison between the actual and the ideal process is illustrated in the figure below [38]:

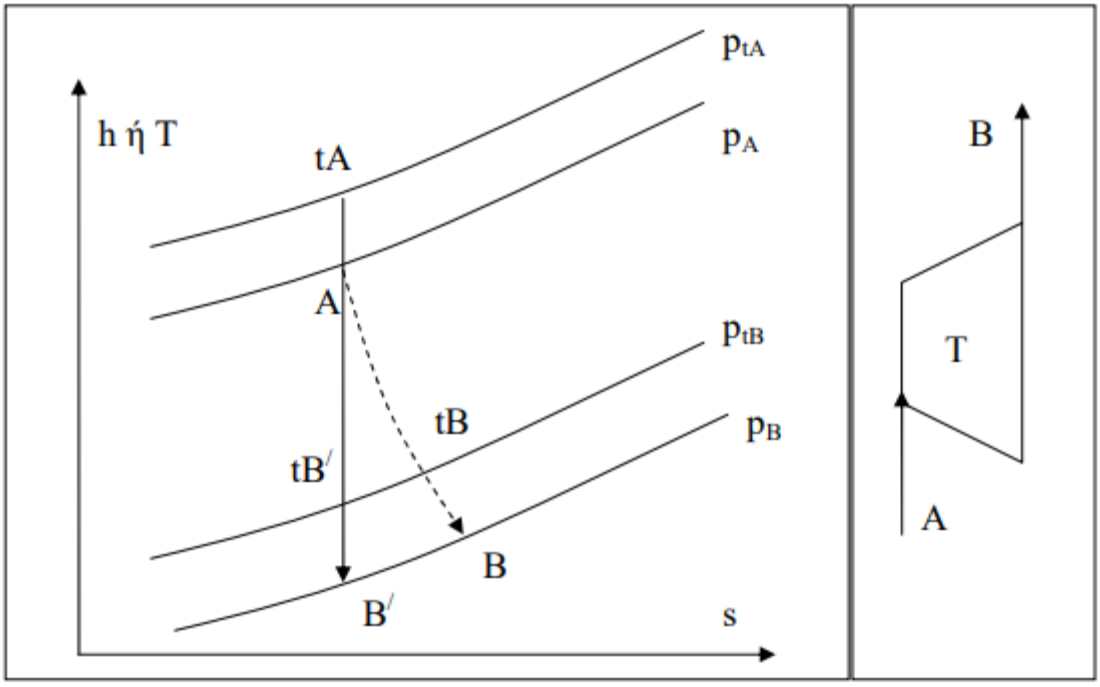

Figure 2.24: Comparison between the actual (dashed line) and ideal process (continuous line) of a turbine [38].

2.4.3. Intake and Exhaust Ducts

The pressure drops taking place in the intake and exhaust ducts of a gas turbine are both modeled with the use of a coefficient called pressure loss factor, which expresses the drop in stagnation pressure as a fraction of the stagnation pressure at the inlet of the duct:

$$K_d = \frac{P_{t,in} - P_{t,out}}{P_{t,in}} \quad (2.37),$$

where $P_{t,in}$ corresponds to the stagnation pressure at the inlet and $P_{t,out}$ corresponds to stagnation pressure at the outlet of the duct. For open loop gas turbines, the total pressure and temperature at the inlet of the intake duct are equal to the atmospheric pressure and ambient temperature, respectively. This is not true for the outlet of the exhaust duct, where the pressure is approximately equal to the atmospheric pressure, but the temperature is higher than the ambient. For inlet ducts, the drop in pressure is caused by the working gas passing through filtration systems, whereas for exhaust ducts, the pressure drop is due to the exhaust gas passing through a silencer or a similar muffling system. Typical values for the pressure loss factor range from 1 to 3%.

2.4.4. Combustion Chamber

In a similar way to the intake and exhaust ducts, the working fluid's pressure drops when it passes through the combustion chamber. These drops are due to the fluid passing through

the diffuser before entering the combustion zone. The pressure loss is again modeled with the help of the pressure loss factor:

$$K_b = \frac{P_{t,in} - P_{t,out}}{P_{t,in}} \quad (2.38),$$

where $P_{t,in}$ corresponds to the stagnation pressure at the inlet and $P_{t,out}$ corresponds to the stagnation pressure at the outlet of the chamber. Typical combustion chamber pressure loss factors at full load range from 5 to 6%, depending on the type of the combustor [43]. For partial loads, the pressure loss factor is given by the following expression [38]:

$$K_{b,PL} = K_b \left(\frac{\dot{m}_{wf} \sqrt{T_{tA}}}{P_{tA}} \right) \quad (2.39),$$

where $\dot{m}_{wf}$ is the working fluid mass flow rate, T_{tA} is the stagnation temperature and P_{tA} is the stagnation pressure at the inlet of the turbine.

In a combustion chamber, heat is provided from the fuel to the working fluid. In practice, not all heat released from the fuel is received by the working fluid. Thus, the efficiency of the combustion chamber must be defined:

$$\eta_b = \frac{(\dot{m}_{wf} + \dot{m}_f) C_{pg} T_{t,out} - \dot{m}_{wf} C_{pwf} T_{t,in}}{m_f q_f} \quad (2.40),$$

where $\dot{m}_{wf}$ corresponds to the working fluid's mass flow rate before the chamber's inlet, $\dot{m}_f$ corresponds to the fuel mass flow rate, $\dot{m}_{wf} + \dot{m}_f$ corresponds to the chamber's exhaust gas mass flow rate at the outlet, C_{pg} is the specific heat capacity of the exhaust gas, $T_{t,out}$ is the exhaust gas stagnation temperature at the outlet of the chamber, C_{pwf} is the specific heat capacity of the fluid before the chamber, $T_{t,in}$ is the stagnation temperature at the inlet of the chamber and q_f is the lower heating value of the fuel. Modern combustion chambers have efficiencies close to 100% (typical range from 99 to 100%) [44].

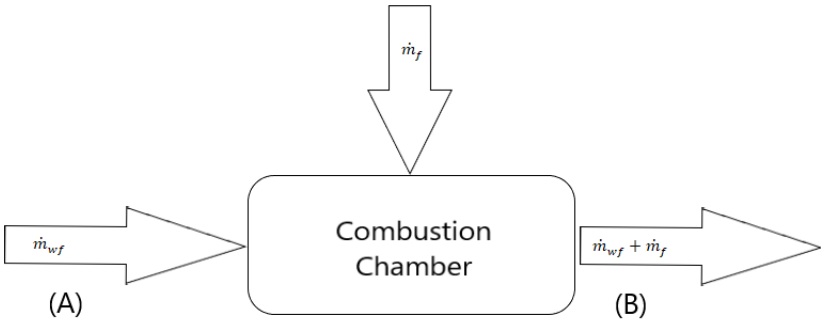

Figure 2.25: Visual Representation of a Combustion Chamber, where the working fluid enters ($\dot{m}_{wf}$), gets mixed with fuel ($\dot{m}_f$) and exits as exhaust gas ($\dot{m}_{wf} + \dot{m}_f$).

2.4.5. Heat Exchangers

As with every other component of the cycle, pressure losses are also present when the working fluid passes through a heat exchanger. For heat exchangers, the pressure loss factor is defined as:

$$K_{HE} = \frac{P_{t,in} - P_{t,out}}{P_{t,in}} \quad (2.41),$$

where $P_{t,in}$ corresponds to the stagnation pressure at the inlet and $P_{t,out}$ corresponds to the stagnation pressure at the outlet of the exchanger.

Finally, at the beginning of the chapter, we mentioned that for heat exchangers of reasonable size, the temperature of the hot fluid at the inlet, is still higher than the temperature of the cold fluid at the outlet, meaning that more heat could ideally be exchanged. In order to describe how effective a heat exchanger is at exchanging heat; we need to compare the temperature increase of the cold fluid to the maximum temperature increase that could theoretically be achieved. To mathematically express the effectiveness of the heat exchanger, the following illustration will be used:

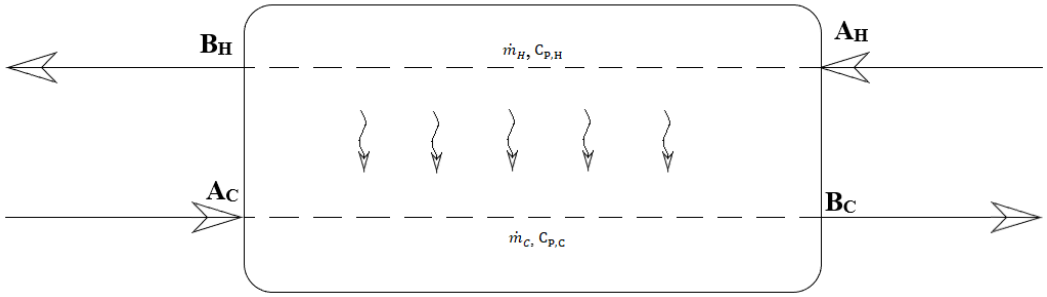

Figure 2.26: Visual Representation of a Heat Exchanger, where a cold fluid ($\dot{m}_C$), gets heated by a warmer fluid ($\dot{m}_H$)

The maximum temperature increase that can be achieved by the cold fluid is when its temperature at the outlet T_{tBC} reaches the temperature of the hot fluid at the inlet T_{tAH}. When we compare this ideal temperature increase to the actual one, we can express the effectiveness of the heat exchanger as:

$$\eta_{HE} = \frac{T_{tBC} - T_{tAC}}{T_{tAH} - T_{tAC}} \quad (2.42)$$

The effectiveness of a heat exchanger is highly dependent on its type, and it can be as high as 90% for state-of-the-art counter-flow plate heat exchangers [45].

3. Supercritical Carbon Dioxide

In this chapter, a summary of the physical and chemical properties of supercritical fluids will be presented, with an emphasis on the supercritical carbon dioxide. Furthermore, the advantages and potential applications of the SCBC will be analyzed and its three main configurations will be described. Finally, the thermodynamic principles behind real gas behavior will be briefly mentioned in order to set the ground for the cycle's modeling in the fourth chapter.

3.1. Properties

A supercritical fluid refers to a fluid above its critical pressure P_C and temperature T_C. At the supercritical state, there is no distinction between the gas and liquid phases. The properties of a supercritical fluid are a mixture of those of a gas and a liquid, and they can be tuned by adjusting the pressure and temperature [46]. For example, we can give the supercritical fluid more liquid-like properties by increasing its pressure, whereas decreasing the pressure will make its properties more gas- like [47]. The most commonly used supercritical fluids are water and carbon dioxide, and they are primarily used for decaffeination, water electrolysis, power generation and other chemical reactions. The critical properties of some commonly used fluids are shown in the table below:

Solvent	Molecular Mass g/kmol	Critical Temperature K	Critical Pressure Mpa	Critical Density g/cm^3
Water	18.015	647.096	22.064	0.322
Carbon Dioxide	44.01	304.1	7.38	0.469
Methane	16.04	190.4	4.6	0.162
Ethane	30.07	305.3	4.87	0.203
Propane	44.09	369.8	4.25	0.217
Methanol	32.04	512.6	8.09	0.272
Ethanol	46.07	513.9	6.14	0.276
Acetone	58.08	508.1	4.7	0.278
Nitrous Oxide	44.013	306.57	7.35	0.452

Table 3.1: Critical properties of various solvents [46]

Carbon dioxide (CO_2) is a chemical compound consisting of one carbon atom double bonded to two oxygen atoms [48]. It is a naturally ocurring substance and a minor component of the Earth's atmosphere formed by the combustion of carbon containing materials, fermentation and animal respiration [49]. At pressures below 5.112 atm it has no

liquid state. In atmospheric pressure, CO_2 is in gas state at room temperature. When the temperature drops below -78.464°C, it directly converts to a solid, also known as dry ice. The liquid state only occurs at pressures above 5.112 atm and the triple point temperature is -56.558°C. The critical point is 30.978°C at 72.808 atm [48]. As illustrated in the following figure [46], the supercritical state lies below the solid- liquid equilibrium line at temperatures and pressures above the critical point. It is possible to convert a liquid into a gas and vice versa with a series of isobaric changes in temperature and isothermal changes in pressure through the supercritical region without incurring a phase transition [50]. Carbon dioxide is minimally toxic, non-flammable [51] and non-corrosive when in gas or supercritical state [52]. It is also 1.5 times denser than air, with a density equal to 1.98 kg/m^3 [48].

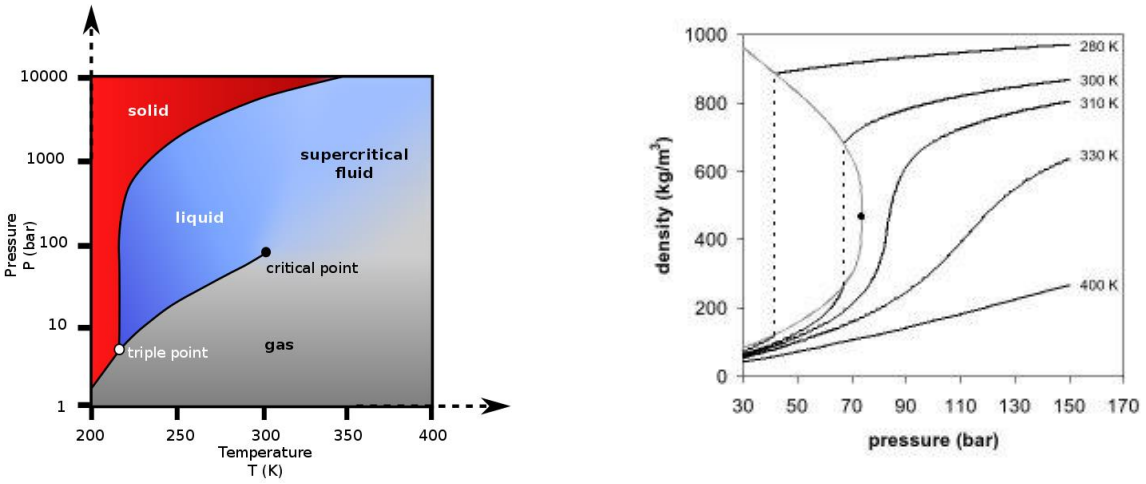

Figure 3.1:Phase Diagram (left) and Density- Pressure Diagram (right) of Carbon Dioxide [46]

Due to their twofold nature, supercritical fluids have many interesting properties. They can easily effuse through porous materials just like a gas; however, they can dissolve materials much better than a gas. Another property of supercritical fluids is that since there is no liquid/ gas phase boundary, there is also no surface tension. Nevertheless, the most interesting property of supercritical fluids is the fine tuning of density near the critical point, where the fluid has a density similar to that of a liquid. This allows for such fluids to be used as the working fluid in closed loop gas turbines of high power and relatively small size. Since CO_2 has a critical temperature close to the ambient temperature, the SCBC can be operated with readily available coolants (e.g., water and air). Factoring in safety, thermal stability, corrosiveness, cost and availability, sCO_2 is the best candidate for being used as the working fluid in a thermal cycle [53]. *Figure 3.2* illustrates a size comparison between a steam turbine and the estimated size of turbines using some supercritical fluids as their working fluid [54].

Property	Density kg/m^3	Viscosity cP	Diffusivity mm^2/s
Gas	1	0.01	1-10
SCF	100-800	0.05-0.1	0.01-0.1
Liquid	1000	0.5-1.0	0.001

Table 3.2: Comparison of physical and transport properties of Gases, Fluids and Supercritical Fluids (SCF) [46]

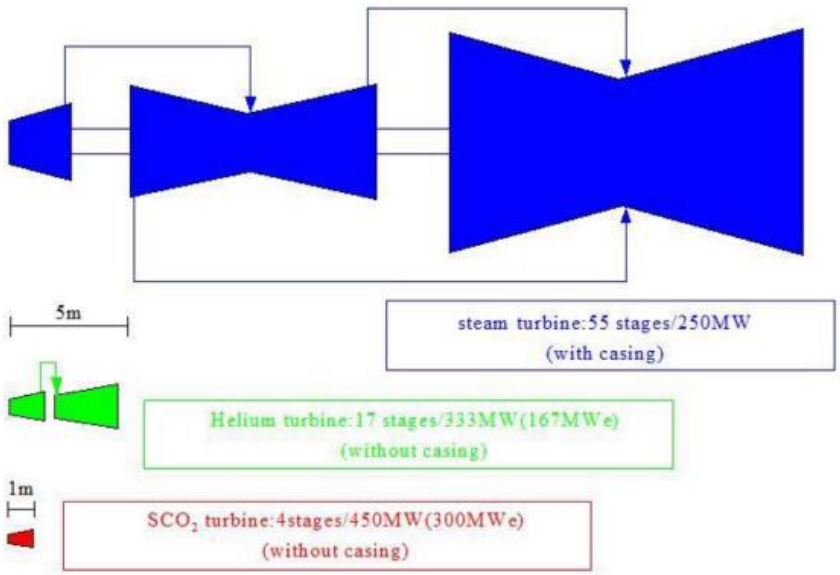

Figure 3.2: Turbine Size Comparison for Helium, Supercritical CO_2, and Steam Cycles [54]

3.2. Advantages and Applications of SCBC

Papers released by SNL [55] and US DOE [53], have done a great job summarizing the potential and challenges of commercializing the SCBC. The cycle offers compact power generation with high thermal efficiency at relatively low turbine inlet temperature ranges [56], thus reducing capital and operating costs. The high efficiency of the cycle can be achieved even under dry cooling, tackling the energy-water nexus problem. The ability for carbon sequestration is also an option, further reducing the environmental impact of the cycle [55]. Other advantages of the SCBC include lower compression work due to the sCO_2 liquid-like density near its critical point, smaller size equipment, lower pressure ratio thus fewer stages in the compressors and turbines and a single-phase working fluid resulting to fewer quality issues and avoidance of the pinch point in the heat exchangers. The SCBC is compatible with a variety of heat sources, from fossil fuels to waste heat, fuel cells, nuclear,

geothermal and solar power, making it an appropriate candidate for many power generation applications.

3.3. Main SCBC Configurations

Over the years, many different SCBC layouts have been developed with the goal of increasing the cycle's efficiency. Each layout offers different advantages and disadvantages in terms of cost and complexity, and for every occasion the layout is chosen depending on the characteristics of the heat source. The three most common layouts are the simple Brayton cycle (SBC), the recuperated Brayton cycle (RBC) and the recompression Brayton cycle (RCBC).

The working principles of the simple Brayton cycle were analyzed in *Chapter 2.3*. The SBC presents the simplest form of a SCBC, so naturally it is expected to have the lowest capital and operating expenses. Its theoretical maximum thermal efficiency is equal to 34.5% at a pressure ratio of 34.9 [53].

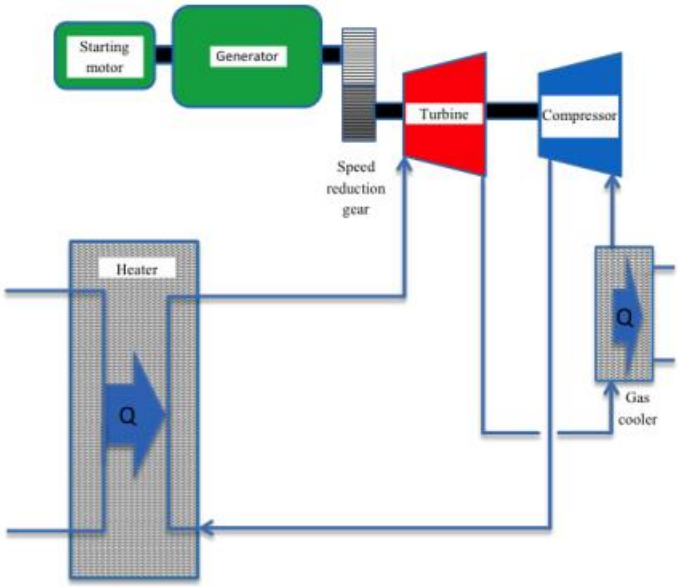

Figure 3.3: Block Flow Diagram for a SBC [53]

The recuperated cycle works in the same way as a Brayton cycle with regeneration, as explained in *Chapter 2.3.1*. In the RBC, a special purpose counter- flow energy recovery heat exchanger, called the recuperator, is placed between the turbine and compressor outlets. By using recuperation, the hot sCO_2 exiting the turbine is used to heat up the working fluid before it enters the heater. Thus, less heat is dumped into the environment by the cooler and less heat needs to be provided by the heater, resulting in a cycle efficiency

improvement. The theoretical maximum thermal efficiency of the RBC is equal to 46.8% and the pressure ratio at which the maximum efficiency occurs is reduced to just 4.5 compared to SBC's 34.9 [53]. One major problem with thermal recuperation is the significant difference in the heat capacity of the sCO_2 at the high- and low-pressure sides of the recuperator (internal pinch point), resulting in a low heat transfer performance. This problem is solved by recompression.

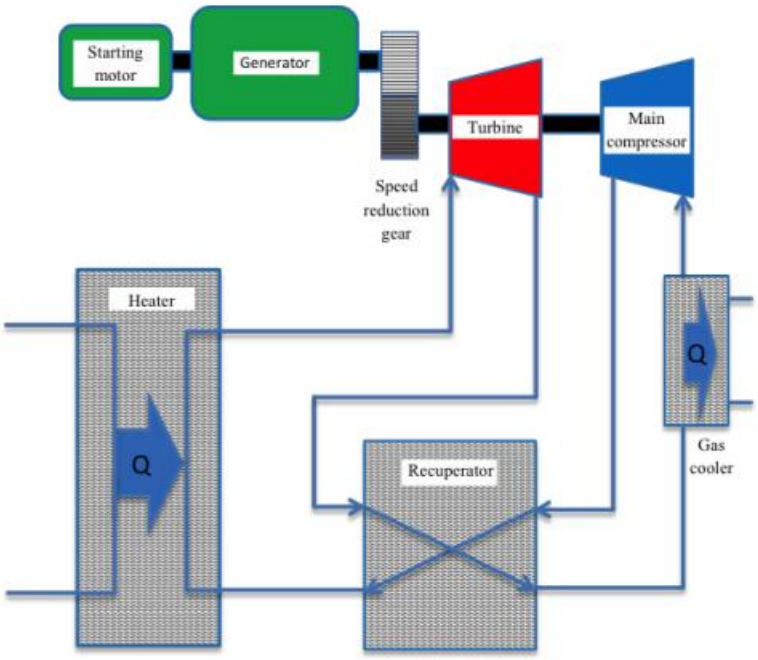

Figure 3.4: Block Flow Diagram of a RBC [53]

The recompression Brayton cycle splits the flow of sCO_2 before it enters the recuperator, thus reducing the mass of the recuperated sCO_2. This arrangement is illustrated in *Figure 3.5* and it features two compressors and two recuperators, one low temperature (LTR) and one high temperature (HTR). The sCO_2 flow is split into two different flows before entering the compression part of the cycle. Only one portion of the flow is cooled before compression. This portion of the flow passes through the low temperature recuperator after the compression. Due to the low mass flow of the fluid that gets heated compared to the mass flow of the fluid that gets cooled in the LTR, the performance of the recuperation is increased. The other portion of the flow is compressed by a different compressor, marked below as re- compressor, without getting cooled first. Then, the two flows are combined at the exit of the LTR and enter the HTR to continue the cycle. The maximum theoretical thermal efficiency of the RCBC is equal to 52.1% at a pressure ratio of 4.4 compared to the RBC's maximum efficiency of 46.8% [53]. All the above efficiencies were calculated for turbomachinery with isentropic efficiency equal to 0.9.

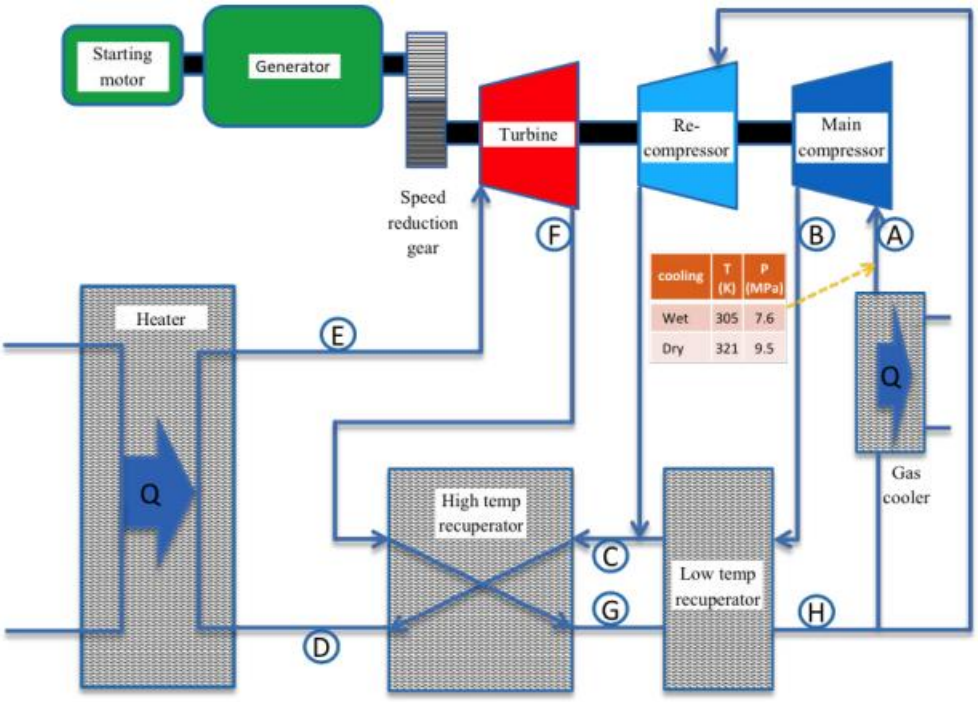

Figure 3.5: Block Flow Diagram of a RCBC [53]

Despite its many advantages, the SCBC has numerous flaws that slow down its wide commercial deployment. The high temperatures exceeding even 500°C in some cases and the high pressure required for high efficiency, require stronger materials for the components. A paper [57] released by SNL in 2014 showed that material erosion is a also a big problem in their SCBC test loop. Factoring in the immaturity of the technology, the yet to be proven performance in real world conditions, the need to scale up the cycle's performance and the remaining R&D on the components, it is understood that several challenges need to be adressed before the cycle is commercialized.

3.4. Real Gas

In *Chapter 2.2.1* we described the thermodynamic behavior of ideal gases with the expression of the ideal gas law. In higher pressures, the gas molecules interact with each other, resulting in a different behavior than that of an ideal gas. Real gases no longer adhere to the ideal gas law, but since most power cycles run on high pressures, it is important to find a way to describe their behavior.

Throughout the years, numerous real gas models have been developed. Similar to the ideal gas law, these models express a relation between the three main thermodynamic properties

of a gas, namely the pressure, the volume and the temperature. The key difference is that real gas models take into consideration the compressibility effects, the differences in specific heat capacity, van der Waals forces, non-equilibrium thermodynamic effects etc. Although the use of such analytical models is not always necessary for most applications, they are very often used at very high pressures, near the critical point or near the condensation point [58]. Thus, they are a particularly important tool for analyzing the behavior of sCO_2. Some of the most commonly used models are the Van der Waals model, Redlich- Kwong model, Berthelot and modified Berthelot model, Dieterici model, Clausius model, Virial model, Peng- Robinson model, Wohl model [58] etc.

Another important tool for studying real gases is the use of thermodynamic tables. Thermodynamic tables are generated using complex models like the ones mentioned above and provide values for the different thermodynamic properties of a fluid at a given state [59]. Their use only requires two of the fluid's properties to be known in advance and provide values for its pressure, temperature, enthalpy and entropy. They are available for a wide variety of fluids and are quite easy to use. Such tables will be used in the fifth chapter, when the SCBC will be modeled in MATLAB.

4. Literature Review

In this section, the scholary sources related to the supercritical carbon dioxide Brayton cycle will be reviewed. The goal of this section is to provide the reader with up to date information about the current research on the cycle, what has been achieved so far on experimental and research level and what is still being researched. This review will also help to understand what obstacles need to be surmounted in order to commercilize the cycle. Before reviewing the most up to date research projects on the cycle, it is important to mention how the closed cycle gas turbine technology has evolved over the last century. A very well rounded historical development of closed cycle gas turbines has been previously presented by Olumayegun et al [56] in 2016. Here, only the most important events will be presented, with a focus on the events of the last decade that are not presented in the aforementioned paper.

4.1. Historical Development

In 1935, professors C. Keller and J. Ackeret filed the initial patent for a closed cycle gas turbine (CCGT) in Berne, Switzerland. This system used air as the working fluid. Nearly four years later, the first CCGT, the AK-36, was built in Zurich, Switzerland by Escher Wyss AG. It was a 2 MW, oil fired gas turbine [60]. In 1949, the first CCGT using air as the working fluid and waste heat as the main heat source was comissioned in Coventry UK. One year later, a patent for a partial condensation CO_2 Brayton Cycle was issued to G. Sulzer.

The main focus during the next fifty years, up until 2000, was to pair closed cycle gas turbines with nuclear reactors. The most important events include, but are not limited to, the US Army's ML-1 project, OKBM Afrikantov's investigation to replace the steam cycle of a 1000 MWh nuclear power plant with a CCGT and a joint program between USA, Russia, France and Japan with the goal of developing a CCGT modular heat reactor. The ML-1 project deserves a special mention, as it took advantage of the main benefit of closed cycle gas turbines, the compact size. It coupled a nitrogen closed Brayton cycle to a small nuclear reactor with the goal of providing portable power generation. The project was shut down for good in 1965 after several mechanical problems with the non nuclear components, that often went undetected until irreversible damage was caused [61]. Despite the project's failure due to the immaturity of CCGT technology, it definately paved the way for small footprint power generation.

The first sCO_2 cycle was designed by Hoffman and Feher in 1970. The cycle produced 150 kW_e and was used to investigate the possibility of pairing sCO_2 cycles with small terrestial nuclear reactors. This was the first and last attempt of using sCO_2 as the working fluid in a power cycle, until 2000, when Massachusetts Institute of Technology (MIT) collaborated

with Idaho National Laboratory (INL), Sandia National Laboratories (SNL) and Argonne National Laboratory (ANL) to revive interest in sCO_2 cycle studies. In 2007, SNL begun investigation of a sCO_2 Brayton cycle using internal funds. The investigation of sCO_2 initially focused on its stability as a working fluid on a double Turbine- Alternator-Compressor (TAC) configuration, each one capable of producing 125 kW of electricity. SNL managed to secure funding from US Department of Energy (DOE) to extend the investigations. In 2010, SNL announced that they managed to produce more electricity than they consumed in a single TAC loop [62] and 2 years later, SNL contractor Barber Nichols Inc completed the design and installation of a megawatt class sCO_2 recompression cycle test assembly. Also in 2012, US DOE funded a project with 8 million dollars with the goal of designing, fabricating and validating a sCO_2 power cycle of nominally 10 MW_e, capable of operation at up to 700°C under dry cooling conditions. The project's team consisted of National Renewable Energy Laboratory (NREL), Abengoa Solar, Echogen, SNL, Electric Power Research Institute (EPRI), UW- Madison and Barber Nichols [63]. Two years later, in 2014, Echogen announced the commercial deployment of a waste heat recovery system using a sCO_2 advanced Rankine cycle, the EPS100, capable of producing 8 MW.

In 2016, the development of a modular nuclear reactor using sCO_2 as both the coolant and the working fluid in a 12 MW Closed Brayton Cycle was announced by Korea Advanced Institute of Science and Technology. During the same year, US DOE announced a 6 year long, 80 million dollar project to develop a sCO_2 test facility. During this project, a team led by Gas Technology Institute, Southwest Research Institute and GE Global Research has to design, build and operate a 10 MW_e closed, inderectly fired sCO_2 recompression Brayton cycle test facility with a turbine inlet temperature of 700 °C, in San Antonio, Texas. The project was named Supercritical Transformational Electric Power (STEP) [64] and begun in 2018 with operations of a 1 MW sCO_2 Brayton cycle with a maximum temperature of 700°C and pressure of 250bar [65]. The STEP team announced in March of 2023 that they achieved supercritical conditions at their 10 MW sCO_2 pilot plant [66]. Meanwhile, nearly a year earlier, in April of 2022, SNL provided power to the Sandia-Kirtland Air Force Base grid for almost an hour, producing up to 10 kW at times. The team's goal now is to demonstrate a 1 MW *sCO_2* Brayton cycle by fall 2024 [67].

4.2. Current Research Overview

In this chapter, a summary of the recent publications on the sCO_2 Brayton cycle will be presented. A bibliometric analysis conducted in 2021 by Yu et al [68] revealed that the publications number related to SCBC had overall increasing trends during 2000- 2019. This means that there is an increasing interest in sCO_2 cycles and their potential is being highly appreciated by the scientific community. The analysis also revealed that the number of issued patents has been decreasing since 2017. This can be interpreted as a proof that the technical bottlenecks of the technology are being gradually solved. From 2000 to 2019, a

total of 1005 patents and 724 publications linked to the sCO_2 Brayton cycle could be found in Scopus, most of them originating from China, the United States and South Korea.

The four main pillars of the SCBC reasearch are: applications of the SCBC, working fluid mixtures, system component development and experiments. Below, these four research fields will be analyzed and some of the most notable publications will be referenced.

4.2.1. Applications of the SCBC

As mentioned in the previous chapter, the SCBC can be paired with a wide variety of heatsouces, namely waste heat, fuel cells, fossil fuels, nuclear, geothermal and solar energy. This aspect of SCBC research is a very broad one, focusing on the characteristics of each heat source and the capabilities of the cycle when paired with a specific heat source. Since there are many cycle configurations and each one of them offers different performance depending on the paired heat source, most of the times different cycle layouts are explored in order to find the most fitting one for the case. Techno- economic analyses of the cycle applications are also oftenly conducted in order to determine whether or not it is worth the potential investment.

The tools used for this study field are mainly simple thermodynamic tools aiming to model the cycle according to the capabilities of the heat source. Exergy analyses are also conducted in order to provide a clear picture of the cycle processes and determine the ones that need to be optimized. The technoeconomic analyses often use financial tools of analysis to assess how this new technology can lower the cost of a process. For example, if we are interested in implementing a SCBC for electrical power generation on the public grid, the cost of electricity provided by this cycle needs to be estimated. If this cost is lower than what is provided by current technologies, it is then worth to proceed with the investment. Such techno- economic analyses consider both the operating and capital expenses of the investment, while also focusing on whether its implementation is possible from a technical point of view (maturity of components, site specific conditions etc).

Along with nuclear power, concentrated solar power (CSP) is considered to be one of the most promising sources of clean energy when paired with a SCBC. Despite the high cost of the technology, programms related to CSP SCBC are some of the few ones that have ever received funding to begin with real world testing. A CSP plant consists of the collector, usually a point focus power tower system, that captures the solar- thermal energy and transfers it to the receiver. The receiver can either be the cycle's working fluid (direct receiver) or any other solid or fluid transport media that then exchanges heat with the working fluid. The biggest challenge with CSP is its inability to stably provide heat. Iverson et al [69] studied the influence of this flactuating thermal input to developmental Brayton turbomachinery and concluded that the system's thermal mass provides for adequate cycle performance for a short period until the thermal input can recover. They also presented a comparison between the effects of short- and long- term thermal storage on the cycle's

performance. Finally, they assesed the cost and financial performance of the cycle while summarizing the key issues that need to be adressed before the SCBC can be used on solar-thermal systems. Guccione et al [70] conducted a techno- economic analysis of a CSP plant combined with photovoltaics and a molten salt thermal energy storage system. They concluded that for a European solar resource location, the levelized cost of energy (LCOE) is lower than 66 €/MWh and the capacity factor is higher than 70% at 10 MW_e. For high irradiance locations, the plant's capacity factor is higher than 85% with a LCOE of 46 €/MWh. Finally, a comparison between a RBC, RCBC, reheated and intercooled layouts revealed that the cycle layout selection has marginal impact on the cycle's performance.

The SCBC is also a great candidate to be paired with a Generation IV nuclear reactor. These reactors are currently being developed and could offer operating temperatures that reach up to 500- 900°C compared to water cooled reactors that operate at around 300°C [68]. Pairing those reactors with a SCBC could offer unprecedented levels of performance and safety. A thermodynamic and exergoeconomic model developed by Luo et al [71] compared the different cycle layouts in terms of performance and revealed that there is an optimal pressure ratio corresponding to the maximum cycle efficiency and lowest total product unit cost for each layout. Meanwhile, the intercooling cycle shows higher performance and comparable costs to the RCBC, whereas the RCBC has the lowest total product unit cost compared to other configurations when the heat exchanger efectiveness exceeds 0.86. The SCBC also shows great potential if paired with nuclear fusion reactors. Even if nuclear fusion is at a very early stage of development, there are studies pairing it with a SCBC and assessing its performance. Hidalgo- Salaverri et al [72] modeled the operation and calculated the performance of a SCBC paired to a helium- cooled pebble bed blanket nuclear fusion reactor with the same characteristics as a demonstration plant planned to start operation in 2050. Two different types of reactors were studied, one pulsive and one steady state. It was concluded that for pulsive reactors, a thermal energy storage unit is necessary to protect the machinery and that the LCOE is not yet competitive with currently available energy producers. On the other hand, steady state reactors offer lower LCOE compared to current electricity prices.

In regards to fossil fuels, CCGT have already been used in the past, so SCBC is a great fit for any fossil fuel power plant due to its compact size and high efficiency. Thanganadar et al [73] conducted a technoeconomic analysis of a supercritical carbon dioxide cycle integrated with a coal- fired power plant where they studied four different SCBC configurations and compared their performance against an advanced ultra- supercritical steam Rankine cycle. The results showed that the SCBC is more efficient than the aforementioned Rankine cycle by about 3 to 4%. The LCOE also saw a reduction of 6 to 8% compared to the steam cycle, however this reduction can be diminished to 0- 3% due to the uncertainty of the SCBC costs. Fossil fuel power plants can also be combined with a directly fired SCBC. This variation of the cycle allows for the working fluid to come in direct contact with the combustion products, just like a typical open loop gas turbine. Direct fired loops allow for greater maximum cycle temperatures, therefore improving the efficiency, while also providing the ability to capture and store the excess CO_2. The

technology is still very immature as the cycle is a lot more complex than indirectly fired loops, due to the necessity of processing the combustion products. Moreover, the range of fuels that can be used with direct fired cycles is narrow. Sleiti et al [74] conducted the thermodynamic and exergoeconomic analyses of a direct oxy- combustion SCBC, studying the effects of preheating in a RBC configuration. They concluded that placing the preheater parallel to both the low- and high temperature recuperators offers the best cycle efficiency, equal to 45.8% and the largest reduction in total product cost per unit equal to 34.6% compared to a simple RBC configuration.

Despite its very limited use to date, geothermal energy is considered to be a great source of clean energy. Typical geothermal power plants use hot water springing from underneath the earth's surface to create steam and power steam turbines. However, a modern development in geothermal energy systems allows for the earth's heat to be utilized in areas without natural underground water reservoirs. Such systems are refered to as hot dry rocks or enhanced geothermal systems (EGS) [75]. In an EGS, a fluid gets injected underground causing pre- existing fractures to open. The first concepts of EGS considered water as the fluid. Since sCO_2 is a better working fluid than water, a SCBC can be used instead of a conventional steam Rankine cycle. Ruiz- Casanova et al [76] presented a comparison between four different SCBC layouts paired with a low grade geothermal heat source. The study results showed that the intercooled RBC layout achieved the highest electric power output, energy and exergy efficiency, followed by the RBC, SBC and intercooled Brayton cycle.

Regarding fuel cells, the potential for clean and efficient energy production is great. The high operating temperatures of solid- oxide fuel cells allow for a SCBC to be used as a bottoming cycle to further improve the performance. Schöffer et al [77] investigated the performance of a solid oxide fuel cell combined with a SCBC and concluded that this hybrid system is more efficient, yet a lot more complex than a directly coupled solid oxide fuel cell- gas turbine system. Furthermore, a comparison between the RBC and RCBC showed that the RCBC offers negligible performance improvement compared to the improvement it offers when running the SCBC as a standalone system, while adding even more complexity to the system.

Finally, due to its compactness, the SCBC can be used as a waste heat recovery (WHR) system, suitable for all sorts of waste heat, from that produced in industrial processes to the exhaust gas of an engine. The WHR industry is currently dominated by steam and organic Rankine cycles (ORC). Due to its increased efficiency, the SCBC might play a big role in WHR in the future. A major problem is that waste heat is not considered a stable heat source as its characteristics greatly depend on the load of the main engine or the process' intensity. Thus, WHR SCBC must be assesed in terms of dynamic performance in different partial load scenarios. Alfani et al [78] analysed five different WHR SCBC configurations and concluded that the sCO_2 technology can reach efficiencies of up to 27.5%, higher than those of an ORC, with a similar specific cost. The simple recuperated cycle with recuperator bypass was deemed to be the most promising configuration and was studied

further in offload conditions. It was concluded that in combination with a CO_2 storage vessel, the cycle has very high and constant efficiency even at 50% of the normalized flue gas mass flow. Xie and Yang [79] studied the performance of a RCBC for waste heat recovery on a low speed marine Diesel engine in three different load conditions (50, 75 and 100%). The results showed that combined with the proper exhaust timing modulation, the total efficiency of the combined system increased by 2.28, 1.04 and 2.07% at each loadcase respectively.

4.2.2. Working Fluid Mixtures

One of the main advantages of closed loop gas turbines is the ability to use a wide variety of working fluids. Thus, it is possible for a broad spectrum of additives to be added to the working fluid in order to modify the cycle's performance. The use of fluid mixtures not only can improve the cycle's efficiency but can also help tackle material corrosion problems which are present, especially at higher temperatures. Since CO_2 is relatively non-corrosive, most of the research around sCO_2 mixtures focuses on improving the thermal efficiency of the cycle, either by modifying the thermodynamic properties of the fluid, or by changing the working fluid's critical temperature and pressure, thus allowing for high efficiency operation in a variety of ambient temperatures with different heat sources.

In 2011, SNL conducted experiments [80] on their test loop, trying to determine the critical point of sCO_2 mixtures with different additives. The results showed that by creating mixtures, the critical pressure and temperature can be modified. Morosini et al [81] investigated the performance of CO_2 with C_6F_6 mixture for use in the hot environment of a CSP plant. Furthermore, they designed a 1D preliminary model of the turbine. This research was part of the European SCARABEUS project for the development of a sCO2 Rankine CSP plant. Since there are more serious challenges that need to be surmounted for the successful deployment of the SCBC, research on working fluid mixtures is still limited. When the fundamentals of the SCBC are covered, it is expected that more experiments will be conducted on the different mixtures in order to optimize the cycle's performance.

4.2.3. Cycle Component Development

Research on the cycle's main components is a vital step for the successful deployment of SCBC systems. The main parts of the SCBC include the compressor, the heat exchangers and the turbine. Each one of the components poses a different challenge in its design and operation when used with sCO_2.

The compressors used on the SCBC operate close to the supercritical region. Thus, due to the acceleration of the flow, condensation is likely to happen, especially at the tips of the compressor blades. Combined with the density variation of sCO_2 in the supercritical region,

the performance of the compressor can sometimes be unpredictable. Compressors are initially designed using one- dimensional models. The results are then validated using three-dimensional computational fluid dynamics (CFD) models, while experiments can also be conducted. Since condensation is an issue for sCO_2 compressors, thermodynamic models are also used to predict the occurrence of a two-phase flow. Saravi and Tassou [82] investigated the performance of the compressor at different regions of the supercritical state using CFD. Du et al [83] investigated the performance of the compressor on off- design conditions. It was found that the behavior of the SCBC is heavily affected by the ambient temperature and that increasing the compressor inlet pressure and speed can improve its performance during the summer. Zhu et al [84] conducted experiments on a 1MW SCBC centrifugal (radial) compressor and compared the experimental and design curves. Finally, Aretis et al [85] investigated the performance of centrifugal compressors at the critical region, focusing on possible condensation phenomena. Furthermore, they presented a methodology for the preliminary design of a centrifugal compressor with a vaned diffuser, suitable for fulfilling a variety of operating requirements.

Regarding the heat exchangers, the main challenge is finding a heat exchanger that can efficiently operate at elevated temperatures and pressures while maintaining a compact size and a low pressure drop. Since regular heat exchangers are considered too big to be used on the highly compact SCBC, micro shell and tube and printed circuit heat exchangers (PCHE) are considered as attractive alternatives. PCHE are ultra- compact heat exchangers with chemically etched fluid micro- channels, bonded together by diffusion welding. They provide excellent heat transfer efficiency with a small footprint [86]. The main parameters that influence the performance of PCHE are the channel's shapes and cross sections. The main methods of studying these state-of-the-art compact heat exchangers are by using semi empirical models and numerical simulations, meanwhile experiments are also usually conducted in order to validate the simulation results [68]. Kwon et al [87] summarized the characteristics of compact heat exchangers for use with sCO_2 at the typical temperature ranges of the SCBC. The main advantages, heat transfer mechanisms and limitations of five different types of compact heat exchangers were presented. They concluded that every compact heat exchanger except for micro shell and tube heat exchangers is susceptible to fouling, whereas the scalability of micro shell and tube heat exchangers is yet to be proven. Seo et al [88] analyzed the design and performance of a sCO_2 heat exchanger. Using three-dimensional CFD codes, they analyzed the flow and thermal characteristics of a tubular type heat exchanger with a staggered tube bundle. Furthermore, they conducted a thermal stress analysis where it was found that the stress satisfied the American Society of Mechanical Engineers (ASME) criteria.

Similar to the compressor, the turbines are usually first designed using one- dimensional models. This initial design is then validated and enhanced with the use of three-dimensional numerical models. Since the CO_2 has a high density in its supercritical state, it is expected that the sCO_2 turbines will have a much smaller size and fewer stages than regular turbines. Combined with the cycle's high temperatures and pressures, turbines need to be designed from the ground up in order to operate the SCBC efficiently and safely. Stepanek et al [89]

estimated the dimensions and characteristics of a sCO_2 turbine by creating a parametric design and running a specialized code. The results showed that the sCO_2 turbines were one-fifth of the size of their steam turbine counterparts, while the majority of turbines only had 3 to 4 stages. Li et al [90] designed and optimized a 25MW turbine rotor and cylinder for use with sCO_2. Finally, Zhang et al [91] investigated the off- design performance of a sCO_2 turbine for use in a CSP power plant. The turbine was designed and three types of nozzle profiles with different leading-edge diameters were examined. The results showed that the leading-edge diameter has a great influence on the performance of the turbine, both on and off- design conditions.

4.2.4. Experiments

To our knowledge, more than five test loops exist to date, including the SNL test loop and the STEP program mentioned in the previous section. Since the SCBC is considered cutting edge technology, it is relatively difficult to find published information, experimental results and specifications for the existing test loops. The SNL test loop has been under testing since 2008 and has operated in many configurations, namely SBC, RBC and GE Waste Heat cycle. During their tests, SNL verified the cycle's performance and developed cycle controls and maintenance procedures. An extensive report [80] was published by SNL in 2010 describing every aspect and component of their setup, while presenting the first experimental results. While their setup has probably changed since then, their goal was to test a 10 MW cycle, yet it is uknown if they managed to achieve this. The following figure [68] summarizes the available information related to some of the current test loop projects.

Project	Starting Year	Main institute	Founding source	Target
Sunshot [138]	2011	Sandia National Lab; the Office of Nuclear Energy	Department of Energy, USA	To ensure component readiness for the successful launch of S–CO_2 Cycle; To support the development of a re-configurable and scalable system, allowing the testing of commercially attractive configurations and system components; To establish the foundations for successful commercialization of the S–CO_2 cycle
A Supercritical CO_2–Cooled Small Modular Reactor [139]	2014	the Korea Advanced Institute of Science and Technology	–	To design the reactor core and S–CO_2 power generation system in one vessel; To validate the performances of PCHE and radial turbomachinery; To investigate the dynamic behaviors and design the reactor control
Research on basic theory and key technology of coal-fired S–CO_2 power generation [140]	2018	North China Electric Power University; Xi'an Jiaotong University	Ministry of Science and Technology of China	To solve the energy cascade utilization, thermodynamic cycle optimization of coal-fired S–CO_2 power system; To investigate the energy and mass conversion and transfer mechanism of key cycle components; To develop prototypes of boiler, recuperator and turbine and design a 1000 MW system with efficiency 51%
10-MW Supercritical Carbon Dioxide Demonstration [141]	2019	Southwest Research Institute; the Gas Technology Institute; GE company	Department of Energy, USA	To demonstrate the scalability of S–CO_2 system, and its performance ability; To develop a megawatt-scale, high-efficiency S–CO_2 hot-gas turbo-expander; To optimize recuperator technology for S–CO_2 applications
SCARABEUS [142]	2019	Politecnico di Milano; Vienna University of Technology; The University of Seville	European Union's Horizon research	To demonstrate the application of CO_2-based mixtures to CSP plants; To investigate the thermal stability of the new working fluid at 700 °C for 300 h in real working conditions; To demonstrate the feasibility of the condensation process performed at high (up to 60 °C) ambient temperature

Figure 4.1: Some of the current sCO_2 projects [68]

The 10 MW scale is considered a very important checkpoint as it represents a direct move from high tech to commercial applications, meaning that more of- the- shelf components can be used and tested. Problems that occur on small scale turbomachinery might not occur on larger ones. The STEP program is on track to reach this checkpoint after its announcement of achieving supercritical conditions in their test facility.

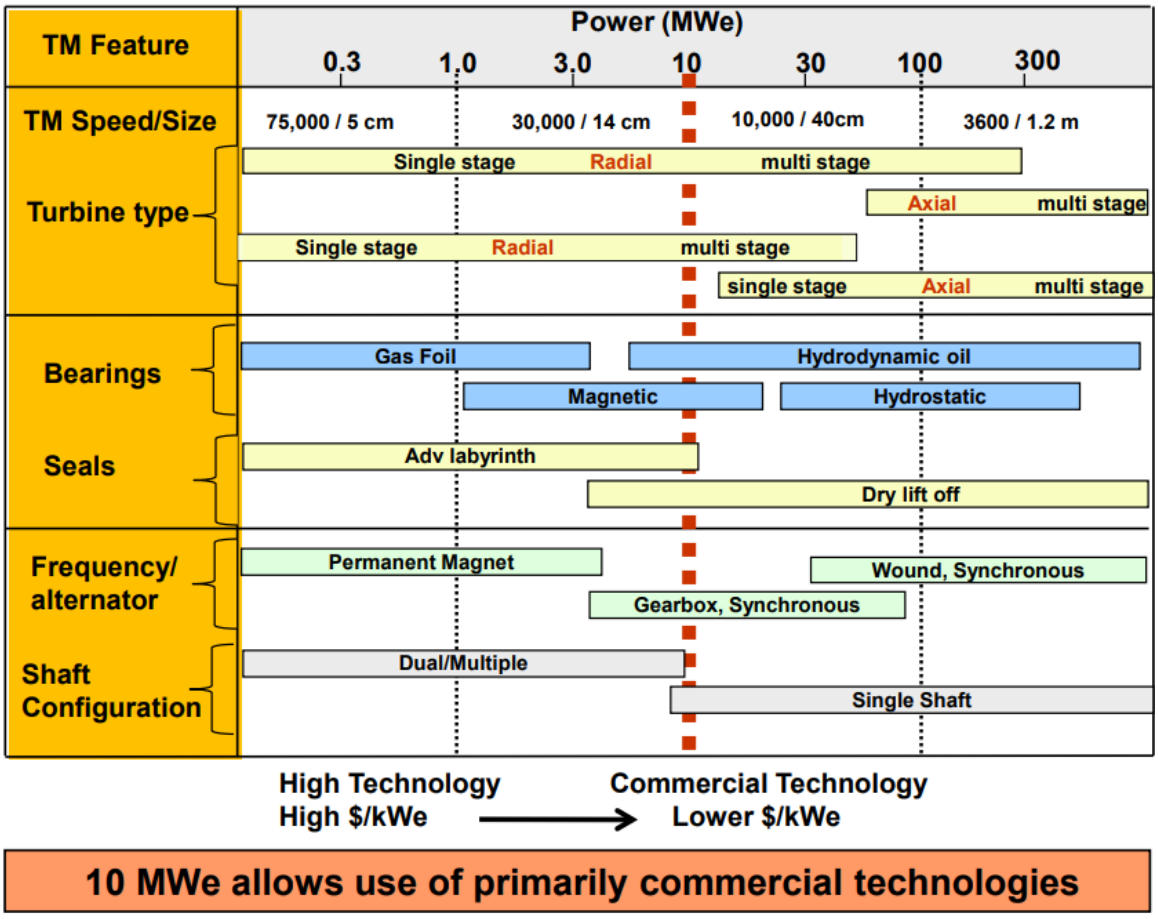

Figure 4.2: Scaling of Cycle Components [55]

Finally, it is important to mention the existence of a commercial WHR sCO_2 system. Despite working on an "advanced Rankine cycle" rather than a Brayton cycle, the Echogen EPS100 shares a lot of the same components with a Brayton Cycle, like the turbine and the heat exchangers. The current available configurations can deliver outputs from 1 to 9 MW but it is feasible for future configurations to deliver up to 500+ MW [92].

Figure 4.3: The Echogen EPS100 WHR system [92]

5. Cycle Modeling and Design

In this chapter, a detailed description of our model and its development process will be presented. First, a suitable configuration for waste heat recovery will be chosen and the mathematical expressions for every thermodynamic state of the cycle will be introduced. Then, our case will be described in detail in order to understand our model parameters and design goals. The rest of the chapter is split in three sections, one for the design and analysis of the system at full load, one for the analysis at partial loads and one for the comparison of our results to similar studies. The goal of the full load design and analysis part is to study our system's behaviour by changing the main parameters and then using the results to choose an operating point. Then, the performance of the SCBC at this point will be calculated and the system's performance improvements will be presented. The full load scenario was the first step in our modeling process, thus a lot of different approaches had to be considered. In this section, one of these alternative approaches is also presented and compared to our final one. For the partial loads modeling, a similar approach to the full load scenario was chosen. Partial loads is a relatively new topic in the SCBC field, thus there is a lack of literature regarding the modelling process. However, some of the most noteworthy publications were mentioned in this section and some of our results were compared to these existing studies. Finally, our simulation results were compared to another similar study on a SCBC WHR system for a marine diesel engine, as well as an ORC, also for WHR for a marine diesel engine. The goal of this last section is to somewhat validate our results while also briefly comparing this state-of-the-art system to an already field-proven one.

5.1. Cycle Configuration

Since the SCBC seems highly unlikely to be used as the main method of propulsion onboard ships in the forseeable future, during the modeling process we are going to focus on the potential of the SCBC as a waste heat recovery system. In 2016, Kim et al [93] compared nine different SCBC layouts for use as a bottoming cycle for a gas turbine. The comparison revealed that the recompression cycle, despite having the highest theoretical thermal efficiency as described in *Chapter 3.3*, is not suitable for bottoming cycle applications. Moreover, it was found that a dual heated Brayton cycle with flow split produces the highest net thermodynamic work; this configuration, however, is extremely complex and requires sophisticated operational strategies. Timothy J. Held, Chief Technology Officer of Echogen Power Systems, submited a paper [94] for the Power Gen International Conference that took place in Nevada in 2015. In this paper, a model of a SCBC for use in a gas turbine combined cycle power plant was presented and various aspects of the technology were analyzed. The configuration of choice was the recuperated Brayton cycle, since more complex architectures like the recompression cycle perform

poorly in bottoming cycle applications. Upon reviewing more papers, it can be concluded that recompression is not a popular option for waste heat recovery applications. Recuperation on the other hand is very popular among the various configurations, with more than one recuperators being used in some cases. Furthermore, the simplicity, smaller size, and allegedly better off- design performance of the recuperated cycle are big advantages when used for waste heat recovery. Due to the aforementioned reasons, the recuperated Brayton Cycle (RBC) will be the main configuration of choice for the modeling process of this chapter.

5.2. Mathematical Expressions

The main working principles of the RBC were presented in *Chapter 3.3*. The working fluid enters the compressor and its pressure is increased $(1 \rightarrow 2)$. Then it passes through a recuperator $(2 \rightarrow 3)$, which utilizes the hot gas exiting the turbine to preheat the working fluid. After the recuperator, the working fluid enters the main heater $(3 \rightarrow 4)$ and its temperature is further increased. Upon exiting the heater, the CO_2 enters the turbine $(4 \rightarrow 5)$ and produces thermodynamic work by rotating the turbine's blades while its pressure decreases. After exiting the turbine, the hot gas enters the recuperator $(5 \rightarrow 6)$, then the cooler $(6 \rightarrow 1)$ and finally repeats the cycle. The aforementioned processes are further illustrated in the figures below [95]:

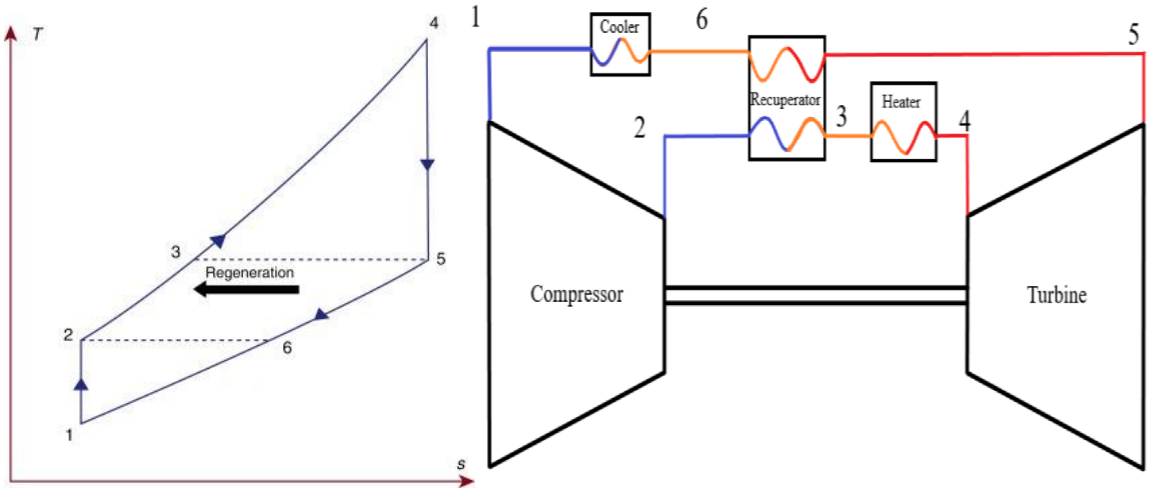

Figure 5.1: T-s Diagram of a Recuperated (Regenerative) Cycle [95] (left); Layout of the RBC (right)

In the following sections, the mathematical equations for every thermodynamic state of the recuperated cycle will be expressed.

5.2.1. State 1 - Compressor Inlet

In a supercritical cycle, the working fluid does not incur a phase transition, thus the pressure and temperature of the fluid must always be kept above the critical point. Due to the already high pressure of the critical point, it is suggested that the cycle's minimum pressure is kept as low as possible. However, as mentioned in *Chapter 4.2.3*, condensation poses a great risk for the safe and efficient operation of the turbomachinery. Therefore, there should always be a safety margin for the cycle's minimum pressure. The same also goes for the cycle's minimum temperature. For this model, the margin for the minimum temperature will be kept at 10 K and the margin for the minimum pressure will be kept at 0.2 MPa. In summary, for the thermodynamic state of the working fluid at the compressor's inlet, the following are true:

$$T_{t1} = T_{CRIT} + 10 \quad [K] \qquad (5.1)$$

$$P_{t1} = P_{CRIT} + 200000 \quad [Pa] \qquad (5.2)$$

$$h_{t1} = f(P_{t1}, T_{t1}) \quad \left[\frac{J}{kg}\right] \qquad (5.3)$$

$$s_{t1} = f(P_{t1}, T_{t1}) \quad \left[\frac{J}{kgK}\right] \qquad (5.4)$$

where T_{t1} is the stagnation temperature, T_{CRIT} is the critical temperature, P_{t1} is the stagnation pressure, P_{CRIT} is the critical pressure, h_{t1} is the stagnation enthaply as a function of the stagnation pressure and temperature and s_{t1} is the stagnation entropy as a function of the stagnation pressure and temperature at the compressor's inlet.

5.2.2. State 2 – Compressor Outlet – Recuperator Cold Side Inlet

The ideal thermodynamic process taking place inside a compressor is an isentropic compression. The real process is not isentropic, however. For the fluid at the compressor's outlet, the following are true:

$$P_{t2} = r \times P_{t1} \quad [Pa] \qquad (5.5)$$

$$s_{t2i} = s_{t1} \quad \left[\frac{J}{kgK}\right] \qquad (5.6)$$

$$h_{t2,i} = f(P_{t2}, s_{t2i}) \quad \left[\frac{J}{kg}\right] \qquad (5.7)$$

$$w_{in} = \frac{w_{in,i}}{\eta_{is,C}} = \frac{h_{t2i} - h_{t1}}{\eta_{is,C}} \quad \left[\frac{J}{kg}\right] \qquad (5.8)$$

$$h_{t2} = h_{t1} + w_{in} \quad \left[\frac{J}{kg}\right] \qquad (5.9)$$

$$T_{t2} = f(P_{t2}, h_{t2}) \quad [K] \quad (5.10)$$

$$s_{t2} = f(P_{t2}, T_{t2}) \quad \left[\frac{J}{kgK}\right] \quad (5.11)$$

where r is the compression ratio, P_{t2} is the stagnation pressure, s_{t2i} is the stagnation entropy at the outlet of the ideal compressor, $h_{t2,i}$ is the stagnation enthalpy at the outlet of the ideal compressor as a function of the stagnation pressure and entropy, w_{in} is the specific thermodynamic work input of the compressor, $w_{in,i}$ is the specific thermodynamic work input of the ideal compressor, h_{t2} is the stagnation enthalpy, T_{t2} is the stagnation temperature as a function of the stagnation pressure and enthalpy and s_{t2} is the stagnation entropy as a function of the stagnation pressure and temperature at the outlet of the compressor.

5.2.3. State 3 – Recuperator Cold Side Outlet – Heater Inlet

Before entering the heater, the fluid first passes through the recuperator to increase its temperature. We are going to assume that inside the recuperator, heat is exchanged at a rate equal to $\dot{Q}_R$. Let us also assume the presence of pressure losses inside the heat exchangers, as explained in *Chapter 2.4.5*. At the inlet of the heater:

$$P_{t3} = P_{t2}(1 - K_R) \quad [Pa] \quad (5.12)$$

$$h_{t3} = h_{t2} + \frac{|\dot{Q}_R|}{\dot{m}} \quad \left[\frac{J}{kg}\right] \quad (5.13)$$

$$T_{t3} = f(P_{t3}, h_{t3}) \quad [K] \quad (5.14)$$

$$s_{t3} = f(P_{t3}, T_{t3}) \quad \left[\frac{J}{kgK}\right] \quad (5.15)$$

where P_{t3} is the stagnation pressure, K_R is the pressure loss factor of the recuperator, h_{t3} is the stagnation enthalpy, $\dot{Q}_R$ is the heat exchange rate in the recuperator in $Watts$, $\dot{m}$ is the working fluid's mass flow rate in $\frac{kg}{sec}$, T_{t3} is the stagnation temperature as a function of the stagnation pressure and enthalpy and s_{t3} is the stagnation entropy as a function of the stagnation pressure and temperature at the inlet of the heater.

5.2.4. State 4 – Heater Outlet – Turbine Inlet

After the recuperator, the working fluid enters the main heater. Assuming that our cycle will be used for waste heat recovery, the high temperature exhaust gas of another thermal engine will be used to heat up the working fluid of the Brayton cycle. Following a similar

approach to the recuperator, we are going to assume that heat is exchanged at a rate equal to $\dot{Q}_H$ inside the heater. Having mentioned the above, at the inlet of the turbine:

$$P_{t4} = P_{t3}(1 - K_H) \quad [Pa] \quad (5.16)$$

$$h_{t4} = h_{t3} + \frac{\dot{Q}_H}{\dot{m}} \quad \left[\frac{J}{kg}\right] \quad (5.17)$$

$$T_{t4} = f(P_{t4}, h_{t4}) \quad [K] \quad (5.18)$$

$$s_{t4} = f(P_{t4}, T_{t4}) \quad \left[\frac{J}{kgK}\right] \quad (5.19)$$

where P_{t4} is the stagnation pressure, K_H is the pressure loss factor of the heater, h_{t4} is the stagnation enthalpy, $\dot{Q}_H$ is the heat exchange rate in the heater in $Watts$, $\dot{m}$ is the working fluid mass flow rate in $\frac{kg}{sec}$, T_{t4} is the stagnation temperature as a function of the stagnation pressure and enthalpy and s_{t4} is the stagnation entropy as a function of the stagnation pressure and temperature at the turbine inlet.

5.2.5. State 5 – Turbine Outlet – Recuperator Warm Side Inlet

For the outlet of the turbine, we are going to follow a similar approach to that of the compressor. A key difference is that the pressure at the outlet turbine is already known, due to the fact that the working fluid has to repeat the cycle. The pressure at the outlet of the turbine however, is different than the minimum pressure of the cycle due to the fact that pressure losses occur in both the cooler and the recuperator before the working fluid re-enters the compressor to repeat the cycle. At the outlet of the turbine:

$$P_{t5} = \frac{P_{t1}}{(1-K_R)(1-K_C)} \quad [Pa] \quad (5.20)$$

$$s_{t5,i} = s_{t4} \quad \left[\frac{J}{kgK}\right] \quad (5.21)$$

$$h_{t5,i} = f\left(P_{t5}, s_{t5,i}\right) \quad \left[\frac{J}{kg}\right] \quad (5.22)$$

$$w_{out} = \eta_T \times w_{out,i} = \eta_T\left(h_{t4} - h_{t5,i}\right) \quad \left[\frac{J}{kg}\right] \quad (5.23)$$

$$h_{t5} = h_{t4} - w_{out} \quad \left[\frac{J}{kg}\right] \quad (5.24)$$

$$T_{t5} = f(P_{t5}, h_{t5}) \quad [K] \quad (5.25)$$

$$s_{t5} = s(P_{t5}, T_{t5}) \quad \left[\frac{J}{kgK}\right] \quad (5.26)$$

where P_{t5} is the stagnation pressure, K_R is the pressure loss factor of the recuperator, K_C is the pressure loss factor of the cooler, $s_{t5,i}$ is the stagnation entropy at the outlet of the ideal

turbine, $h_{t5,i}$ is the stagnation enthalpy at the outlet of the ideal turbine as a function of the stagnation pressure and entropy, w_{out} is the specific thermodynamic work output of the turbine, $w_{out,i}$ is the specific thermodynamic work output of the ideal turbine, h_{t5} is the stagnation enthalpy, T_{t5} is the stagnation temperature as a function of the stagnation pressure and enthalpy and s_{t5} is the stagnation entropy as a function of the stagnation pressure and temperature at the turbine outlet.

5.2.6. State 6 – Recuperator Warm Side Outlet – Cooler Inlet

Following a similar approach to the cold side of the recuperator, at the outlet of the warm side of the recuperator:

$$P_{t6} = P_{t5} \times (1 - K_R) \quad [Pa] \quad (5.27)$$

$$h_{t6} = h_{t5} - \frac{|\dot{Q}_R|}{\dot{m}} \quad \left[\frac{J}{kg}\right] \quad (5.28)$$

$$T_{t6} = f(P_{t6}, h_{t6}) \quad [K] \quad (5.29)$$

$$s_{t6} = f(P_{t6}, T_{t6}) \quad \left[\frac{J}{kgK}\right] \quad (5.30)$$

where P_{t6} is the stagnation pressure, K_R is the pressure loss factor of the recuperator, h_{t6} is the stagnation enthalpy, $\dot{Q}_R$ is the heat exchange rate in the recuperator in $Watts$, $\dot{m}$ is the working fluid mass flow rate in $\frac{kg}{sec}$, T_{t6} is the stagnation temperature as a function of the stagnation pressure and enthalpy and s_{t6} is the stagnation entropy as a function of the stagnation pressure and temperature at the inlet of the cooler.

5.2.7. Performance

The performance of a thermal cycle includes the values for the net power production and thermal efficiency of the cycle among other metrics used to evaluate a system's performance. Here, we are only going to focus on the power and efficiency of the cycle:

$$P = \dot{m}(w_{out} - w_{in}) \quad [Watt] \quad (5.31)$$

$$\eta = \frac{P}{\dot{Q}_H} \quad (5.32)$$

where P is the power produced by the cycle in $Watt$, $\dot{m}$ is the mass flow rate of the working fluid in $\frac{kg}{sec}$, w_{out} is the specific thermodynamic work output of the turbine, w_{in} is the specific thermodynamic work input of the compressor, η is the thermal efficiency of the cycle and $\dot{Q}_H$ is the heat input rate in $Watt$.

5.3. Case Study

For the purposes of this thesis, a supercritical carbon dioxide Brayton cycle will be used as a bottoming cycle for a marine engine. The engine of choice is the state-of-the-art MAN B&W 6G70ME-C10.5-GA-EGRBP, a six cylinder dual fuel engine aimed at the LNG carrier sector [96], paired with a MHI MET53-MBII turbocharger. The engine is based on the premixed Otto principle and is capable of operating on low pressure fuel supply. It also features an exhaust gas recirculation system (EGR), further reducing NO_X emissions. It is designed to reduce the methane slip on low pressure dual fuel engines while focusing on keeping the capital expenses low. It is fully Tier III compliant when running on dual fuel mode as well as on conventional fuel oils with the help of EGR. Finally, it is capable of producing 16980 kW at 78 rpm at its specified maximum continuous rating (SMCR).

The mindset behind this choice is that the SCBC is not yet a widely available technology. In fact, it will probably take a couple of years to become comercially ready. Pairing it to marine engines used on older ships, although beneficial in terms of increasing the ship's energy efficiency, does not make any sense, as those ships will probably have already been scrapped by the time SCBC systems come to market. On the other hand, alternative fuels are a hot topic in the maritime industry. Liquified natural gas is considered an alternative fuel and is being used by all modern LNG carriers. Despite not being the fuel that will achieve IMO's 2050 goals for decarbonization, LNG carriers are currently being built in large quantities to serve the global demand for LNG. Having this in mind, it is expected that in a couple of years, LNG carriers, despite currently being the most advanced ships, might no longer meet the IMO's rules for energy efficiency, thus, retrofitting new systems may become a necessity. Those systems may be some kind of exhaust gas treatment device, similar to the scrubbers outfitted in some older vessels. Using a waste heat recovery system is also an option, due to the fact that part of the electricity used onboard ships could be produced by such a system with no further fuel consumption, resulting in an improvement of the ship's overall operational efficiency.

5.4. System Design and Full Load Performance Modelling

In a waste heat recovery system, the heat input rate of the cycle is determined by the main engine's exhaust gas temperature and mass flow rate. In our case, MAN's Computerised Engine Application System (CEAS) was used to acquire the necessary data for the main engine's exhaust gas at various load conditions. The engine will be operated in Tier III mode with the use of fuel oil (MDO or MGO) in ISO ambient conditions (ambient air: 25°C, scavenge air coolant: 25°C). The main engine's exhaust gas particulars at various loading conditions are summarised in the table below.

Load [% SMCR]	Power [kW]	SFOC [g/kWh]	Exhaust Gas Amount [kg/s]	Exhaust Gas Temperature [^{o}C]
100	16980	179	23.4	270
95	16131	176.1	23	243
90	15282	174	22.6	219
85	14433	172.5	21.8	215
80	13584	171.5	20.9	213
75	12735	171.1	20	212
70	11886	171	18.8	213
65	11037	171	17.7	215
60	10188	171.2	16.4	218
55	9339	171.5	15.1	223
50	8490	172	13.8	229
45	7641	172.6	12.3	238
40	6792	173.4	10.8	249
35	5943	174.4	9.1	284
30	5094	175.6	7.5	322
25	4245	177	6.2	337

Table 5.1: MAN B&W 6G70ME-C10.5-GA-EGRBP Exhaust Gas Particulars on ISO Ambient Conditions. Via: MAN CEAS.

According to the MEPC.281(70) Resolution, the lower calorific value of fuel oil is $LCV = 42700\ \frac{kJ}{kg}$. This value is also confirmed by the engine manufacturer's documents. Finally, the exhaust gas specific heat capacity has to be determined. The specific heat capacity heavily depends on the parameters of the combustion process, the engine type, the load condition, the fuel used, the temperature of the exhaust gas, the ambient conditions etc. Ideally, it should be calculated using the exact composition and temperature of the exhaust gas. Since the engine manufacturer does not provide a specific value, an average value equal to $C_P = 1.15\ \frac{kJ}{kgK}$ will be used, which is within the range of exhaust gas heat capacity for internal combustion engines.

Before we design our model, it is important to understand what exactly our objective is. A waste heat recovery device utilizes the exhaust gas of an engine to produce power. The heat input for such a device comes exclusively from the main engine's exhaust gas, thus no further fuel is consumed. The ultimate design goal for those devices is to improve the overall efficiency of the main engine in combination with the waste heat recovery device as a combined system. This is achieved by designing a bottoming cycle that produces the maximum possible power. In this way, the exact same amount of fuel is utilized by the main engine in order to produce the maximum possible power. Cycle efficiency is of no particular interest when designing a WHR device, as it is possible to design a more efficient yet less productive device that contributes less to the overall efficiency of the system

compared to a device that produces more power with less efficiency. The bottoming cycle's efficiency is only useful when comparing two waste heat recovery devices of similar power output. During this thesis, the performance of the SCBC for different pressure ratios will be studied and its contribution to the system's efficiency in various main engine load conditions will be calculated. In the second section of this chapter, the expressions for every thermodynamic state of the recuperated Brayton cycle were presented. During the same section we mentioned that the minimum pressure and temperature of the cycle are known in advance. Thus, for every compression ratio, only the heat input rate, the working fluid mass flow rate and the recuperated heat rate remain to be calculated.

Now that we have set our objective and determined the characteristics of the heat source, it is time to move on to the code that will be used in our model. The expressions presented in *Chapter 5.2* were programed in MATLAB and the COOLPROP library was used to calculate the fluid's thermodynamic properties. In the beginning of this chapter we chose the recuperated Brayton cycle as our configuration, as it is more suitable for waste heat recovery applications. In *Chapter 2.3* we also introduced the concept of the optimal pressure ratio. Above this pressure ratio, thermal recuperation can not be used due to the fact that the temperature at the outlet of the turbine is lower than the temperature at the outlet of the compressor. Despite this concept being valid for ideal gasses, meaning that it is not directly applicable in our case, we expect that it will have some effect on real gases too. If we were to handle carbon dioxide as an ideal gas at a temperature of about 250ºC and high pressure, its adiabatic coefficient would be roughly equal to 1.25 [97]. Using the expression 2.34 for a temperature ratio $t = 1.70$, the optimal pressure ratio is calculated at $r_{opt} = 3.77$. With the use of a simple Brayton cycle model at the above temperature ratio, the temperature difference at the outlet of the turbine and the compressor as a function of the compression ratio was plotted in *Figure 5.2*. As we can see, at a pressure ratio between 3.5 and 4, the temperature difference becomes negative, thus thermal recuperation is no longer possible. This means that in our final model, these temperatures must be compared in advance in order to decide if thermal recuperation is possible.

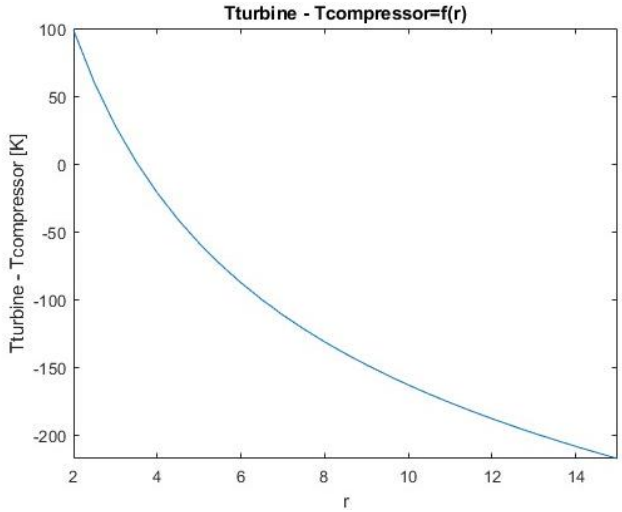

Figure 5.2: Temperature difference at the outlet of the turbine and the compressor as a function of the compression ratio in a SBC.

The next problem that needs to be tackled is the calculation of the cycle's heat input rate. In *Chapter 2.3* we concluded that in order to maximize the specific work output of the cycle, the temperature ratio of the cycle also needs to be maximized. Thus, we are going to assume that the maximum temperature of the cycle is almost equal to the temperature of the engine's exhaust gas. Moreover, a temperature difference between the two streams equal to 10K will be applied in all of the heat exchangers in order to provide enough driving force (temperature difference) for the heat exchange to actually take place. In contrast to subcritical cycles, no phase transition takes place inside our heat exchangers, thus this temperature difference will be applied at the ends of the heat exchanger. In order for the cycle heat input rate to be calculated, the temperature of the exhaust gas at the outlet of the main heater must also be determined. Since our goal is to maximize the cycle's power output, the cycle should be provided with the maximum possible heat. This is achieved when the temperature difference of the exhaust gas at the inlet and outlet of the heater is maximized. The minimum possible temperature of the exhaust gas is 10K above the temperature of the working fluid at the inlet of the heater. Thus, the cycle's heat input rate can now be calculated by the formula $\dot{Q} = \dot{m}_g C_{Pg}(T_{g,in} - T_{g,out})$, where $\dot{m}_g$ is the exhaust gas mass flow rate, C_{Pg} is the exhaust gas specific heat capacity, $T_{g,in}$ is the temperature of the exhaust gas exiting the main engine and $T_{g,out}$ is the temperature of the exhaust gas exiting the heater. Due to the balance of energy inside the heat exchanger, this heat is also equal to the heat absorbed by the working fluid, which can be calculated by the formula $\dot{Q} = \dot{m} \times (h_{t4} - h_{t3})$ where $\dot{m}$ is the working fluid's mass flow rate, h_{t4} is the stagnation enthalpy at the outlet of the heater and h_{t3} is the stagnation enthalpy at the inlet of the heater. Thus, the working fluid mass flow rate for maximum power output can then be calculated. Finally, some limitations for the exhaust gas temperature should be set. This temperature should never drop below a certain point, called the acid dew point. Below this temperature, the sulphur oxides produced during the combustion react with the water present in the exhaust gas to form sulphuric acid. These acids are corrosive and thus they are capable of causing damage to the heat exchangers or any other part of the exhaust gas system they come in contact with. It is a common belief that the dew point limit comes from the condensation of sulphur dioxide. This is not true, as a small part of the sulphur dioxide further oxidizes to sulphur trioxide. Despite the sulphur trioxide being in much lower quantities than sulphur dioxide, it has a condensation temperature of about 120°C-130°C compared to the dioxide's 50°C [98]. Knowing the above limit, some "safety" conditions were integrated into our code to improve its robustness. If the exhaust gas temperature drops below the acid dew point, the code shall return an error. A schematic of the cycle's heater is provided below in order to help the reader understand its main working principles.

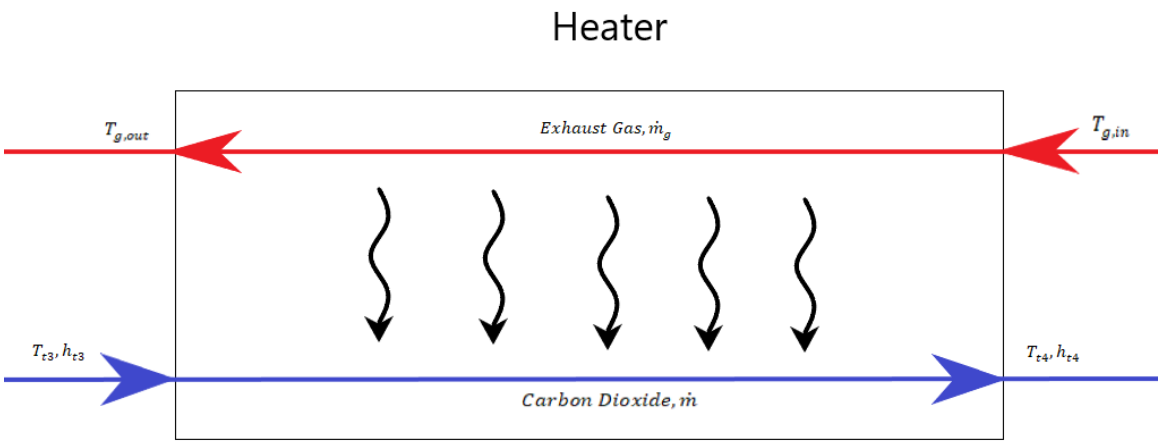

Figure 5.3: A schematic of the cycle's heater.

The final part of the problem is the calculation of the recuperated heat rate when a recuperated cycle is used. The purpose of thermal recuperation is to increase the cycle's efficiency. In a RBC, the specific net work output doesn't increase when compared to a SBC, however, the power output may increase due to an increase in mass flow rate. When we presented our objective, we mentioned that thermal efficiency matters little on bottoming cycles. Thermal recuperation, however, is important to be applied whenever possible due to a larger part of the necessary heat being provided internally. In our case this translates in higher main engine exhaust gas temperatures at the exit of the heater, thus the exhaust gas can be further utilized to provide heat to other systems. A prime example of such a system is a boiler, often called economiser, which is present in most modern ships and utilizes the engine's flue gas to produce steam. For thermal recuperation to be done correctly, the temperature of the CO_2 exiting the compressor must reach the temperature at the outlet of the turbine. Using the ideal gas theory we would expect that the temperature difference at the inlet and the outlet of the warm side of the recuperator would be smaller than that of the cold side due to the larger heat capacity. Once again, the ideal gas theory leads to false conclusions when working on real gasses. Using a simple heat exchanger model, the temperature profiles of the warm and cold streams of the recuperator were plotted in *Figure 5.5*. As we can see, the warm carbon dioxide "loses" temperature at a faster rate than the rate that the cold stream "gains" temperature. This practically means that inside the recuperator, the temperature of the fluid exiting the compressor will never reach the temperature of the fluid exiting the turbine before the exact opposite happens. Thus, the heat exchange is limited by the temperature difference of the two streams at the outlet of the warm side of recuperator. In our model, the recuperated heat rate is calculated by the drop in enthalpy of the warm stream. The temperature at the outlet of the warm side of the recuperator was set 10K above the temperature of the working fluid exiting the compressor. The specific recuperated heat is then calculated by the formula $q_R = |h_{t6} - h_{t5}|$ where h_{t6} is the stagnation enthalpy of the working fluid exiting the warm side of the recuperator and h_{t5} is the stagnation enthalpy of the working fluid exiting the turbine. Then, the stagnation enthalpy at the outlet of the cold side of the recuperator can be

calculated by the formula $h_{t3} = h_{t2} + q_R$, where h_{t2} is the stagnation enthalpy of the working fluid at the compressor's outlet. In a similar way to the heater, "safety" conditions were integrated into our code for extra robustness in order to ensure that the heat exchange will actually take place. If the temperature difference of the two streams at the inlet or the outlet of the recuperator is lower than 10K, our code shall return an error.

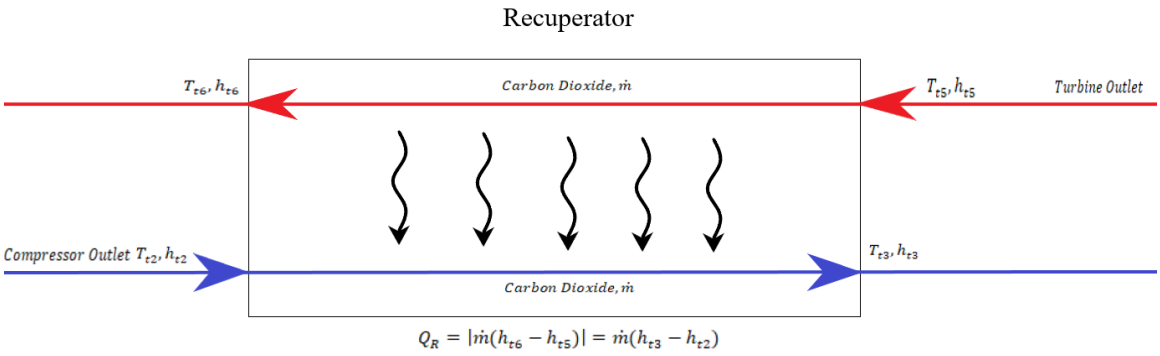

Figure 5.4: A schematic of the recuperator

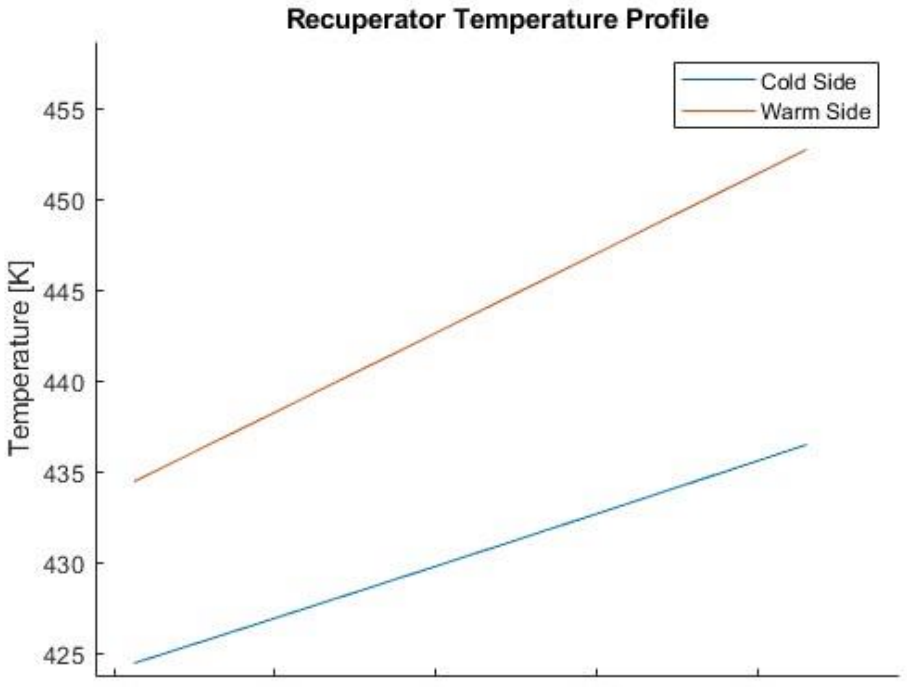

Figure 5.5: Temperature profile in the recuperator. Note that the recuperator is a counter- flow heat exchanger.

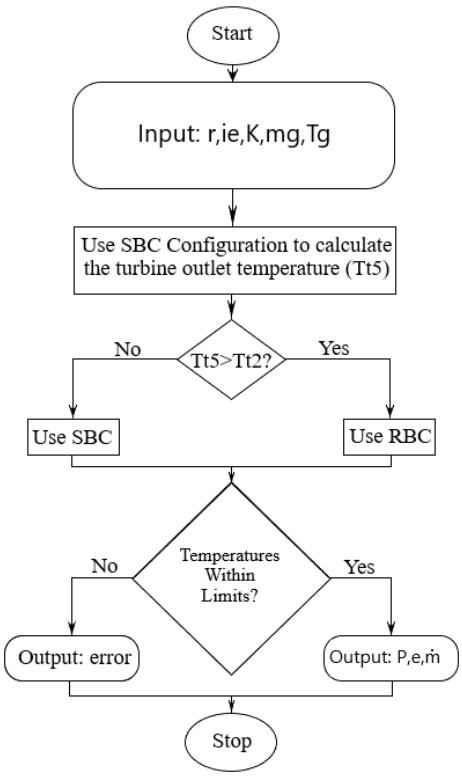

Figure 5.6: Flowchart Diagram of the Code

Model Input		
Symbol	**Description**	**Unit**
r	Pressure Ratio	-
ie	Turbomachinery Isentropic Efficiency	-
K	Heat Exchanger Pressure Loss Factor	-
mg	Exhaust Gas Mass Flow Rate	kg/s
Tg,in	Exhaust Gas Temperature	^{o}C
Cycle Characteristics		
Parameter	**Value**	**Unit**
Minimum Pressure	7477300	Pa
Minimum Temperature	314.1282	K
Maximum Temperature	Tg,in-10	K
Configuration	Dependent on the Pressure Ratio and Load	-
Model Output		
Symbol	**Description**	**Unit**
e	Thermal Efficiency	-
m	Working Fluid Mass Flow Rate	kg/s
P	Power Output	kW

Table 5.2: A summary of the cycle characteristics, model input and output

Summarizing the above methodology, our model can be broken down into 11 discrete steps:

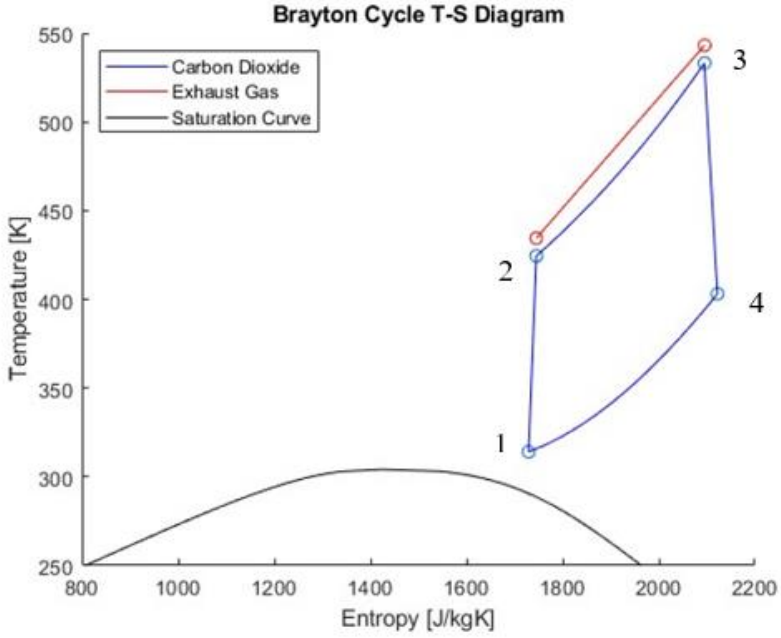

Figure 5.7: Simple Brayton Cycle T-s Diagram.

Step 1: Given T_{t1}, P_{t1}, the pressure ratio r and the compressor's isentropic efficiency ie_C, T_{t2} and P_{t2} can be calculated.

Step 2: First, for a simple Brayton cycle, we are going to assume that $T_{g,out} = T_{t2} + 10\ [K]$ and $T_{t3} = T_{g,in} - 10\ [K]$. Also, P_{t3} can be calculated given the heater's pressure loss factor K_H.

Step 3: Given the cooler's pressure loss factor K_C and the turbine's isentropic efficiency ie_T, T_{t4} and P_{t4} can be calculated. Thermal recuperation is only possible if $T_{t4} > T_{t2}$. For a simple Brayton cycle, steps 4 to 7 may be skipped.

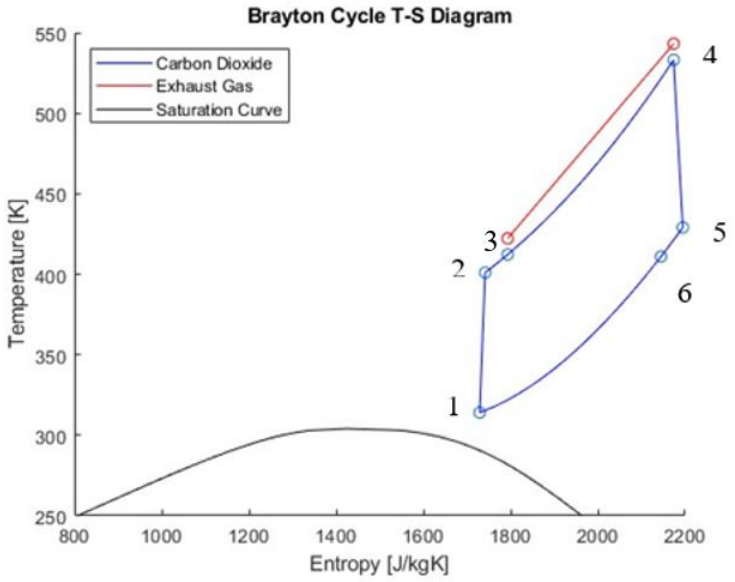

Figure 5.8: Recuperated Brayton Cycle T-s Diagram.

Step 4: For the recuperated cycle, T_{t2} and P_{t2} are calculated in the same way as a simple Brayton Cycle. Furthermore we are going to assume that $T_{t4} = T_{g,in} - 10\ [K]$ and we are going to calculate $P_{t4} = P_{t2} \times (1 - K_R) \times (1 - K_H)$. For now, T_{t3} remains unknown.

Step 5: Knowing the pressure loss factors of the cooler K_C and the recuperator K_R as well as the isentropic efficiency of the turbine ie_T, P_{t5} and T_{t5} can be calculated.

Step 6: We are going to assume that $T_{t6} = T_{t2} + 10\ [K]$. The pressure is then calculated $P_{t6} = \frac{P_{t1}}{(1-K_R)\times(1-K_C)}$ and the specific recuperated heat can be calculated too by the formula $q_R = |h_{t6} - h_{t5}|$.

Step 7: The enthalpy at the inlet of the heater is calculated by the formula $h_{t3} = h_{t2} + q_R$. The corresponding temperature can then be calculated as a function of the pressure $P_{t3} = P_{t2} \times (1 - K_R)$ and the enthalpy h_{t3}. We are also going to assume that the temperature of the exhaust gas at the outlet of the heater is $T_{g,out} = T_{t3} + 10\ [K]$.

Step 8: The turbine's specific work output w_{out} can be calculated as the difference in enthalpy at the inlet and the outlet of the turbine. The compressor's specific

work input w_{in} can be calculated as the difference in enthalpy at the outlet and the inlet of the compressor.

Step 9: The specific heat input q_{in} of the cycle can be calculated as the difference in enthalpy at the outlet and the inlet of the heater. Given that the heat input rate of the cycle is $\dot{Q} = \dot{m}_g C_{Pg}\left(T_{g,in} - T_{g,out}\right) = \dot{m} \times q_{in}$, the working fluid's mass flow rate can also be calculated.

Step 10: Knowing the carbon dioxide's mass flow rate, the power output of the cycle is calculated $P = \dot{m} \times (w_{out} - w_{in})$. The thermal efficiency $\eta = \frac{P}{\dot{Q}}$ can also be calculated.

Step 11: The temperature differences at the inlets and the outlets of the heat exchangers are calculated. If the differences are below 10 K, an error wil be printed in MATLAB's command window. The same will also happen in case the temperature of the exhaust gas drops below the acid dew point.

5.4.1. Exploring an Alternative Approach

During the development of our model, many different approaches had to be considered and compared with each other. By far one of the most interesting ones was the one regarding the complete utilization of the engine's exhaust gas. During this approach, referred to as scenario 2 hereafter, a simple configuration was used and the temperature of the exhaust gas at the outlet of the heater was set at the acid dew point (130°C) while the cycle's maximum temperature was still held 10K below the engine's exhaust gas. The main difference between scenario 2 and our final approach described in the previous section and referred to as scenario 1 hereafter, is that the majority of the heat required by the cycle is provided by the flue gas, whereas in scenario 1 a large part of the heat is provided internally by thermal recuperation. Having said that, we expect that in scenario 2, the cycle's efficiency will be lower due to the larger amount of heat wasted in the cooler. However, the goal for a WHR system is to maximize the power output. The two scenarios have the same maximum temperature. The maximum temperature is the sole factor that dictates the specific work output of a Brayton cycle according to the ideal gas theory, thus we expect that the two scenarios will have similar specific net work output. Power, however, is a function of the specific net work output and working fluid mass flow rate. It is unclear how the mass flow rate compares between the two scenarios due to the fact that enthalpy is not a linear function of temperature. The two scenarios had to be compared in order to draw a safe conclusion.

In *Figure 5.9* the net power output of the SCBC as a function of the pressure ratio is displayed for both scenarios. As we can see, the first scenario produces more power than the second one. *Figure 5.10* presents the SCBC thermal efficiency as a function of the pressure ratio for both scenarios. We can see that the second scenario showcases lower

thermal efficiency, due to the fact that a large part of the required heat is no longer provided internally via recuperation.

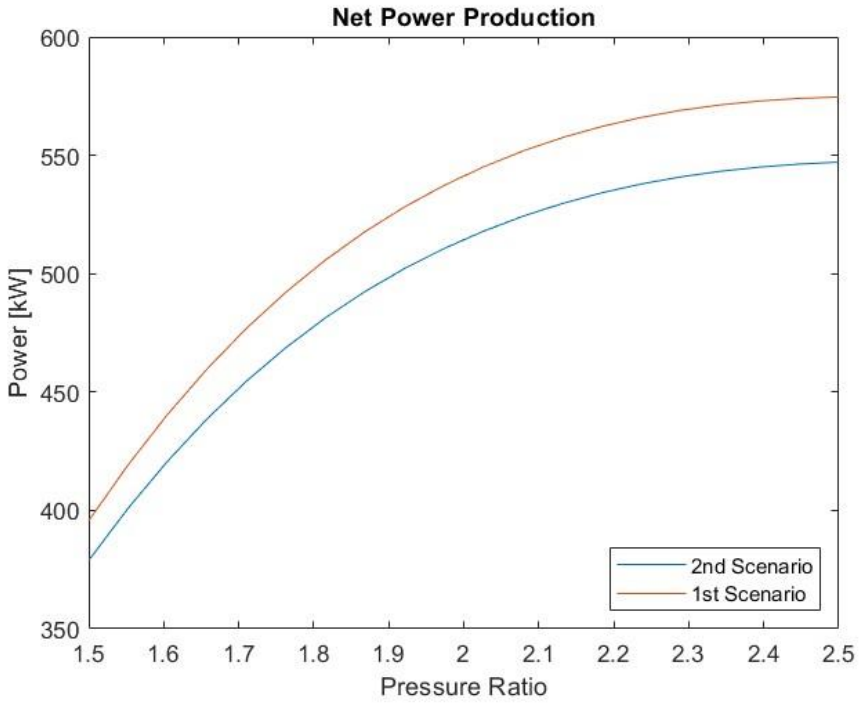

Figure 5.9: Net Power Production as a Function of the Pressure Ratio

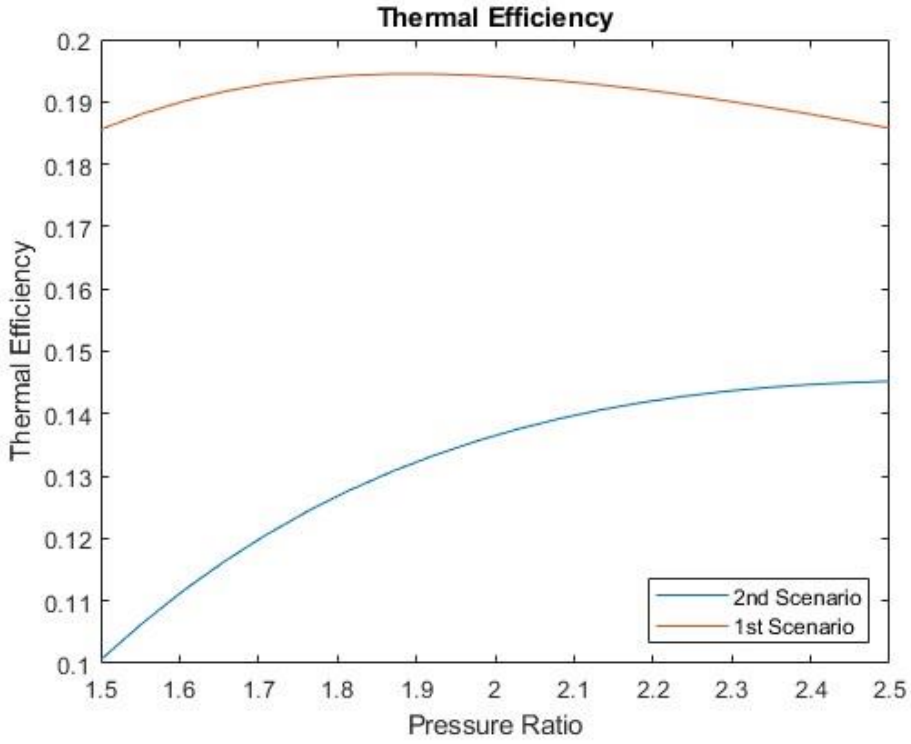

Figure 5.10: Thermal Efficiency as a Function of the Pressure Ratio

Figure 5.11 presents the specific net work output against the pressure ratio for both scenarios whereas in *Figure 5.12* the carbon dioxide's mass flow rate is displayed as a function of the pressure ratio for both scenarios as well. Since the specific net work output is the same for both scenarios, the increase in power is exclusively the result of an increase in mass flow rate, meaning that the heat input is utilized more "efficiently" in the first scenario. This is a direct consequence of the non linear relationship between the temperature and enthalpy of real gasses. To further backup our theory, the temperature-enthalpy diagram of carbon dioxide at 18.7 MPa was plotted and examined in *Figure 5.13*. Keeping in mind that in our model, the temperature change of the working fluid is equal to $\Delta T = T_4 - T_3 = T_{g,in} - 10 - T_{g,out} + 10 = T_{g,in} - T_{g,out}$, two different cases will be studied. In the first case, the temperature of the working fluid is raised from $T_3 = 403.15\ K$ to $T_4 = 533.15\ K$. The enthalpy difference between states 3 and 4 is equal to $\Delta H = 184848 \frac{J}{kg}$ and the required heat is $Q = m_g \times C_p \times \Delta T_g = 130 \times m_g \times C_p$. In the second case, the temperature of the working fluid is raised from $T_3 = 468.15\ K$ to $T_4 = 533.15\ K$. The enthalpy difference between 3 and 4 is equal to $\Delta H = 84979 \frac{J}{kg}$ and the required heat is $Q = m_g \times C_p \times \Delta T_g = 65 \times m_g \times C_p$. As we can see, the temperature difference and thus the heat input are cut in half in the second case, however the enthalpy difference is not. Knowing that the working fluid's mass flow rate is calculated by the formula $\dot{m} = \frac{\dot{Q}}{\Delta H}$, it can be seen that the second case allows for a larger mass flow rate. These two cases are representative of our two scenarios. In the 1st scenario, the heat input process occurs in higher temperatures than the 2nd one, thus a larger carbon dioxide mass flow rate is allowed. In conclusion, the first scenario showcases better performance than the second one in every aspect, mainly due to the non linear relationship between the cycle's mass flow rate and temperature ratio.

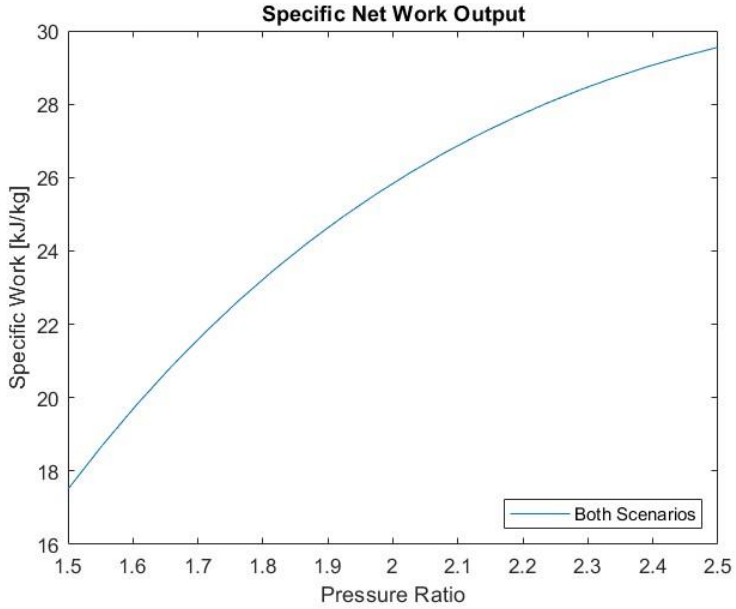

Figure 5.11: Specific Net Work Output as a Function of the pressure ratio.

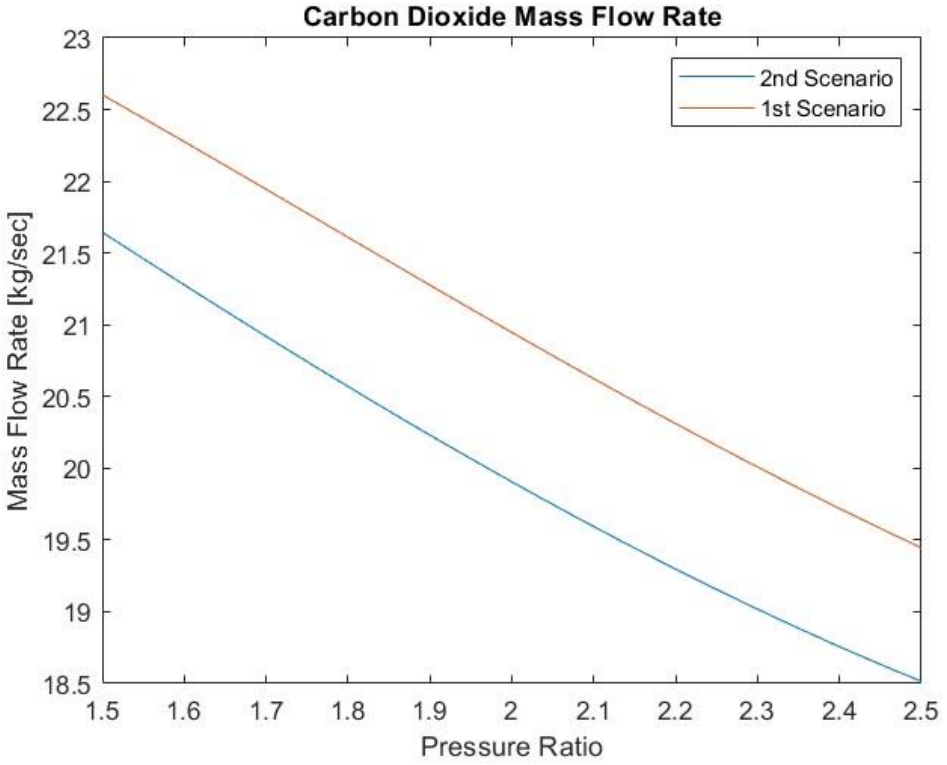

Figure 5.12: Carbon Dioxide Mass Flow Rate as a Function of the Pressure Ratio

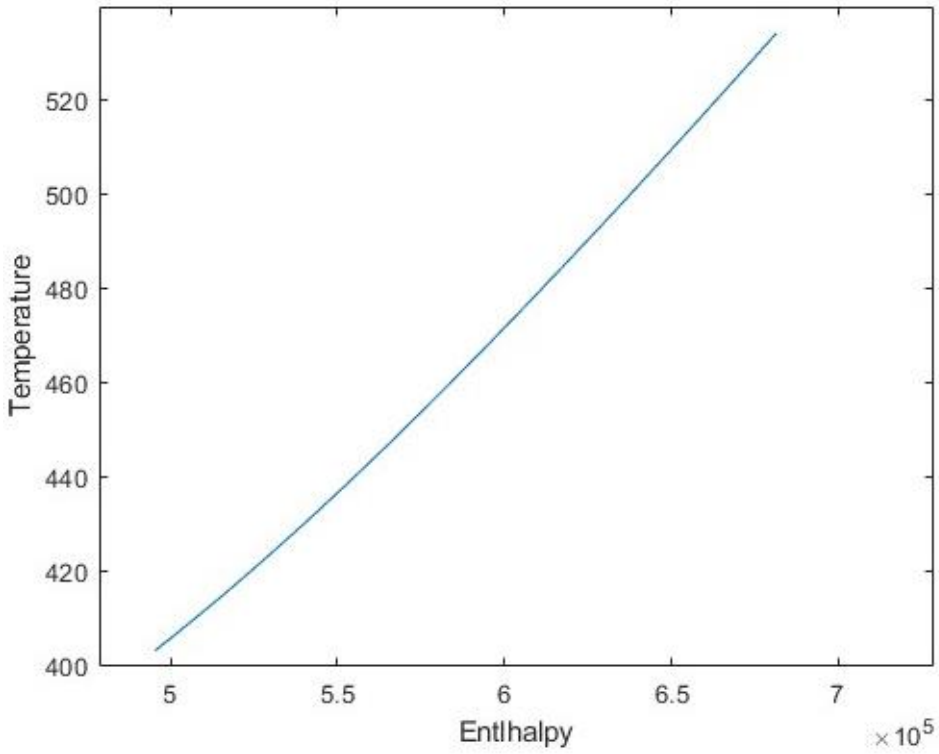

Figure 5.13: Temperature- Enthalpy Diagram of Carbon Dioxide at 18.7 MPa

5.4.2. Results

With the use of our model, the performance of the SCBC as a standalone WHR system as well as a system combined with the main engine, was evaluated at the engine's SMCR. First, the power output, thermal efficiency and CO_2 mass flow rate of the cycle were calculated for various pressure ratios. Furthermore, the performance of the recuperated configuration was compared to a simple configuration to further confirm our initial speculation that a recuperated Brayton cycle is a more suitable configuration for WHR. For our simulations, the following assumptions were made based on an existing review of the constrains and assumptions for the steady state modeling of sCO_2 systems [99]:

- The isentropic efficiency was assumed 0.85 for the compressor and 0.9 for the turbine.
- Pressure loss factor was assumed 1% for all heat exchangers, including the heater.
- Pressure losses inside the ducts were considered negligible.
- Pressure losses of the main engine's exhaust gas inside the heater were considered negligible and the performance of the main engine was not affected in any way by the use of the WHR system.

As we can see in the figures below, at the main engine's SMCR, the recuperated cycle can be operated for pressure ratios up to 3.35. In *Figure 5.14*, the net power output of the SCBC as a function of the cycle's pressure ratio is presented for both the recuperated and simple layout. As we can see, both configurations have a similar power output, with the recuperated cycle producing slightly more power for pressure ratios lower than 2.75 and the simple configuration surpassing the recuperated in terms of power production in higher pressure ratios. If we were to assume that no pressure losses occur inside the recuperator, the recuperated configuration would produce more power for every pressure ratio as a result of the heat input phenomenon explained in the previous section.

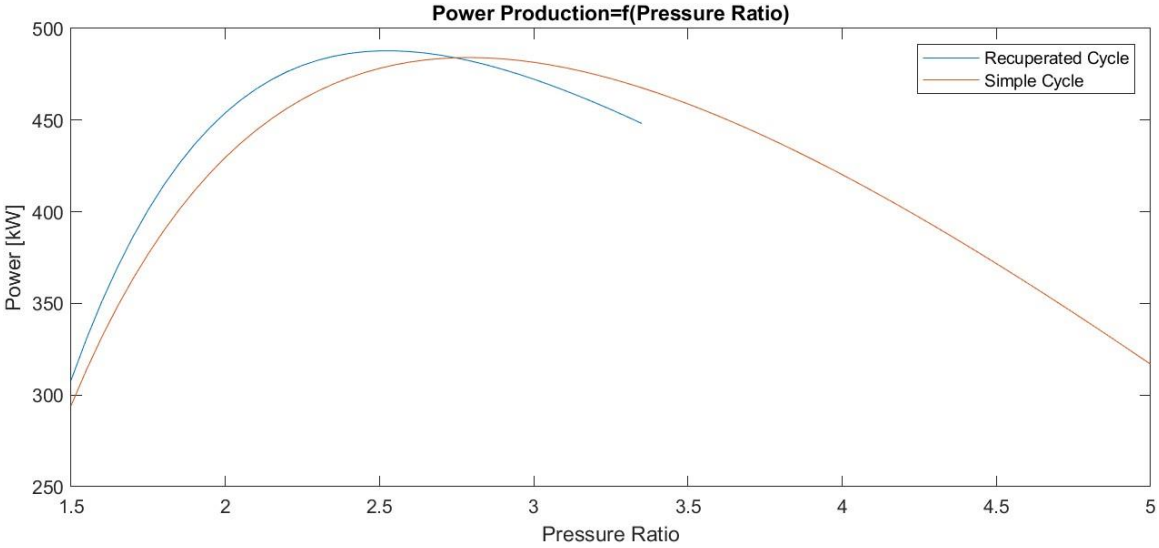

Figure 5.14: Net Power Production of the Recuperated and Simple Configurations as a Function of the Pressure Ratio.

Figure 5.15 presents the SCBC thermal efficiency as a function of the pressure ratio. As we can see, the thermal efficiency is higher for the recuperated cycle with the simple configuration surpassing it only for pressure ratios higher than 3.24 as a result of the pressure losses inside the recuperator. A higher thermal efficiency was indeed expected for the recuperated configuration due to the fact that a large part of the required heat is provided internally. It is also noteworthy that the cycle's thermal efficiency does not necessarily increase with the increase of the pressure ratio as explained in *Chapter 2.3*. This is due to the irreversibilities of the cycle making it to no longer adhere to the ideal gas laws.

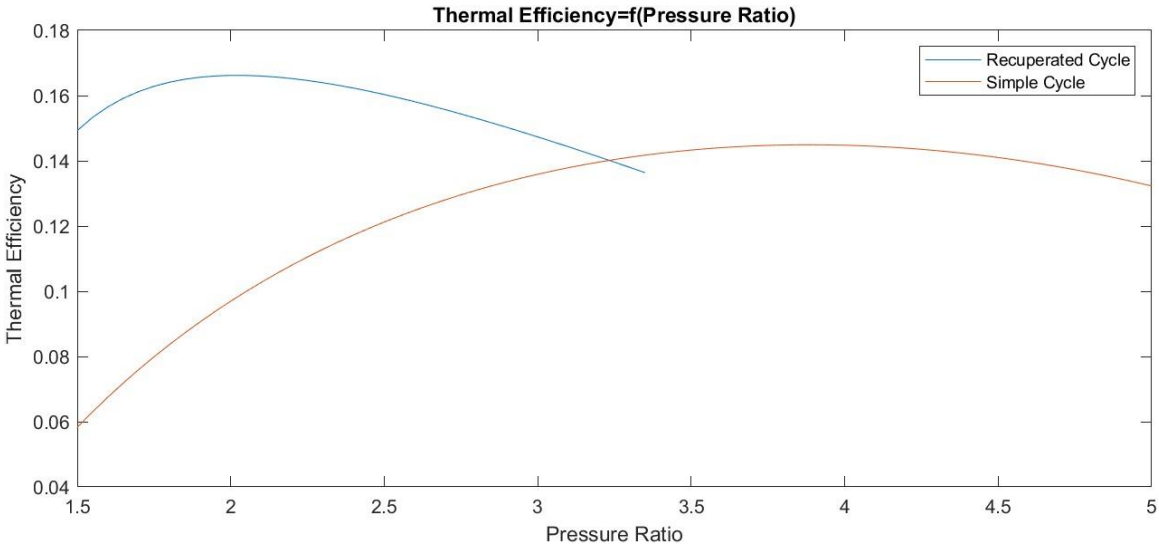

Figure 5.15: Thermal Efficiency of the Recuperated and Simple Configurations as a Function of the Pressure Ratio.

In *Figure 5.16*, the carbon dioxide mass flow rate as a function of the pressure ratio is displayed. As we can see, the recuperated cycle allows for a larger working fluid mass flow rate resulting in a higher power output. If we were to assume that no pressure losses occur inside the recuperator, we would find out that the specific net work output is exactly the same for both configurations.

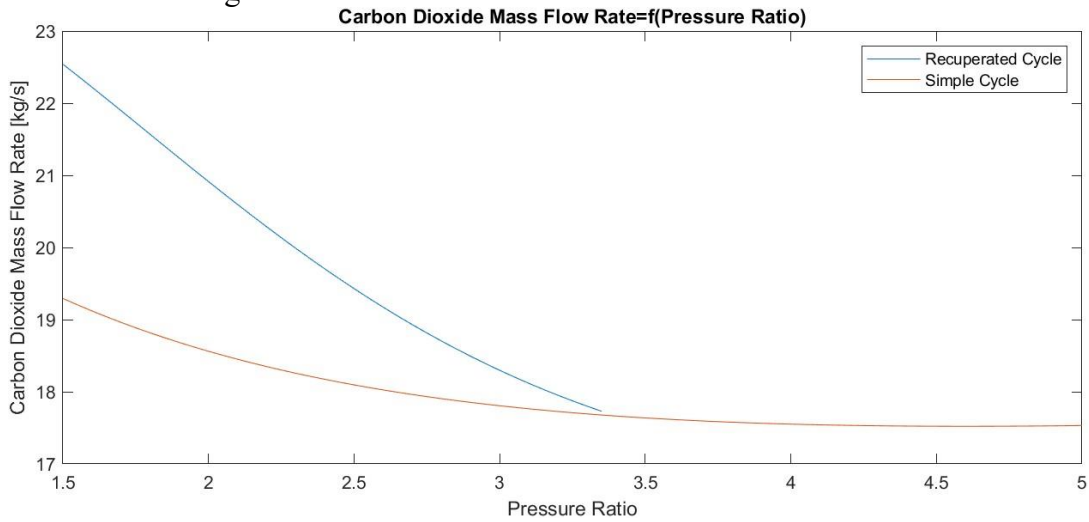

Figure 5.16: Carbon Dioxide Mass Flow Rate of the Recuperated and Simple Configurations as a Function of the Pressure Ratio.

Finally, in *Figure 5.17* the main engine's exhaust gas temperature at the outlet of the heater is displayed for both configurations. Due to its higher thermal efficiency and thus lower waste heat usage, the recuparated cycle has a higher exhaust gas temperature at the outlet of the heater for every pressure ratio that it is applicable for. This means that the exhaust gas can be further utilized for other purposes like generating steam. Another important thing to note, is that the simple configuration cannot be operated with the limitations and assumptions of our model for pressure ratios lower than 2.71, due to the fact that the exhaust gas temperature drops below 130^{o}C, which is the exhaust gas acid dew point. It is important to note that our model was created having the maximum possible power production in mind, thus the simple configuration could theoretically be used below the aforementioned pressure ratio by limiting the heat input and producing less power as a result.

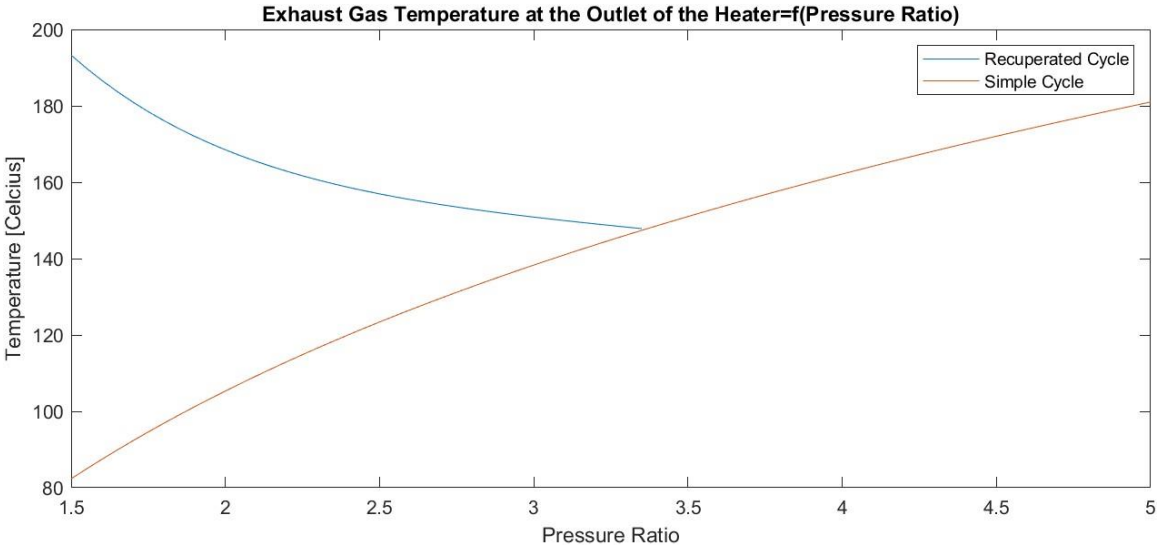

Figure 5.17: Exhaust Gas Temperature at the Outlet of the Heater of the Recuperated and Simple Configurations as a Function of the Pressure Ratio.

Summarizing the obove, the optimal operating point of the system has to be determined. Our goal in a waste heat recovery system is to maximize the power output. This occurs in the recuperated cycle for a pressure ratio equal to 2.55. The characteristics of the main engine, supercritical Brayton cycle, as well as the combined system for the above pressure ratio are summarized in *Table 5.3*. A temperature- entropy diagram of the SCBC at the optimal pressure ratio is also displayed in *Figure 5.18*.

Supercritical CO_2 Brayton Cycle		Main Engine	
Configuration	Recuperated	Load	100 [%]
Pressure Ratio	2.550	Power Output	16980 [kW]
Minimum Pressure	7.577 [MPa]	SFOC	179 [g/kWh]
Maximum Pressure	19.322 [MPa]	Exhaust Gas Amount	23.4 [kg/sec]
Minimum Temperature	40.98 [Celcius]	Exhaust Gas Temperature	270 [Celcius]
Maximum Temperature	260 [Celcius]	Thermal Efficiency	0.47
Power Output	487.78 [kW]	**Combined System**	
Thermal Efficiency	0.159	**Power Output**	**17467.78 [kW]**
Working Fluid Mass Flow Rate	19.299 [kg/sec]	**Thermal Efficiency**	**0.485**
Heat Input Rate	3063.1 [kW]	**SFOC**	**174.002 [g/kWh]**
Heat Recuperation Rate	1115.03 [kW]	**Exhaust Gas Temperature**	**156.172 [Celcius]**
Cooling Rate	2575.32 [kW]	**Efficiency Increase Percentage**	**2.873 [%]**
Heater Effectiveness	0.919	**Power Increase Percentage**	**2.873 [%]**
Recuperator Effectiveness	0.832	**SFOC Reduction Percentage**	**2.792 [%]**

Table 5.3: WHR System Particulars (Left); Main Engine Particulars (Upper Right); Combined System Performance (Lower Right).

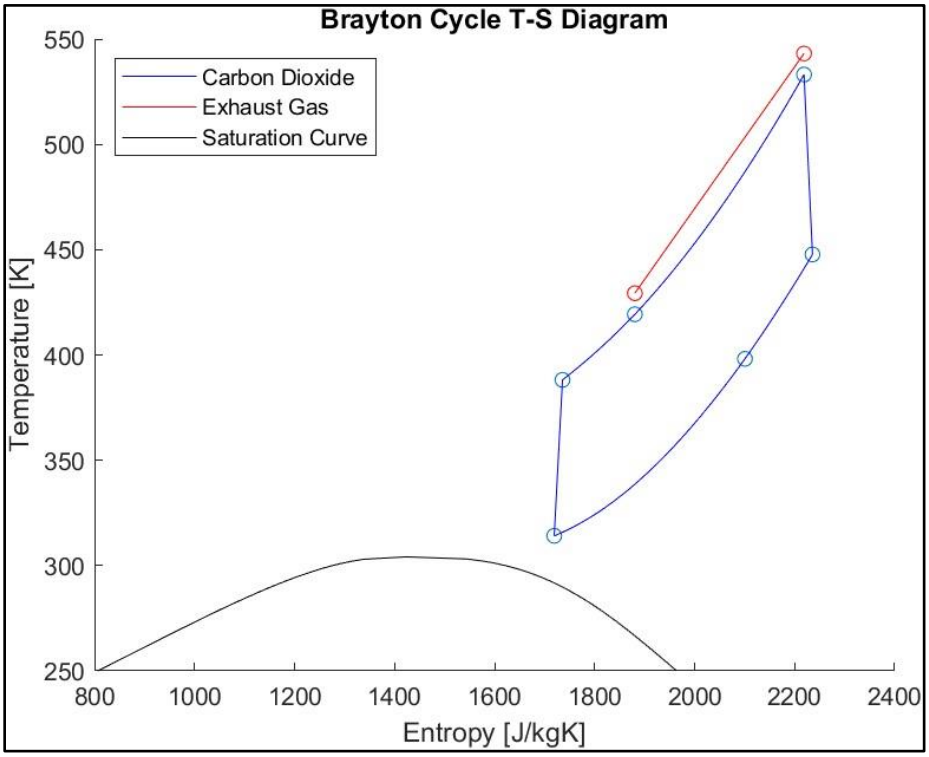

Figure 5.18: T-S Diagram of the SCBC at the Optimal Pressure Ratio

Some of the values in *Table 5.3* were not provided by the engine's manufacturer and were calculated by methods not explained in the previous chapters, thus the mathematical expressions used will be introduced below.

For the main engine, given the engine's specific fuel oil consumption ($SFOC_{ME}$ in $\frac{g}{kWh}$), power (PWR_{ME} in kW) and the fuel's lower calorific value (LCV in $\frac{kJ}{kg}$), the thermal efficiency (η_{ME}) can be calculated by the following equation:

$$\eta_{ME} = \frac{PWR_{ME}}{\dot{Q}_{in,ME}} = \frac{3600000 \times PWR_{ME}}{LCV \times SFOC_{ME} \times PWR_{ME}} = \frac{3600000}{LCV \times SFOC_{ME}} \quad (5.33),$$

where $\dot{Q}_{in,ME}$ is the heat input rate of the main engine.

For the combined system:

- The total power output of the system is calculated by the following equation:
$$PWR_{CC} = PWR_{ME} + PWR_{WHR} \quad (5.34),$$
where PWR_{CC} is the power output of the combined cycle and PWR_{WHR} is the power output of the WHR system.
- The thermal efficiency of the combined cycle (η_{cc}) was calculated using the following equation:
$$\eta_{CC} = \frac{PWR_{CC}}{\dot{Q}_{in,ME}} = \frac{3600000 \times PWR_{CC}}{LCV_{ME} \times SFOC_{ME} \times PWR_{ME}} \quad (5.35)$$
- The specific fuel oil consumption for the combined cycle ($SFOC_{CC}$ in $\frac{g}{kWh}$) is calculated by the following equation:
$$SFOC_{CC} = \frac{3600000}{\eta_{CC} \times LCV} \quad (5.36)$$

As we can see from the results of our simulation, the SCBC shows excellent performance as a waste heat recovery system at a relatively low pressure ratio. Compared to a recompression model developed by Xie and Yang [79] for use with a smaller marine Diesel engine, both models have about the same efficiency, at similar pressure ratios, which further confirms that in order to achieve the maximum theoretical efficiency of the recompression cycle, a higher level heat source is required. Furthermore, Xie and Yang [79] suggest that the system's performance can be further improved with exhaust gas modulation.

A big advantage of the SCBC as a WHR system is that besides its small footprint, it can be cooled by readily available coolants like water or even air in some cases, due to the fact that the cycle's minimum temperature is always above the carbon dioxide's critical temperature. In our case, the minimum temperature is 41°C which means that our system can be easily cooled by the sea water.

Finally, it is worth noting how such a WHR system could actually reduce the ship's total energy efficiency. The main engine's exhaust gas at the outlet of the WHR system is 156°C. This means that there is only a narrow margin of 26°C before the exhaust gas starts entering the acid dew point region. Therefore, it would be difficult to find an application further utilizing the exhaust gas. Most modern ships, however, already use WHR systems in the form of boilers called economisers. Using a SCBC as a waste heat recovery method means than an economiser can no longer be used, at least according to our own model. Thus, a

more detailed study and comparison between those systems shall be conducted in order to determine which one is more beneficial in terms of ship energy efficiency.

5.5. Partial Loads Performance Modelling

Studying a system's performance at partial loads is of great importance, especially when used for heat recovery on engines that they themselves are oftenly operated at partial loads. A vessel's main engine is a prime example of an engine that is constantly required to be operated at variable loads due to port calls, course and speed adjustments, manouvers, different sea conditions etc. When an engine is operated at partial loads, its exhaust gases have a lower mass flow rate and sometimes lower temperature. This means that the thermal input for the bottoming cycle, which is directly dependant on the thermal energy of the exhaust gases, is lower at partial loads. Studies on partial load performance are a relatively new topic in the SCBC field. Many methods have been developed over the last few years, with most of them requiring a detailed design of the cycle's components. Sandia National Laboratories conducted a detailed study [80] on a sCO_2 compressor based on exprerimental data in 2010. This study provided important insight on the behaviour of the compressor and can be used to predict its performance at partial loads, as long as some of its geometric and operational characteristics have been determined. Dyreby et al [100] predicted the heat exchangers' part load performance by scaling their conductance and pressure losses with mass flow rate. Once again, this method requires some degree of detail in the design of the cycle's heat exchangers, thus it cannot be used with our current model due to the fact that a simpler thermodynamic approach was chosen. Therefore, we are going to study the partial load performance using a similar approach to the one used in the previous chapter.

Operating and control strategies are significantly more complex in closed loop gas turbines than in open loop ones. In an open loop gas turbine, the cycle's maximum temperature can be easily controlled by regulating the amount of fuel burnt in the combustion chamber. In closed loop systems, the turbine inlet temperature is limited by the capabilities of the heat source as well as the heat exchanger itself. For example, in a concentrated solar power plant, the heat input of the cycle depends on the weather conditions and cannot be regulated on demand. The same holds true in heat recovery applications. The heat input of the cycle can be somewhat regulated by decreasing the amount of exhaust gas that enters the heater, thus decreasing the thermal input. Increasing the thermal input however is not possible as it is limited by the main engine's load. Another big difference in the control stategy of gas turbines is the adjustment of the compressor's operating point. In most open loop gas turbines, the use of variable inlet guide vanes allows for the working fluid's mass flow rate to be regulated. This is simply not an option in closed loop systems where the fluid's mass is enclosed within the loop and remains constant. The power output and rotational speed of closed loop cycles can be controlled with two different methods, namely compressor back flow control and the use of an accumulator [101]. With the first method, a portion of the CO_2's mass flow exiting the compressor returns to the cooler via a valve, completely

bypassing the turbine. This way, the pressure in front of the turbine falls while the cycle's minimum pressure increases resulting in a reduced turbine output. The working fluid's mass flow inside the loop remains constant during this process. The CO_2's inventory can be regulated with the use of an accumulator. In full load, most of the gas flows inside the system while in partial loads a portion of it stays inside the accumulator. The cycle's pressure and power output behave proportionally to the gas density in the cycle [101]. The bypass method offers the ability of rapid unloading of the shaft, thus it is ideal for use in systems hooked to electrical generators.

Before we explain our methodology, it is important to understand our problem in terms of its variables and constraints. A heat recovery system like this in a vessel is going to be used for electrical power generation. For a generator to produce electricity, its shaft must rotate at a constant speed. In our system, the shaft speed is determined by the compressor's rotational speed, thus the cycle's pressure ratio and mass flow rate have a direct effect on the generator's speed. These two variables also have an important impact on the cycle's performance and can be optimized depending on the load scenario. Changing either one of these variables, however, is going to require a change in the other one too, in order to maintain constant shaft speed. Having in mind the available control strategies explained in the previous chapter, we can assume that implementation of such complex systems will have a negative impact on the capital and operating expenses of a heat recovery system that accounts for less than 3% of the system's efficiency. Therefore, after careful consideration of all the available control strategies and system limitations, we have decided that keeping both the pressure ratio and CO_2 mass flow rate constant in partial loads is our best option in the current stage of this study. The implementation of more complex control strategies would require a detailed technoeconomic study, due to the complexity of a ship's operation (i.e., time spent in ports, changes in main engine's load etc.), that is outside the current thesis' boundaries.

As explained in the previous section, many models for SCBC partial load performance have been developed over the last few years. Most of these models require a detailed design of the system's components, something that was not done in our model. Therefore, a thermodynamic approach like that of the previous section will be used to simulate our cycle at partial loads. A detailed description of our model will be given in the following paragraphs.

Contrary to the previous sections, we have now fully designed our system, thus the working fluid's mass flow rate and cycle's pressure ratio are already known and will be kept constant. This is something possible to achieve as the working fluid does not incur any phase transition inside the loop, therefore its mass flow rate does not depend on the cycle's heat input, something that is true for Rankine cycles. Knowing the CO_2's mass flow rate and pressure at the exit of the compressor, only the cycle's maximum temperature remains to be determined. Because a recuperator is present in our loop and that its use depends on the turbine outlet temperature, which is not known in advance, assumptions on the cycle's maximum temperature must be made. If a very high temperature is assumed, the main

engine's exhaust gas temperature at the outlet of the heater will be lower than the carbon dioxide's temperature at the inlet of the heater due to the balance of energy. Therefore, the two streams inside the heater will be considered incompatible and a lower temperature will be assumed. The temperatures at the recuperator's ends are calculated in the exact same way as in the full load scenario. While the cycle's maximum temperature gets progressively lower, a point where recuperation can no longer be used will eventually be reached. At this point, the recuperator must be bypassed, and our methodology must change. When recuperation is not used, there is no longer a need to assume the cycle's maximum temperature. The main engine's exhaust gas temperature at the outlet of the heater will be set at the dew point limit and the cycle's maximum temperature will be calculated via the balance of energy in the heater.

Summarizing the above, a step-by-step description of our methodology based on the below T-s diagrams will be given:

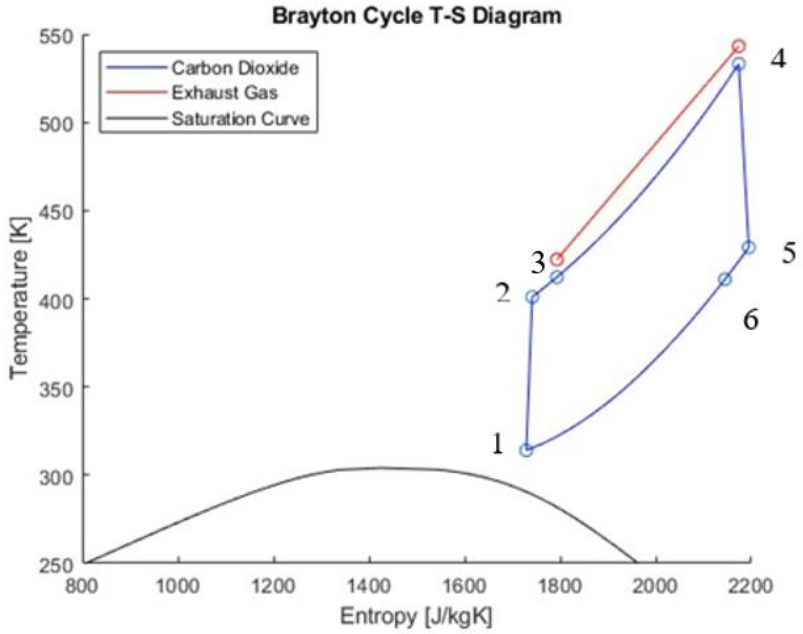

Figure 5.19: Recuperated Brayton Cycle T-s Diagram

Step 1: Given the cycle's pressure ratio and the compressor's isentropic efficiency, the working fluid's temperature (T_2) and pressure at the outlet of the compressor will be calculated.

Step 2: Given the main engine's exhaust gas temperature, an assumption on the cycle's maximum temperature (T_4) will be made. As an initial value, a temperature of 10K lower than the exhaust gas will be used.

Step 3: The temperature at the outlet of the turbine (T_5) will be calculated. If T_5 is lower than T_2 +10K, the recuperated cycle cannot be used, thus steps 4 and 5 may be skipped.

Step 4: The temperature of the working fluid at the outlet of the warm side of the recuperator (T_6) will be set to 10K above T_2 (see *Chapter 5.4* for a more detailed

explanation), thus T_3 may be calculated via the balance of energy inside the recuperator ($h_{t5} - h_{t6} = h_{t3} - h_{t2}$).

Step 5: Given the working fluid's mass flow rate $\dot{m}$, the cycle's heat input $\dot{Q_H} = \dot{m} \times (h_{t4} - h_{t3})$ can be calculated. Given the main engine's exhaust gas mass flow rate $\dot{m}_g$ and temperature $T_{g,in}$, its temperature at the outlet of the heater $T_{g,out}$ can also be calculated via the balance of energy inside the heater $\dot{m} \times (h_{t4} - h_{t3}) = \dot{m}_g \times C_{pg} \times (T_{g,in} - T_{g,out})$. If $T_{g,out}$ is lower than T_3+10K, our initial assumption of T_4 was too high. Therefore, its value will be reduced by 0.5K and steps 3 to 5 will be repeated. If our loop ends with the use of a recuperated cycle, step 6 may be skipped.

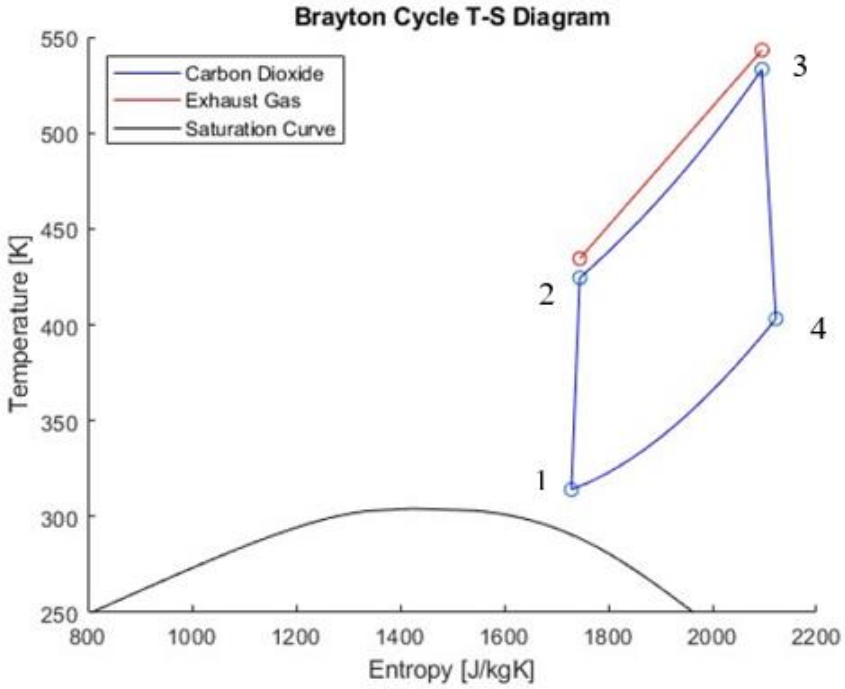

Figure 5.20: Simple Brayton Cycle T-s Diagram.

Step 6: In the case that thermal recuperation is not possible, the recuperator will be bypassed, and a simple Brayton cycle will be used. Using a simple cycle will no longer require making assumptions on the cycle's maximum temperature. Instead, the temperature of the main engine's exhaust gas at the outlet of the heater will be set to its dew point. This is an assumption that we will be making since the temperature of the working fluid at the outlet of the compressor is way below the dew point limit, and the dew point temperature is the lowest allowable temperature that will maximize our heat input. The cycle's heat input can then be calculated $Q_H = \dot{m}_g \times C_{pg} \times (T_{g,in} - T_{g,out})$. Finally, the cycle's maximum temperature T_3 can be calculated as a function of the stagnation enthalpy via the balance of energy inside the heater $\dot{m} \times (h_{t3} - h_{t2}) = \dot{m}_g \times C_{pg} \times (T_{g,in} - T_{g,out})$. The rest of the cycle's thermodynamic states can be calculated according to the theory explained in *Chapter 5.2*.

Step 7: The temperature differences at the ends of the heat exchangers will be checked. If the two temperature profiles are incompatible, an error will occur. An error will also occur if the exhaust gas dew point temperature limit is surpassed for whatever reason. Finally, the cycle's efficiency and net power production will be calculated in a similar manner to the full load scenario.

Step 8: The heater's conductance $UA = \frac{Q}{LMTD}$, where $LMTD = \frac{\Delta T_1 - \Delta T_2}{\ln\left(\frac{\Delta T_1}{\Delta T_2}\right)}$, ΔT_1 and ΔT_2 are the temperature differences of the two streams at the ends of the heat exchanger, will be calculated and compared to Dyreby's method at every load scenario. Finally, the heater's effectiveness will also be calculated.

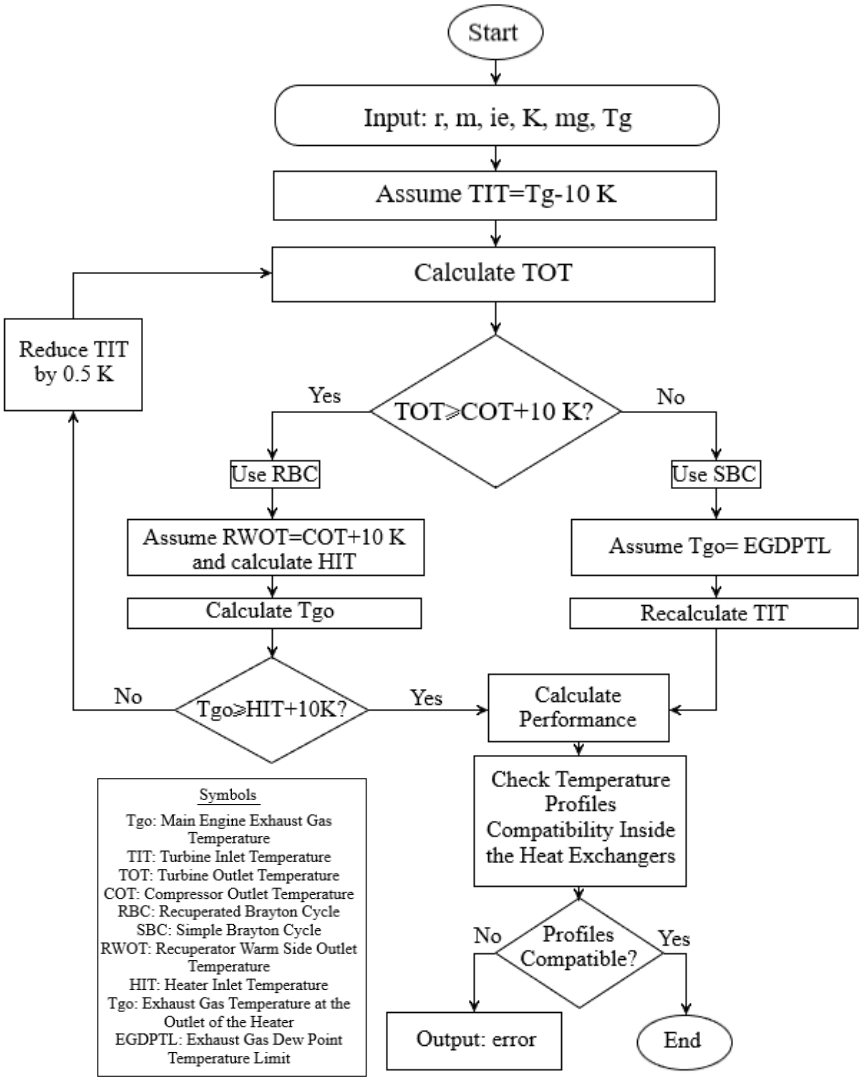

Figure 5.21: Flowchart Diagram of the Code

Model Input		
Symbol	**Description**	**Unit**
ie	Turbomachinery Isentropic Efficiency	-
K	Heat Exchanger Pressure Loss Factor	-
mg	Exhaust Gas Mass Flow Rate	kg/s
Tg,in	Exhaust Gas Temperature	^{o}C
Cycle Characteristics		
Parameter	**Value**	**Unit**
Minimum Pressure	7477300	Pa
Minimum Temperature	314.1282	K
Pressure Ratio	2.55	-
Working Fluid Mass Flow Rate	19.299	kg/s
Model Output		
Symbol	**Description**	**Unit**
e	Thermal Efficiency	-
P	Power Output	kW
UA	Heater Conductance	W/K
eH	Heater Efficiency	-

Table 5.4: A summary of the cycle's characteristics, model input and output at partial loads.

5.5.1. Results

Using our model, the performance of the SCBC as a waste heat recovery system for an engine at partial loads will be evaluated. The system's net power output and efficiency as well as some other important system metrics will be plotted for the various main engine load scenarios (from 100% of the SMCR down to 25% of the SMCR). The main engine's performance data at partial loads will be once again obtained via MAN's CEAS. To proceed with our simulations, the following assumptions will be made:

- The turbine and compressor isentropic efficiencies remain constant at partial loads as the working fluid's mass flow rate and pressure ratio are also kept constant.
- Heat exchanger pressure loss factor does not change at partial loads. It is assumed as 1% for all heat exchangers as well as the recuperator's bypass ducts. Pressure losses in the other ducts are considered negligible.
- Pressure losses of the main engine's exhaust gas inside the heater are considered negligible and the performance of the main engine is not affected in any way by the use of the WHR system.

Our simulations showed that thermal recuperation cannot be used at loads lower than 95 % of the SMCR, thus a recuperator bypass is necessary in order to keep the system operational at partial loads. *Figure 5.22* displays the net power output of the SCBC as a function of the

main engine load. As we can see, there is a steep decrease in power during the 100 to 90% range followed by a more gentle decline in the 90 to 40% range and finally a sudden spike at lower loads. The higher gradient in the 100 to 90% range is due to a big change in exaust gas temperature compared to the rest of the load scenarios. More specifically, in this range, the exhaust gas temperature drops by 51°C compared to the 3°C drop in the 90 to 80% range. As for the spike in the 35 to 25% range, there is also a similar explaination. In this range, the exhaust gas temperature starts increasing significantly, thus there is a higher cycle heat input rate. In general, the exhaust gas mass flow rate increases with the increase of the main engine load, therefore it is normal that the power output of the cycle has an increasing trend as the engine gets more loaded.

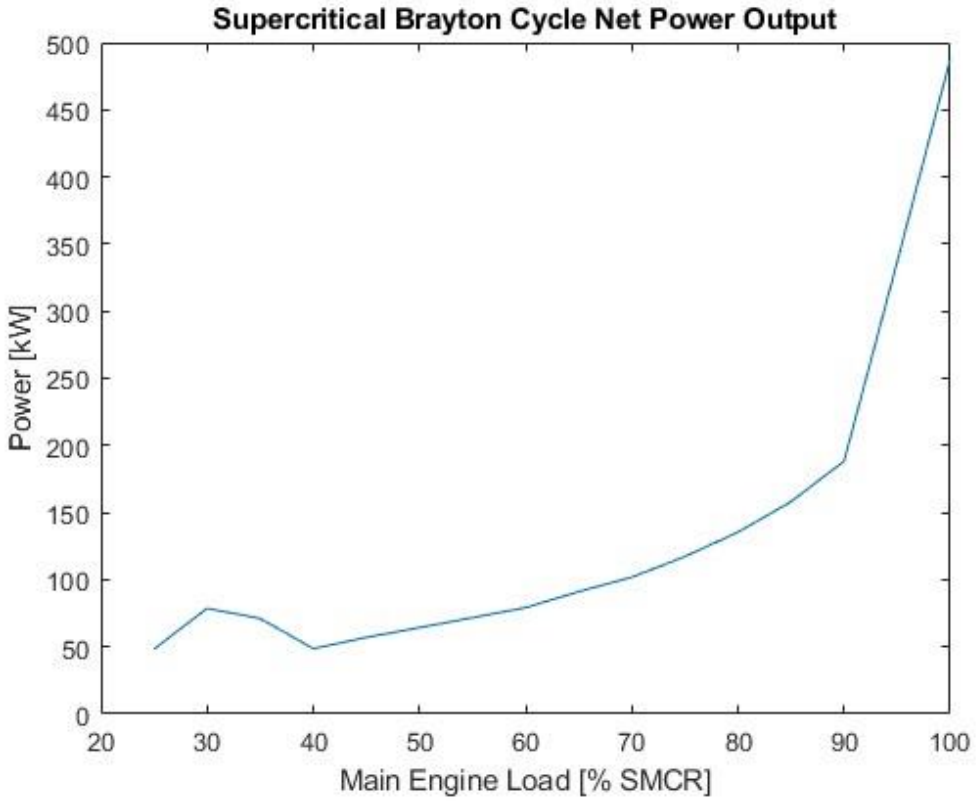

Figure 5.22: Net Power Output of the SCBC as a Waste Heat Recovery Method for the Vessel's Main Engine at Partial Loads

In *Figure 5.23* the SCBC's thermal efficiency is displayed as a function of the main engine's load. Thermal efficiency follows a similar trend to the net power output. Once again, we see that the thermal efficiency of the cycle changes at partial loads, despite the pressure ratio being constant. This happens due to the cycle having irreversibilities and not being ideal.

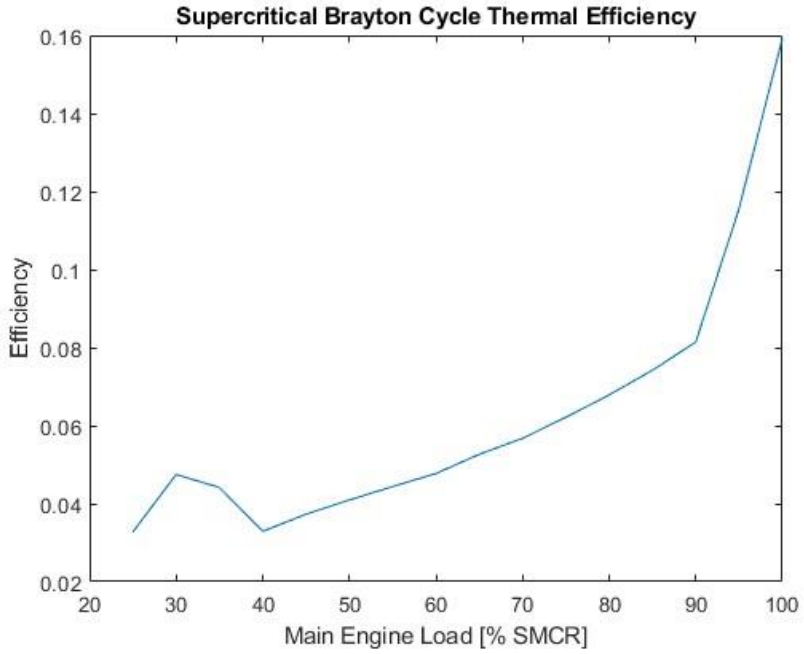

Figure 5.23: Thermal Efficiency of the SCBC as a Waste Heat Recovery Method for the Vessel's Main Engine at Partial Loads

In *Figure 5.24* the net power output of the combined cycle is displayed, whereas in *Figure 5.25* the combined cycle's thermal efficiency is presented for different main engine loads. The combined cycle's net power output increases with the increase of the main engine load and maximizes at the SMCR. On the other hand, the combined cycle's efficiency maximizes in the 65 to 75% range, which is also the range in which the main engine's efficiency maximizes.

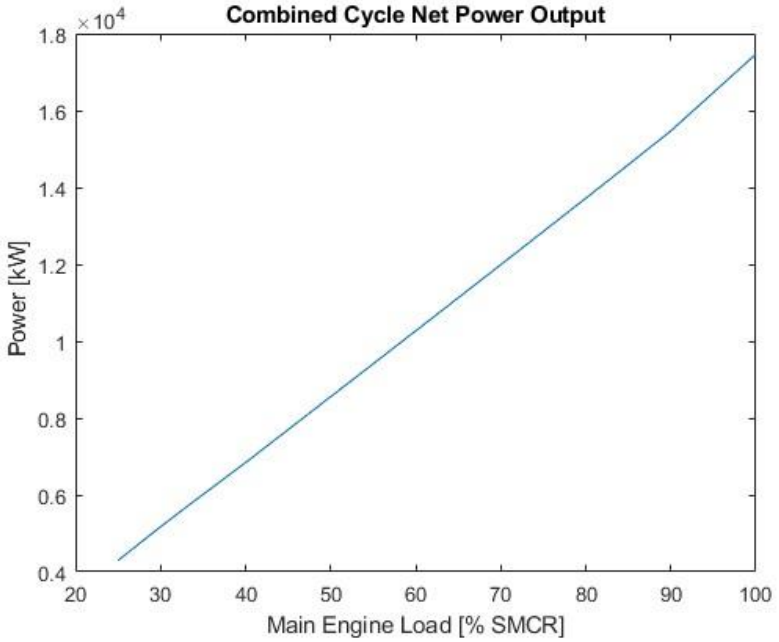

Figure 5.24: Net Power Output of the Combined Cycle at Different ME Loads

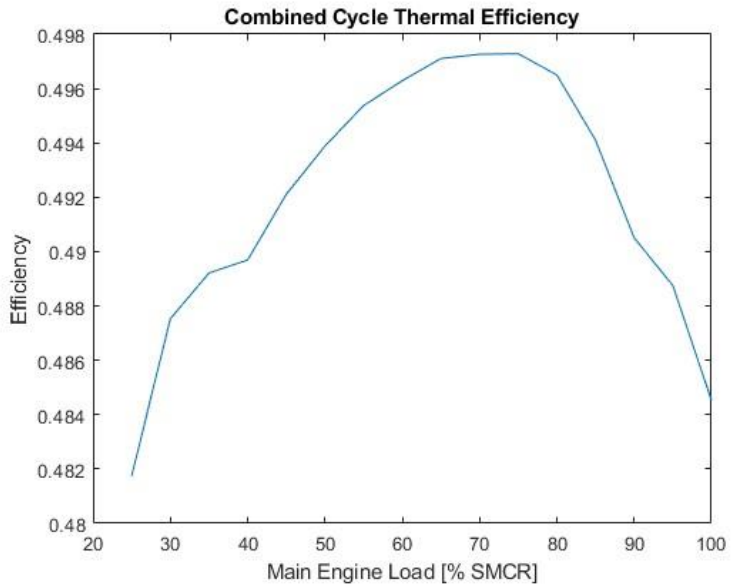

Figure 5.25: Thermal Efficiency of the Combined Cycle at Different ME Loads

In *Figure 5.26* the system's net power production increase percentage and thermal efficiency increase percentage by using the SCBC for waste heat recovery at different loads are presented. Furthermore, the specific fuel oil consumption reduction percentage at different engine loads is also displayed in *Figure 5.27*. The SCBC offers a significant improvement in the system's performance when used for waste heat recovery. This improvement is especially noticeable at higher loads where the SCBC can provide an up to 2.9% increase in power and efficiency and an up to 2.8% decrease in specific fuel oil consumption. It may seem that this improvement is insignificant, but considering the large amount of fuel consumed by vessels, even this small improvement could result in a noticeable decrease in greenhouse gas emissions and operating costs.

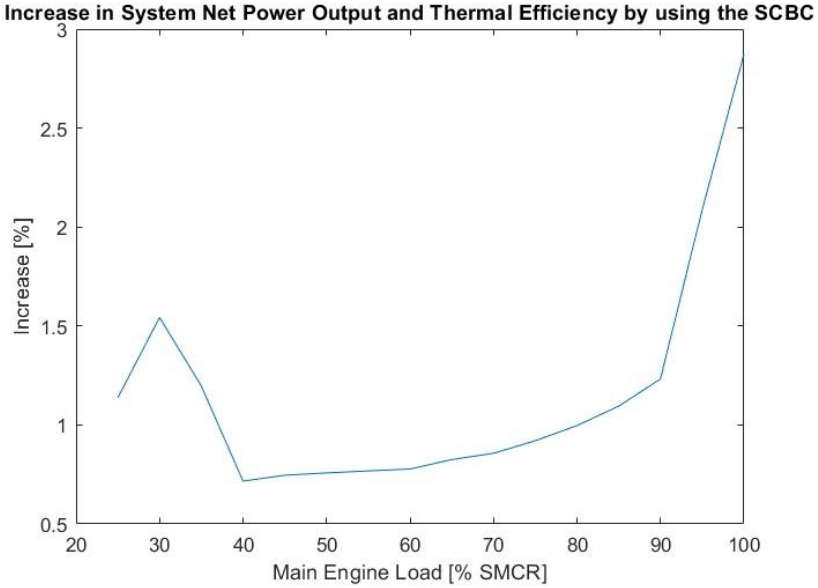

Figure 5.26: Increase in System Net Power Output and Thermal Efficiency by using the SCBC for Waste Heat Recovery

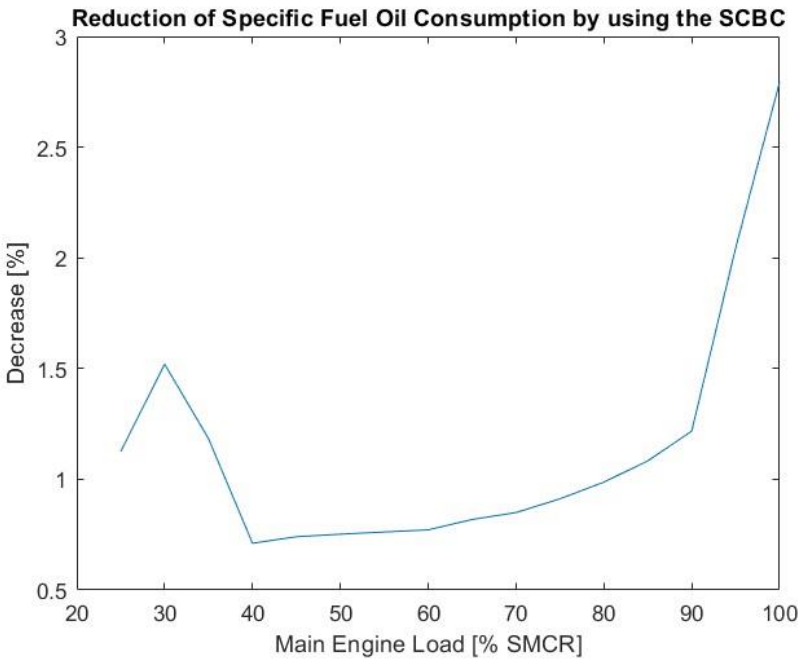

Figure 5.27: Reduction of Specific Fuel Oil Consumption by using the SCBC for Waste Heat Recovery

In *Figure 5.28* the SCBC's contribution to the combined system's net power output as a function of the main engine load is displayed. It is noteworthy that there is a noticeable performance improvement at lower loads too. This could be useful when approaching ports near urban areas, as a reduction in SFOC could theoretically help reduce the pollution in big cities. The use of a bottoming cycle in lower loads, however, is a questionable practice as the significant difference between the exhaust gas and sCO_2 mass flow rate raises questions about the feasibility of the heat exchange inside the heater.

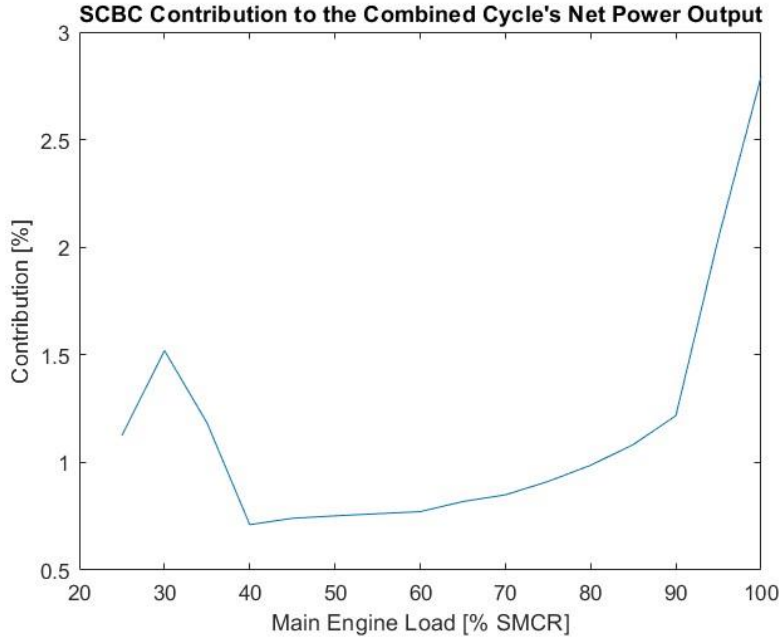

Figure 5.28: Contribution of the SCBC to the Combined System's Net Power Output

Studying the system's heater performance was also a part of our simulations. Although not detailed enough, this part of the study provides important insight on how realistic is our approach of the cycle's heat input. In *Figure 5.29* the heater's effectiveness at different main engine loads is displayed. As we can see, the effectiveness decreases with the decrease of the engine's load, which was to be expected, as the drop in exhaust gas mass flow rate and temperature makes it harder for heat to be exchanged between the two streams inside the heater. It is important to remember that the working fluid's mass flow rate inside the Brayton cycle is kept constant and it is not being scaled according to the exhaust gas mass flow rate. Finally, the heater's conductance at different main engine loads was plotted in *Figure 5.30* and compared to the Dyreby et al method. Our model results in a sudden drop in conductance in the 90 to 100% range followed by a smoother decline at lower loads. According to the Dyreby et al method, there should be a smooth decline in conductance across the whole range of loads. The Dyreby et al method, although not applicable in our case, provides more accurate results, as it is based on experimental data and component specific studies. Our method is not as realistic but it should provide an upper limit for the cycle's performance at partial loads.

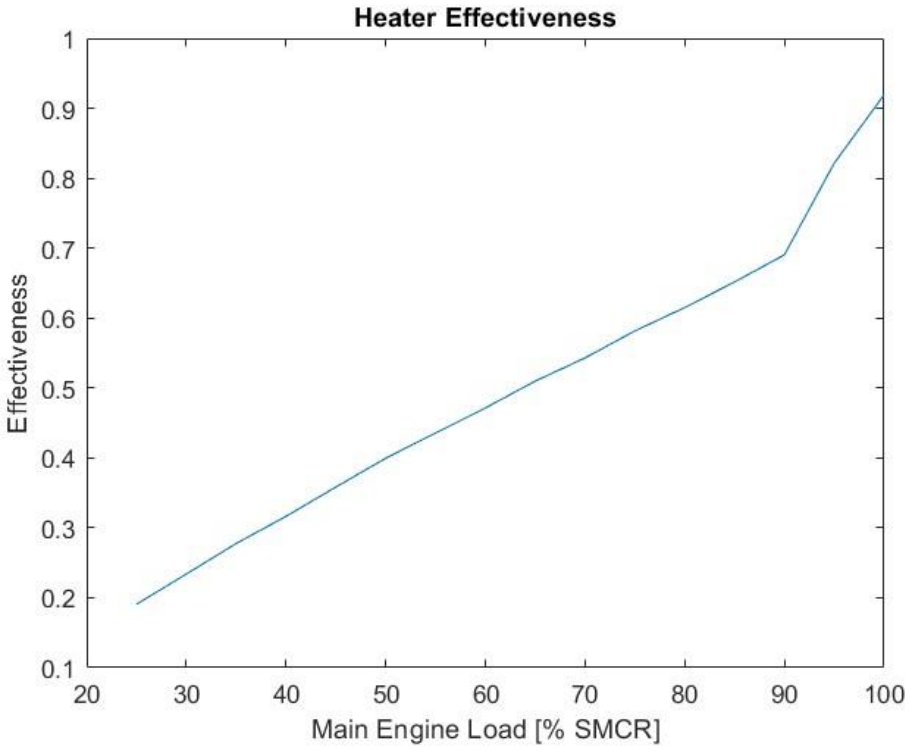

Figure 5.29: Heater Effectiveness at Partial Loads

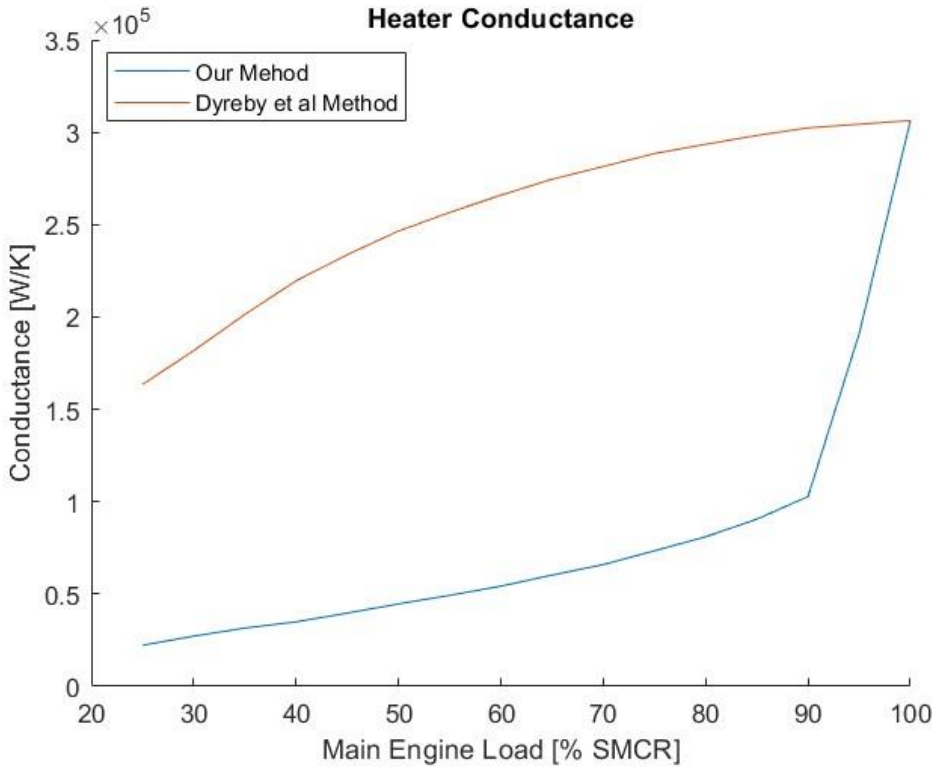

Figure 5.30: Heater Conductance Compared to the Dyreby et al Method [100].

5.6. Effect of Main Engine Power on SCBC Performance

In this section, the effect of the main engine's power output on the performance of the supercritical carbon dioxide Brayton cycle will be presented. For this, seven MAN Diesel engines of the same injection technology (GI- Gas Injection) with power outputs ranging from 8340 to 82440 kW were chosen and the performance of the SCBC in terms of optimal pressure ratio, power recovery, thermal efficiency and power contribution to the combined cycle was analyzed. This study was conducted at the engine's SMCR and the approach was the same as the one presented in *Chapter 5.4*. The characteristics of the main engines used in our simulations are presented in *Table 5.5*.

Model No.	Power [kW]	Cylinders	Cylinder Bore [cm]	Speed [rpm]	SFOC [g/kW]	EGA [kg/s]	EGT [Celcius]
6G45ME-C9.5-GI-HPSCR	8340	6	45	111	172	17.4	270
6G60ME-C10.5-GI-HPSCR	17040	6	60	103	167	36.4	245
6G80ME-C10.5-GI-HPSCR	28260	6	80	72	162	58.5	242
6G95ME-C10.5-GI-LPSCR	41220	6	95	80	161	79.4	265
8G95ME-C10.5-GI-LPSCR	54960	8	95	80	165	112.4	255
10G95ME-C10.5-GI-LPSCR	68700	10	95	80	161	132.4	265
12G95ME-C10.5-GI-LPSCR	82440	12	95	80	161	158.9	265

Table 5.5: MAN ME-GI Marine Engine Characteristics (EGA= Exhaust Gas Amount, EGT= Exhaust Gas Temperature)

As we can see, there is an increase in exhaust gas amount as the power increases, which is to be expected, due to the fact that higher engine power means more working fluid and thus higher exhaust gas mass flow rate. This is not true for the exhaust gas temperature, which is maximum for the low power and minimum for the medium to low power engines with high power engines standing somewhere in between. The exhaust gas temperature is a difficult to predict parameter as it depends on a variety of factors like the chamber's geometry, air and fuel mixture and other combustion process parameters. Even though the exhaust gas amount is the main influencing factor for the bottoming cycle's heat input, the exhaust gas temperature also plays an important role.

Therefore, the engine's waste heat rate $Q_{WH} = \dot{m}_g C_{pg} T_g$ was plotted as a function of the main engine power in *Figure 5.31*, where $\dot{m}_g$ is the exhaust gas amount, C_{pg} is the exhaust gas specific heat capacity and T_g is the exhaust gas temperature. The relationship between the main engine power and its waste heat rate is almost linear with a slight abnormality in the 50000 to 60000 kW range. As expected, the waste heat rate has an increasing trend with power, which means that the recovered power should also increase with the increase of main engine power.

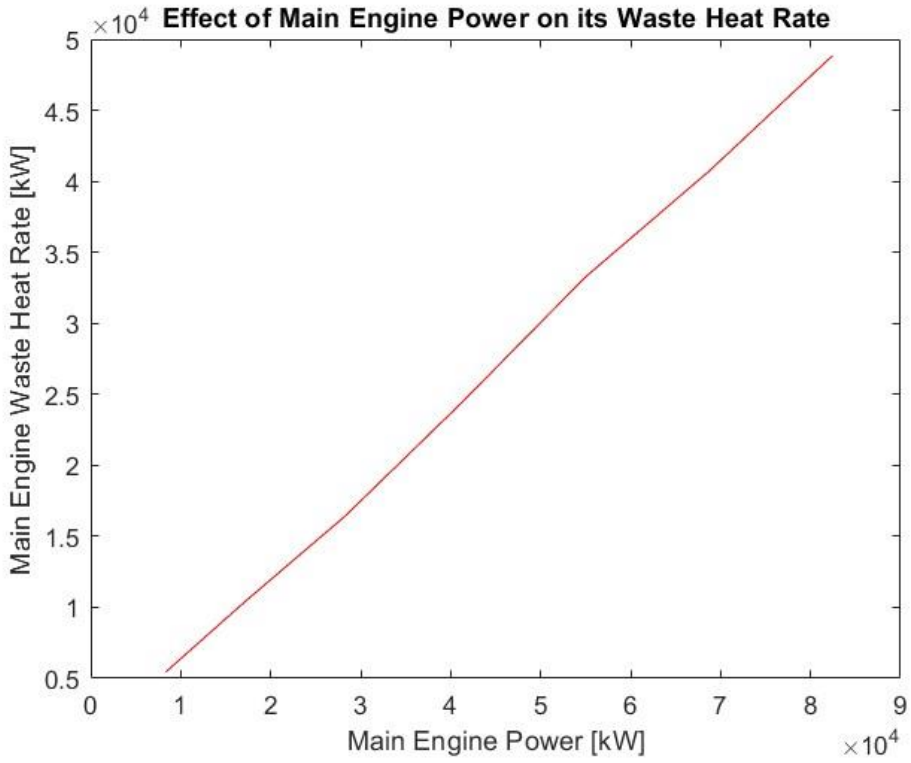

Figure 5.31: Effect of Main Engine Power on its Waste Heat Rate

In *Figure 5.32,* the recovered power against the main engine's power is presented. As expected, due to the higher waste heat rate, the recovered power increases with the increase of main engine power, which means that the SCBC produces more power when paired to a high power engine.

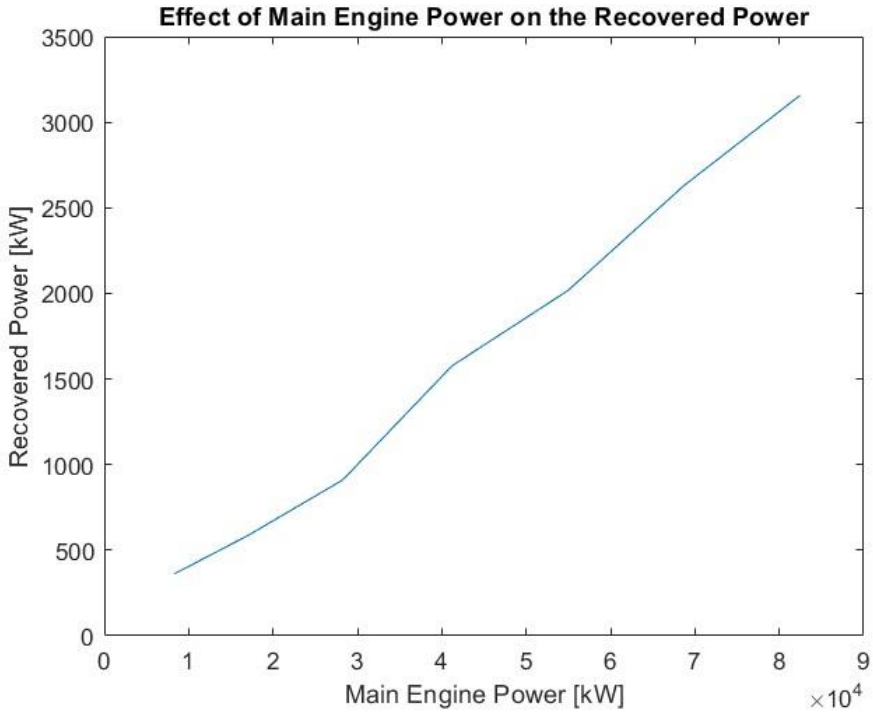

Figure 5.32: Effect of Main Engine Power on the Power Recovered by the SCBC

In *Figure 5.33*, the optimal pressure ratio as a function of the main engine's power is displayed. As we can see, the optimal pressure ratio does not have a specific dependency on the engine power. If we examine the engine data closely, we will figure out that the engines that have the same exhaust gas temperature also share the same optimal pressure ratio.

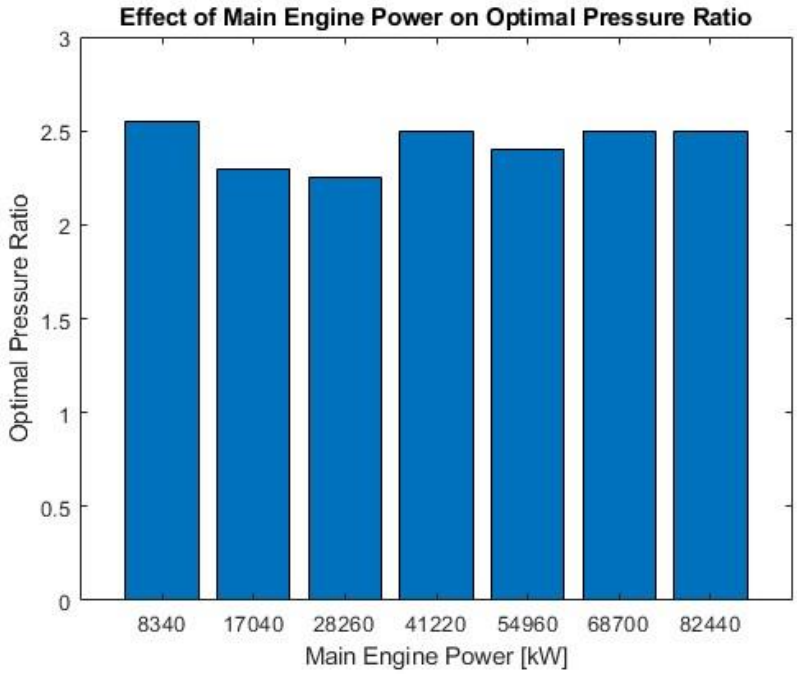

Figure 5.33: Effect of Main Engine Power on SCBC Optimal Pressure Ratio

In *Figure 5.34*, the cycle's thermal efficiency against the main engine's power is presented. In a similar way to the optimal pressure ratio, the cycle's thermal efficiency does not have a specific dependency on the engine power but increases with the increase of the exhaust gas temperature. In *Figure 5.35*, the SCBC contribution to the combined system's net power output against the main engine's power is presented. As we can see, the contribution follows a similar trend to the optimal pressure ratio and cycle thermal efficiency. This means that engines with higher exhaust gas temperature could potentially benefit more by the use of such a WHR system at the cost of using higher pressure ratios. However, it is not safe to draw such a conclusion with such a small engine sample size.

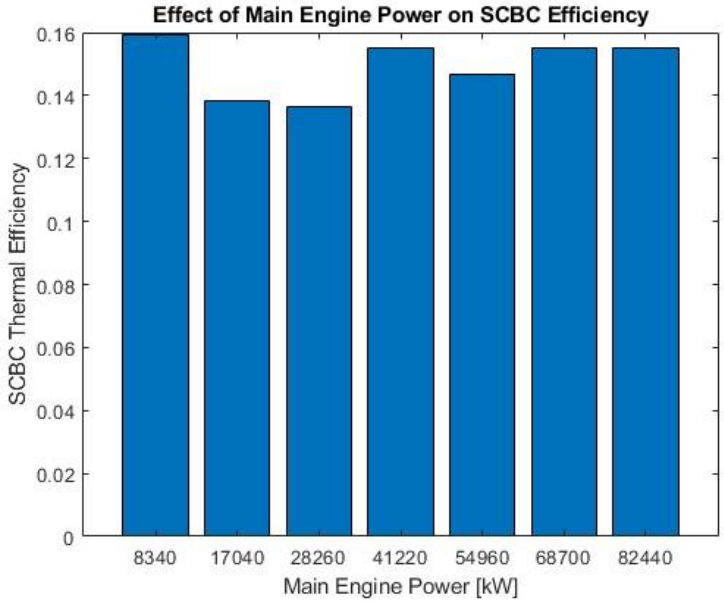

Figure 5.34: Effect of Main Engine Power on SCBC Thermal Efficiency

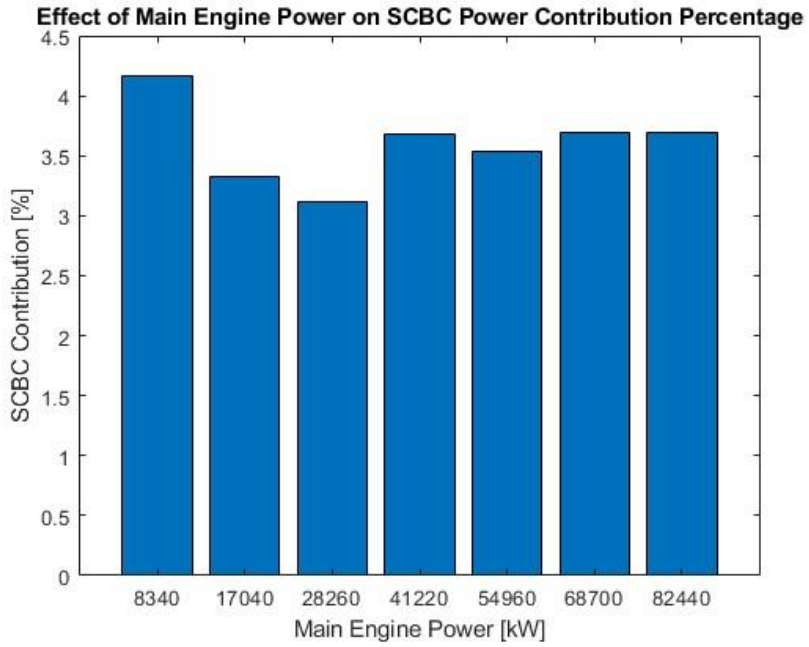

Figure 5.35: Effect of Main Engine Power on the SCBC Power Contribution to the Combined Cycle

5.7. Performance Comparison

In this section, we will compare the performance of our model against some models found in the literature, in order to examine how it stacks up against other layouts and similar WHR technologies. More specifically, our model will be compared against a recompression SCBC model developed by Xie and Yang [79] as well as an ORC model developed by Akman and Ergin [102], both used for marine Diesel engine waste heat recovery. For both cases, our model input was adjusted to match that of the literature and an approach similar to the one presented in *Chapter 5.4* was followed. Then, the performance in terms of recovered power, efficiency increase percentage and specific fuel oil consumption reduction percentage was analyzed and plotted in a bar diagram.

Figure 5.36 presents the recovered power for both our and the recompression model. As we can see, our recuperated model produces more power, which means it is more suitable for waste heat recovery applications. In *Figure 5.37* the system's efficiency increase percentage is highlighted whereas in *Figure 5.38* the specific fuel oil consumption reduction percentage is displayed for both models. As we can see, our recuperated model exhibits better performance benefits than its recompression counterpart, which further confirms what was discussed in the very beginning of this chapter regarding the most suitable SCBC layout for waste heat recovery. Despite the recompression layout being popular for its higher efficiency, higher heat source temperatures are a requirement in order to benefit from such a layout. Factoring in the added size, maintenance and operating complexity, recompression seems to be unsuitable for waste heat recovery applications, especially for diesel engines which have notoriously low waste heat temperatures.

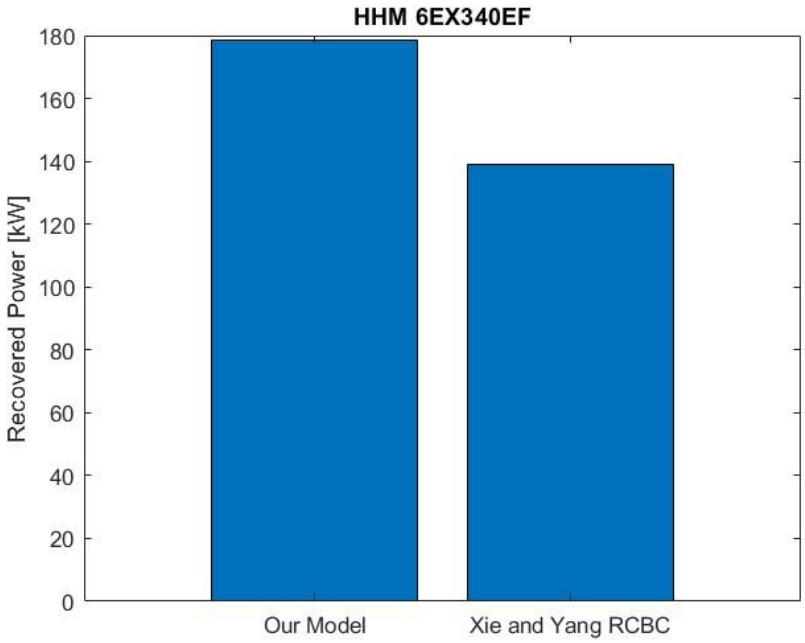

Figure 5.36: Power Recovered with our model compared to Xie and Yang's recompression model for an HHM 6EX340EF.

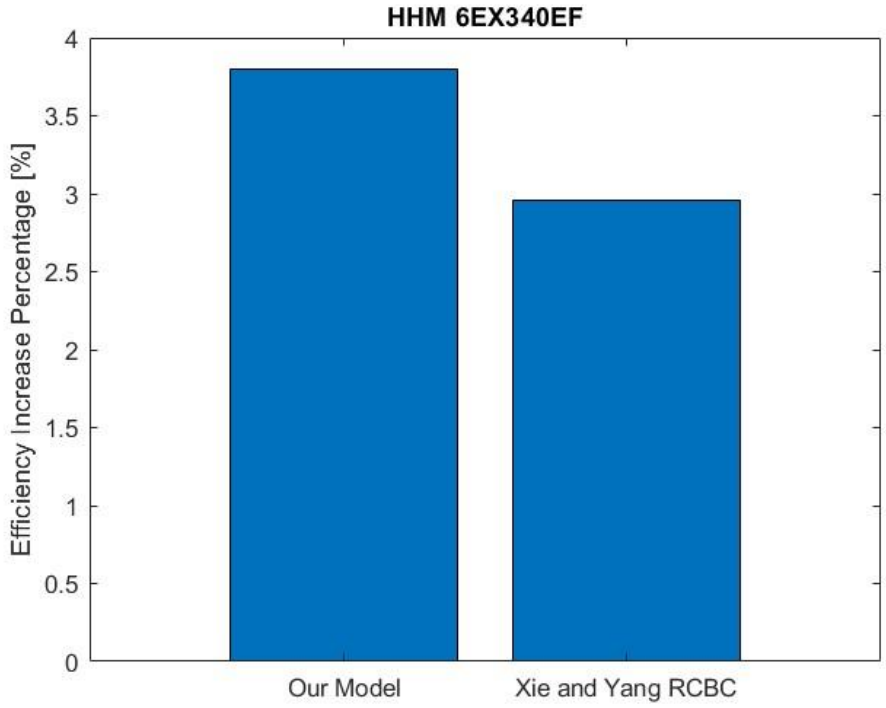

Figure 5.37: Efficiency Increase Percentage with our model compared to Xie and Yang's recompression model for an HHM 6EX340EF.

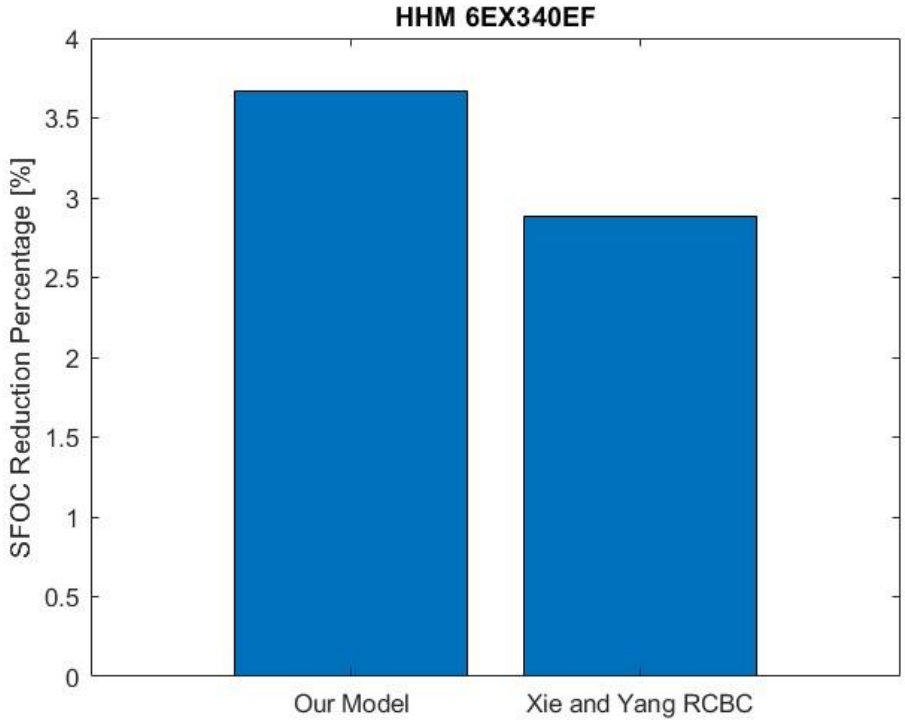

Figure 5.38: Specific Fuel Oil Consumption Reduction Percentage with our model compared to Xie and Yang's recompression model for an HHM 6EX340EF.

In *Figure 5.39*, the power output of our model was compared to Akman and Ergin's ORC model. The comparison showed that the organic rankine cycle offers slightly better performance. In *Figure 5.40* the system's efficiency increase percentage is presented whereas in *Figure 5.41* the specific fuel oil consumption reduction percentage is displayed for both models. In a similar way to the power output, the ORC showcases better performance benefits compared to the SCBC. However, a more detailed look into the Akman and Ergin's model revealed that pressure losses were not modeled inside the heat exchangers and that a heat exchanger efficiency factor was used. Due to the very high cycle pressures, pressure losses have a significant impact on our model's performance, thus it is not fair to compare it against models without pressure losses. Moreover, the heater's efficiency was not modeled in our case, thus our model is in the advantageous position this time around. In order to draw a safer conclusion, a more detailed study with respect to each system's limitations and constraints is required.

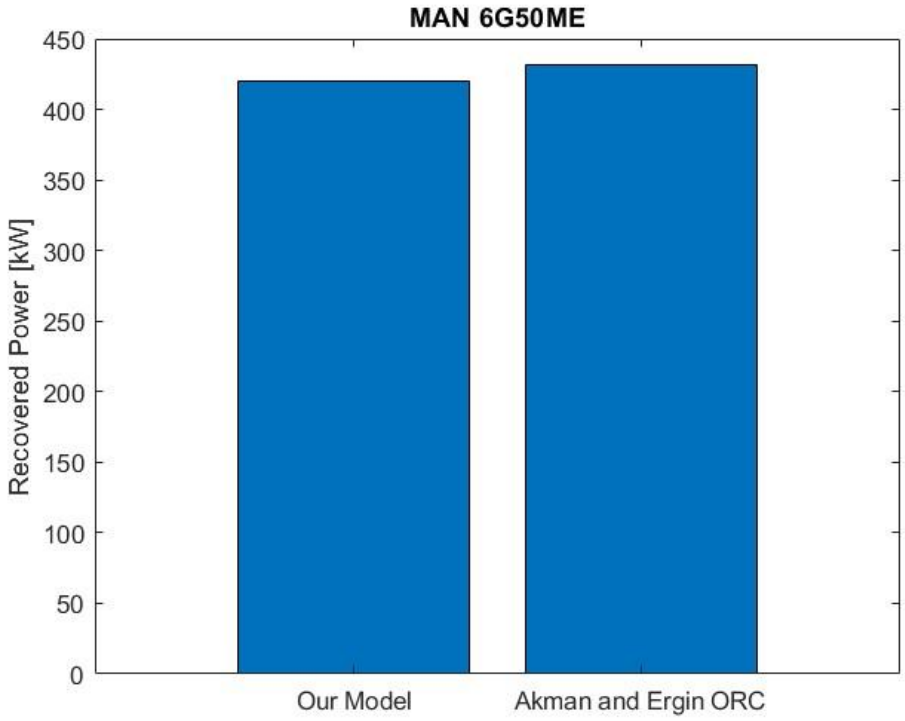

Figure 5.39: Power Recovered with our model compared to Akman and Ergin's Organic Rankine Cycle model for an MAN 6G50ME.

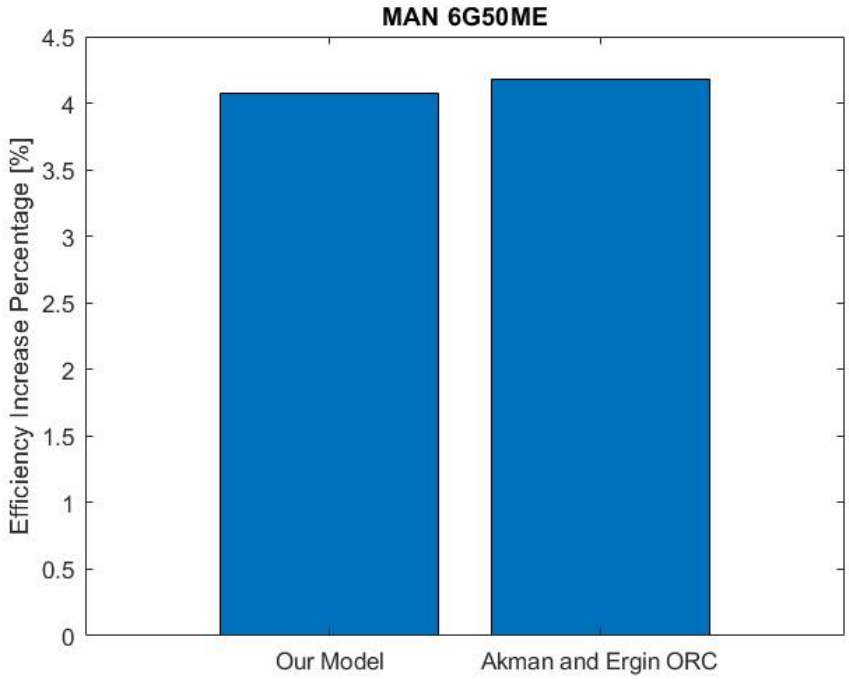

Figure 5.40: Efficiency Increase Percentage with our model compared to Akman and Ergin's Organic Rankine Cycle model for an MAN 6G50ME.

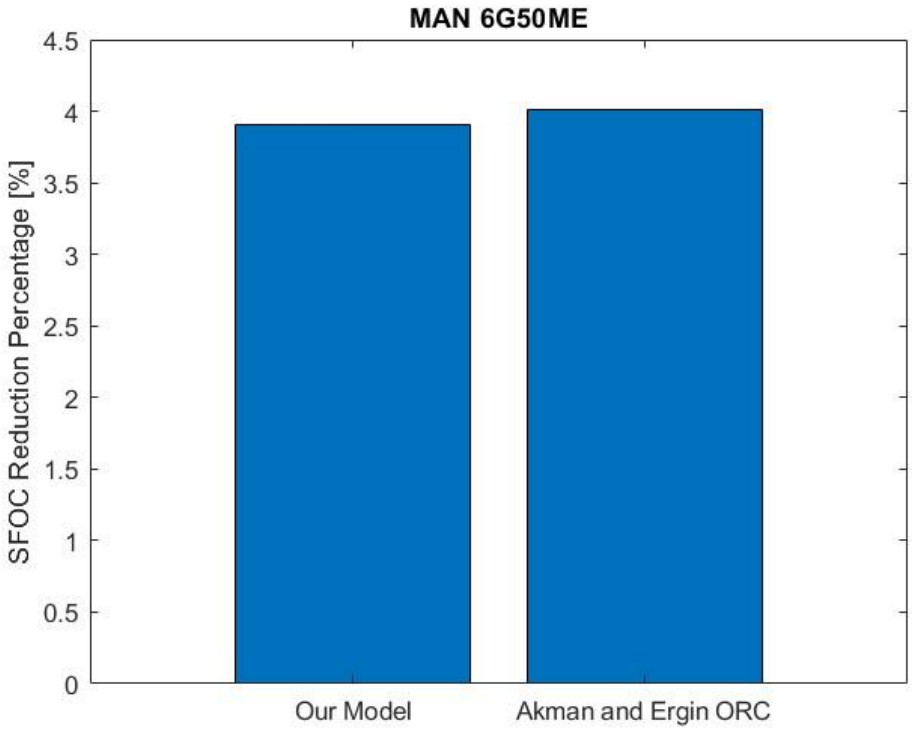

Figure 5.41: Specific Fuel Oil Consumption Percentage with our model compared to Akman and Ergin's Organic Rankine Cycle model for an MAN 6G50ME.

Conclusions

The supercritical carbon dioxide Brayton cycle has the potential to revolutionize power generation in the future. With a small form factor, a user friendly working fluid and unprecedented levels of performance, this technology is a direct upgrade in every aspect to traditional power generation methods like steam and gas turbines. The SCBC is compatible with any standard heat source, from fossil fuels to nuclear energy, with the more enviromentally friendly heat sources, like geothermal and solar energy, being in the center of attention for the SCBC researchers.

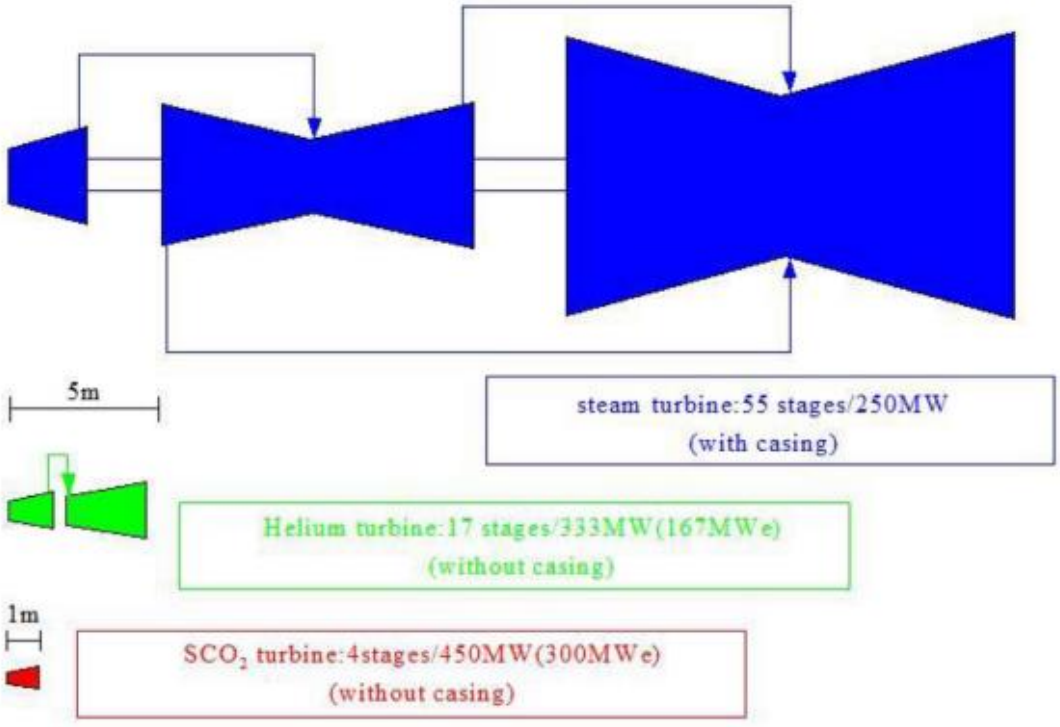

Figure A: Turbine Size Comparison for Steam, Helium and Supercritical CO_2 Cycles [54]

The main objectives of this thesis were to provide important insight on this new and to many still unknown technology, as well as develop a thermodynamic model of the cycle for waste heat recovery of a marine engine. Among the many configurations considered for our model, a recuperated layout was chosen and its performance was parametrically analysed. Our SCBC model was specifically optimized for maximum power generation and the effects of the pressure ratio were carefully studied at the engine's SMCR. Furthermore, the performance of the recuperated layout was compared to a simple layout in order to cover a broader spectrum of pressure ratios.

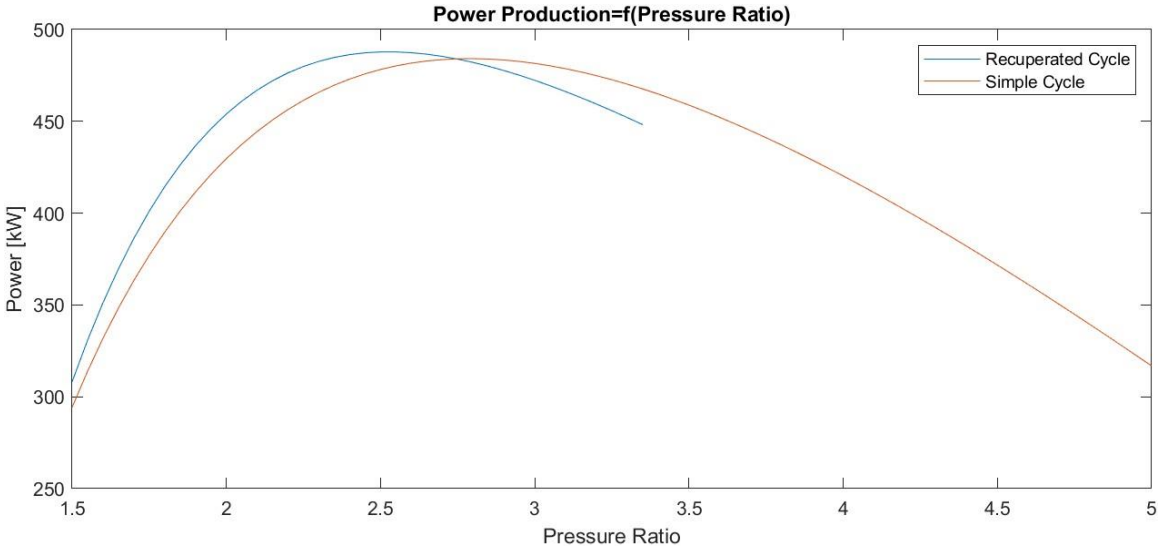

Figure B: Effect of Pressure Ratio on the SCBC Performance When Used for Waste Heat Recovery of a MAN 6G70ME-C10.5-GA-EGRBP Dual Fuel Marine Engine.

As we can see, there is always an optimal pressure ratio for maximum power generation, which was found to be different than the optimal pressure ratio for maximum cycle efficiency. What is interesting is the fact that the recuperated layout almost consistently outperforms the simple configuration in terms of power production. In theory, thermal recuperation should only increase the cycle's efficiency, but in reality, a more careful examination of the cycle's behaviour revealed that the heat is utilized more effectively when supplied at higher temperatures, therefore a higher CO_2 mass flow rate is allowed. Our results revealed that with the use of a SCBC for WHR, the engine's efficiency can be increased by 2.9% and its specific fuel oil consumption can be reduced by 2.8%.

Supercritical CO_2 Brayton Cycle		**Main Engine**	
Configuration	Recuperated	Load	100 [%]
Pressure Ratio	2.550	Power Output	16980 [kW]
Minimum Pressure	7.577 [MPa]	SFOC	179 [g/kWh]
Maximum Pressure	19.322 [MPa]	Exhaust Gas Amount	23.4 [kg/sec]
Minimum Temperature	40.98 [Celcius]	Exhaust Gas Temperature	270 [Celcius]
Maximum Temperature	260 [Celcius]	Thermal Efficiency	0.47
Power Output	487.78 [kW]	**Combined System**	
Thermal Efficiency	0.159	**Power Output**	**17467.78 [kW]**
Working Fluid Mass Flow Rate	19.299 [kg/sec]	**Thermal Efficiency**	**0.485**
Heat Input Rate	3063.1 [kW]	**SFOC**	**174.002 [g/kWh]**
Heat Recuperation Rate	1115.03 [kW]	**Exhaust Gas Temperature**	**156.172 [Celcius]**
Cooling Rate	2575.32 [kW]	**Efficiency Increase Percentage**	**2.873 [%]**
Heater Effectiveness	0.919	**Power Increase Percentage**	**2.873 [%]**
Recuperator Effectiveness	0.832	**SFOC Reduction Percentage**	**2.792 [%]**

Table A: MAN 6G70ME-C10.5-GA-EGRBP Performance Improvement by Using the SCBC for Waste Heat Recovery

Another important part of our modeling process was the simulation of the SCBC at partial loads. A vessel's engine is constantly required to operate at various load conditions, therefore it is important to examine the behaviour of the bottoming cycle when the engine operates at partial loads. Deciding not to deploy advanced closed loop gas turbine control strategies, the cycle's pressure ratio and working fluid mass flow rate were kept constant. The results showed that even at lower loads, there are significant performance benefits by using the SCBC for WHR.

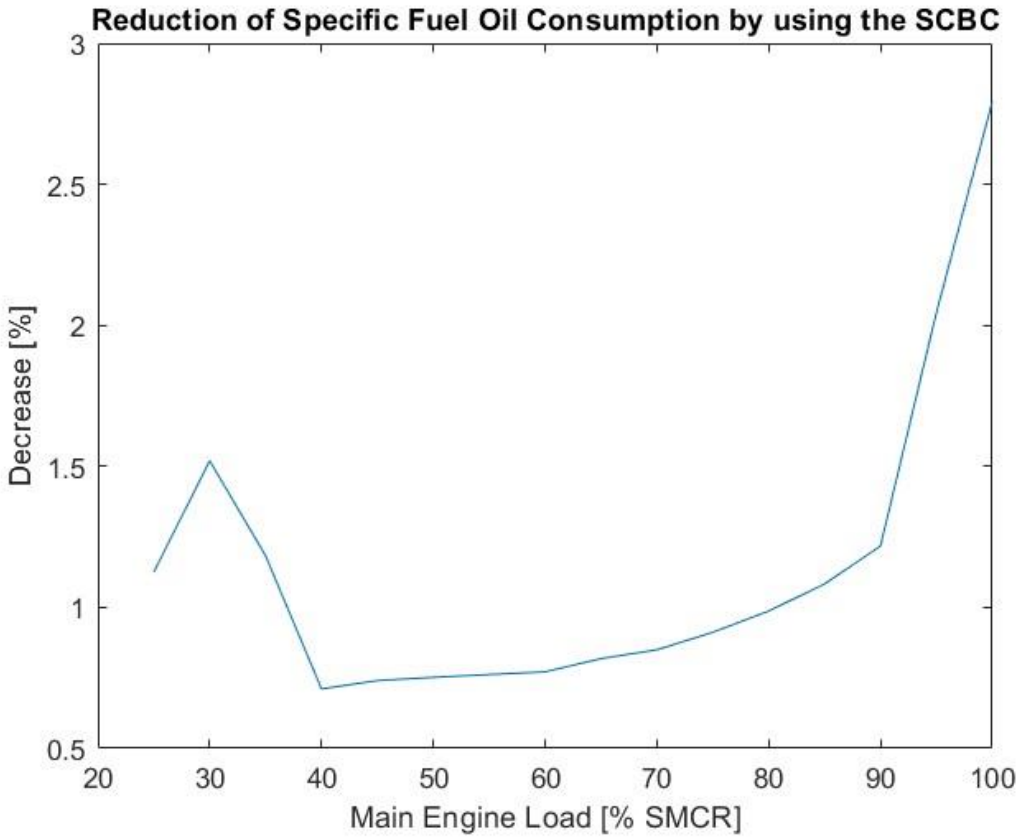

Figure C: Specific Fuel Oil Consumption Reduction Percentage by Using the SCBC for WHR of a 6G70ME-C10.5-GA-EGRBP .

Finally, the effects of main engine power to the SCBC performance were studied. For this, 7 engines of the same injection technology and different power outputs were chosen and the performance of the SCBC was calculated at the SMCR using our previous model. The results showed that there is a possible relationship between the main engine exhaust gas temperature and optimal pressure ratio as well as the system's performance improvement. This means that pairing the SCBC to higher level heat sources might offer a greater performance improvement at the cost of higher pressure ratios.

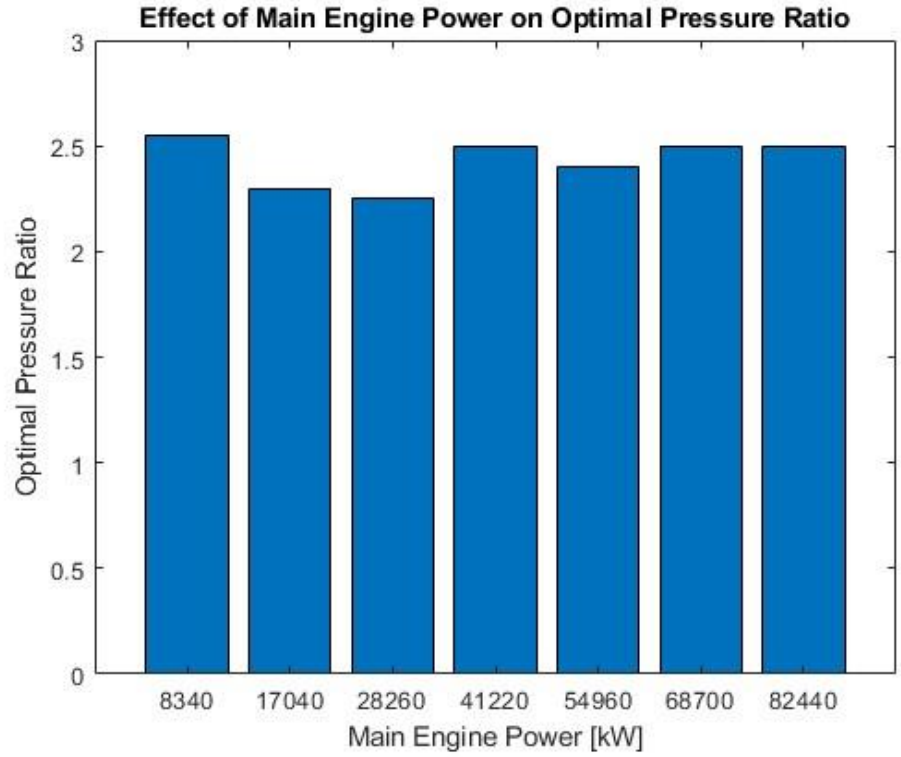

Figure D: Effect of Main Engine Power on Optimal Pressure Ratio

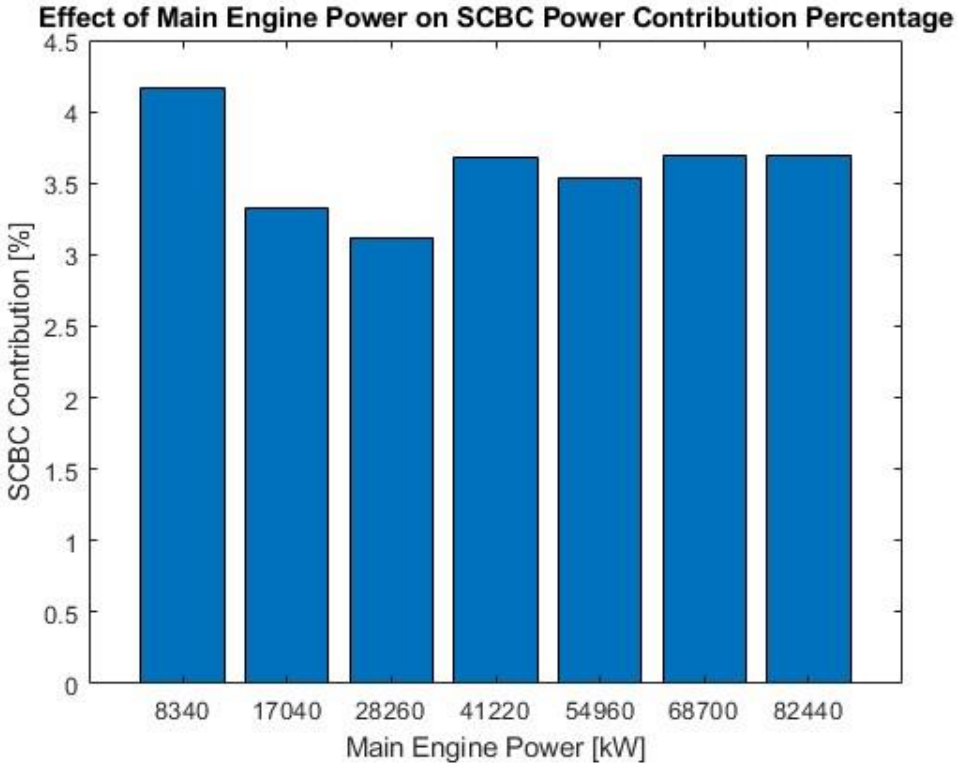

Figure E: Effect of Main Engine Power on the SCBC Power Contribution to the Combined Cycle

Overall, the SCBC has good performance as a WHR system. With a supposedly smaller form factor and similar performance to ORCs, it is possible that the SCBC could replace the traditional WHR methods in the future. However, it goes without saying that the commercial deployment of such a system onshore or onboard a vessel might be several years away. The use of specialized components, high cost, yet to be scaled performance and remaining research and development on the cycle components are major challenges that need to be surmounted first. With the current research momentum, it is only certain that the fate of this technology will be known in the very near future.

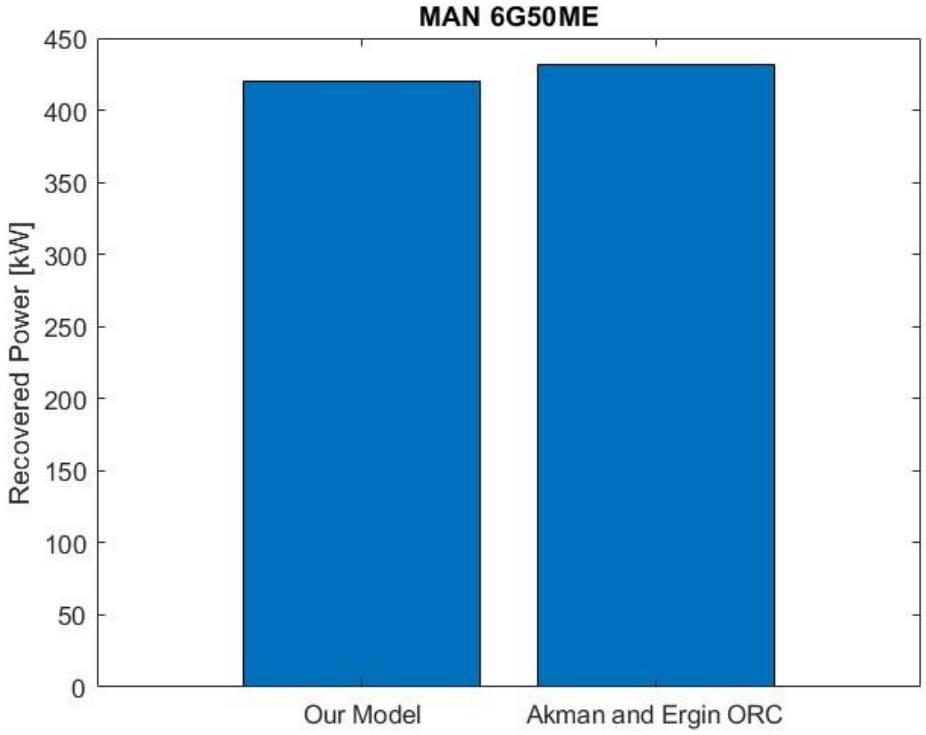

Figure F: Power Recovered by the SCBC compared to the ORC on a MAN 6G50ME.

Recommendations for Future Research

The fifth chapter of this thesis can be regarded as a preliminary design of a supercritical CO_2 Brayton cycle used for recovering the waste heat of a marine engine. Aiming to further develop the current models and enrich the available literature, some of the most crucial topics are proposed below for future research purposes:

- Advanced exergy analysis of the sCO_2 cycle with the goal of determining the cycle's performance limits and specifying the components that need to be further optimized.
- Development of a recompression model for waste heat recovery and optimization of the flow split ratio. A direct comparison with the results of this thesis should also be conducted.
- Supercritical CO_2 flow analysis in a compressor with the goal of developing a model to predict condensation phenomena. A combination of both thermodynamic and CFD tools shall be used.
- Development of an analytical printed circuit heat exchanger model to accurately predict its size and performance at off- design conditions.
- Enhancement of our model by adding preheating using jacket cooling water. Moreover, a detailed recap of the major challenges of commercializing the SCBC can also be presented.
- Technoeconomic analysis of deploying advanced closed loop gas turbine control strategies in order to optimize the cycle's performance at partial loads.
- Technoeconomic analysis of pairing a small modular reactor with a supercritical carbon dioxide Brayton cycle for the propulsion of ships.

References

[1] European Comission, “Reducing emissions from the shipping sector,” Climate Action. Accessed: Apr. 04, 2023. [Online]. Available: https://climate.ec.europa.eu/eu-action/transport-emissions/reducing-emissions-shipping-sector_en

[2] International Maritime Organization, “IMO’s work to cut GHG emissions from ships,” Hot Topics. Accessed: Apr. 04, 2023. [Online]. Available: https://www.imo.org/en/MediaCentre/HotTopics/Pages/Cutting-GHG-emissions.aspx

[3] P. Balcombe *et al.*, “How to decarbonise international shipping: Options for fuels, technologies and policies,” *Energy Conversion and Management*, vol. 182, pp. 72–88, Feb. 2019, doi: 10.1016/j.enconman.2018.12.080.

[4] Dorthe Marie Sveistrup Jacobsen, Randall Krantz, Lara Mouftier, and Emma Skov Christiansen, “Ammonia as a shipping fuel.” Accessed: Apr. 04, 2023. [Online]. Available: https://www.globalmaritimeforum.org/news/ammonia-as-a-shipping-fuel

[5] Max, “Quick Guide: The Difference Between Gas Turbine and Diesel Engine - Industrial Manufacturing Blog | linquip.” Accessed: Apr. 04, 2023. [Online]. Available: https://www.linquip.com/blog/quick-guide-the-difference-between-gas-turbine-and-diesel-engine/

[6] V. Hariram and R. Bharathwaaj, “Application of zero-dimensional thermodynamic model for predicting combustion parameters of CI engine fuelled with biodiesel-diesel blends,” *Alexandria Engineering Journal*, vol. 55, no. 4, pp. 3345–3354, Dec. 2016, doi: 10.1016/j.aej.2016.08.021.

[7] “Gas turbine,” *Wikipedia*. Mar. 18, 2023. Accessed: May 01, 2023. [Online]. Available: https://en.wikipedia.org/w/index.php?title=Gas_turbine&oldid=1145271000

[8] O. Cleynen, *Six different configurations for a gas turbine (gas-based turbomachine). From top to bottom: gas generator (with no inherent use); turbojet; turboprop; turboshaft (electric generator); high-bypass (civilian) en:turbofan; low-bypass afterburning (military) turbofan.* 2013. Accessed: May 01, 2023. [Online]. Available: https://commons.wikimedia.org/wiki/User:Ariadacapo#/media/File:Gas_turbine_configurations.svg

[9] T. Rogoway, “General Electric’s GE9X Engine Looks Absurdly Huge Mounted On This 747 Testbed,” The Drive. Accessed: May 03, 2023. [Online]. Available: https://www.thedrive.com/the-war-zone/19276/general-electrics-ge9x-engine-looks-absurdly-huge-mounted-on-this-747-testbed

[10] “Compressor Basics,” PURDUE University College of Engineering. Accessed: May 02, 2023. [Online]. Available: https://engineering.purdue.edu/~propulsi/propulsion/jets/basics/comp.html

[11] Nancy Hall, “Axial Compressors,” NASA. Accessed: May 03, 2023. [Online]. Available: https://www.grc.nasa.gov/www/k-12/airplane/caxial.html

[12] “Combustor,” *Wikipedia*. Apr. 07, 2023. Accessed: May 03, 2023. [Online]. Available: https://en.wikipedia.org/w/index.php?title=Combustor&oldid=1148594729

[13] “Classification of Combustion Chamber,” Aerospace Notes. Accessed: May 03, 2023. [Online]. Available: https://aerospacenotes.com/classification-of-combustion-chamber/

[14] "Turbine," *Wikipedia*. Apr. 10, 2023. Accessed: May 06, 2023. [Online]. Available: https://en.wikipedia.org/w/index.php?title=Turbine&oldid=1149073563
[15] General Electric, "9HA Gas Turbine | 9HA.01 and 9HA.02 | GE Gas Power," GE Gas Power. Accessed: May 12, 2023. [Online]. Available: https://www.ge.com/gas-power/products/gas-turbines/9ha
[16] General Electric, "LMS100 Aeroderivative Gas Turbine | GE Gas Power," GE Gas Power. Accessed: May 12, 2023. [Online]. Available: https://www.ge.com/gas-power/products/gas-turbines/lms100
[17] General Electric, "Combined Cycle Power Plant | GE Gas Power," GE Gas Power. Accessed: May 06, 2023. [Online]. Available: https://www.ge.com/gas-power/resources/education/combined-cycle-power-plants
[18] "Heat exchanger," *Wikipedia*. Mar. 22, 2023. Accessed: May 08, 2023. [Online]. Available: pla
[19] "Plate heat exchanger," *Wikipedia*. Apr. 12, 2023. Accessed: May 10, 2023. [Online]. Available: https://en.wikipedia.org/w/index.php?title=Plate_heat_exchanger&oldid=1149442585
[20] B. Zohuri, "Compact Heat Exchangers Application in NGNP," 2017, pp. 315–337. doi: 10.1007/978-3-319-29835-1_7.
[21] "Ideal Gas Law," *Wikipedia*. Mar. 29, 2023. Accessed: Apr. 15, 2023. [Online]. Available: https://en.wikipedia.org/w/index.php?title=Ideal_gas_law&oldid=1147263500
[22] "Internal energy," *Wikipedia*. Jan. 19, 2023. Accessed: Apr. 15, 2023. [Online]. Available: https://en.wikipedia.org/w/index.php?title=Internal_energy&oldid=1134647427
[23] R. Nave, "Internal Energy." Accessed: Apr. 15, 2023. [Online]. Available: http://hyperphysics.phy-astr.gsu.edu/hbase/thermo/inteng.html
[24] "Enthalpy," *Wikipedia*. Mar. 15, 2023. Accessed: Apr. 15, 2023. [Online]. Available: https://en.wikipedia.org/w/index.php?title=Enthalpy&oldid=1144755745
[25] "First law of thermodynamics," *Wikipedia*. Apr. 11, 2023. Accessed: Apr. 14, 2023. [Online]. Available: https://en.wikipedia.org/w/index.php?title=First_law_of_thermodynamics&oldid=1149356415
[26] "Second law of thermodynamics," *Wikipedia*. Mar. 16, 2023. Accessed: Apr. 14, 2023. [Online]. Available: https://en.wikipedia.org/w/index.php?title=Second_law_of_thermodynamics&oldid=1145026195
[27] I. Dincer and Y. Bicer, "Chapter 2 - Fundamentals of energy systems," in *Integrated Energy Systems for Multigeneration*, I. Dincer and Y. Bicer, Eds., Elsevier, 2020, pp. 33–83. doi: 10.1016/B978-0-12-809943-8.00002-9.
[28] V. K. Patel, V. J. Savsani, and M. A. Tawhid, "Thermal Design and Optimization of Heat Engines and Heat Pumps," *Thermal System Optimization*, pp. 99–198, 2019, doi: 10.1007/978-3-030-10477-1_4.
[29] Dimitrios Koubogiannis, "Ch. B: Thermodynamic Principles for Turbomachinery." Nov. 24, 2020. Accessed: Apr. 14, 2023. [Online]. Available: https://eclass.uniwa.gr/modules/document/file.php/ET173/%28%CE%9D%CE%AD

%CE%B5%CF%82%29_%CE%A3%CE%B7%CE%BC%CE%B5%CE%B9%CF%8E%CF%83%CE%B5%CE%B9%CF%82_%CE%9C%CE%B1%CE%B8%CE%AE%CE%BC%CE%B1%CF%84%CE%BF%CF%82_%CE%95%CE%9A%CE%98%CE%A3/2_stTT.pdf
[30] Israel Urieli, "Increase in Entropy Principle - (Updated 5/18/11)," Increase in Entropy Principle. Accessed: Apr. 15, 2023. [Online]. Available: https://www.ohio.edu/mechanical/thermo/Intro/Chapt.1_6/Clausius/S_increase.html
[31] "Stagnation enthalpy," *Wikipedia*. Apr. 08, 2023. Accessed: Apr. 16, 2023. [Online]. Available: https://en.wikipedia.org/w/index.php?title=Stagnation_enthalpy&oldid=1148769604
[32] "Mach number," *Wikipedia*. Apr. 07, 2023. Accessed: Apr. 16, 2023. [Online]. Available: https://en.wikipedia.org/w/index.php?title=Mach_number&oldid=1148667200
[33] "Brayton cycle," *Wikipedia*. Mar. 03, 2023. Accessed: Apr. 17, 2023. [Online]. Available: https://en.wikipedia.org/w/index.php?title=Brayton_cycle&oldid=1142640944
[34] Dimitrios Koubogiannis, "Chapter D: Ideal Gas Turbine Cycles." Nov. 24, 2020. Accessed: Apr. 18, 2023. [Online]. Available: https://eclass.uniwa.gr/modules/document/file.php/ET173/%28%CE%9D%CE%AD%CE%B5%CF%82%29_%CE%A3%CE%B7%CE%BC%CE%B5%CE%B9%CF%8E%CF%83%CE%B5%CE%B9%CF%82_%CE%9C%CE%B1%CE%B8%CE%AE%CE%BC%CE%B1%CF%84%CE%BF%CF%82_%CE%95%CE%9A%CE%98%CE%A3/3_stTT.pdf
[35] Jason Sebring, "Increasing Efficiency - The Brayton Cycle," University of Alaska Fairbanks. Accessed: May 19, 2023. [Online]. Available: http://ffden-2.phys.uaf.edu/webproj/212_spring_2015/Jason_Sebring/jason_sebring_web/increasing-efficiency.html
[36] "Single vs. Multi-Stage Compressors," CASCO USA. Accessed: May 19, 2023. [Online]. Available: https://cascousa.com/compressed-air-101/types-of-compressors/single-versus-multi-stage-compressors/
[37] "BRAYTON CYCLE WITH REHEATING," ENGINEERING APPLICATIONS. Accessed: May 19, 2023. [Online]. Available: https://www.hkdivedi.com/2016/12/brayton-cycle-with-reheating.html
[38] Dimitrios Koubogiannis, "Chapter E: Actual Cycles and Gas Turbine Modeling." Nov. 24, 2020. Accessed: Apr. 19, 2020. [Online]. Available: https://eclass.uniwa.gr/modules/document/file.php/ET173/%28%CE%9D%CE%AD%CE%B5%CF%82%29_%CE%A3%CE%B7%CE%BC%CE%B5%CE%B9%CF%8E%CF%83%CE%B5%CE%B9%CF%82_%CE%9C%CE%B1%CE%B8%CE%AE%CE%BC%CE%B1%CF%84%CE%BF%CF%82_%CE%95%CE%9A%CE%98%CE%A3/4_stTT.pdf
[39] Emerson Morin, "Gas Power Cycles," SlideServe. Accessed: Apr. 19, 2023. [Online]. Available: https://www.slideserve.com/emerson-morin/gas-power-cycles
[40] "Isentropic process," *Wikipedia*. Feb. 08, 2023. Accessed: Apr. 17, 2023. [Online]. Available: https://en.wikipedia.org/w/index.php?title=Isentropic_process&oldid=1138196880#Isentropic_efficiencies_of_steady-flow_devices_in_thermodynamic_systems

[41] Sangeeta Das, “Compressor Isentropic Efficiency: What, How, Several Types, Examples -.” Accessed: Apr. 19, 2023. [Online]. Available: https://lambdageeks.com/compressor-isentropic-efficiency/
[42] Nuclear Power, “Isentropic Efficiency - Turbine/Compressor/Nozzle,” Nuclear Power. Accessed: Apr. 19, 2023. [Online]. Available: https://www.nuclear-power.com/nuclear-engineering/thermodynamics/thermodynamic-processes/isentropic-process/isentropic-efficiency-turbinecompressornozzle/
[43] H. Alkhareef, A. Farad, M. Salem, F. Piao, H. Yujing, and Z. Yang, “Development of Ultra-Low Emissions Gas Turbine Combustor System,” 2017. doi: 10.13140/RG.2.2.18290.40642.
[44] Axel Rossmann, “11.2.2 The Combustion Chamber,” Aeroengine Safety. Accessed: Apr. 20, 2023. [Online]. Available: https://aeroenginesafety.tugraz.at/doku.php?id=11:112:1122:1122
[45] Swiss Rotors, “How do you calculate the efficiency of a plate heat exchanger?,” Swiss Rotors. Accessed: Apr. 21, 2023. [Online]. Available: https://swissrotors.com/blog/how-do-you-calculate-the-efficiency-of-a-plate-heat-exchanger/
[46] “Supercritical fluid,” *Wikipedia*. Mar. 22, 2023. Accessed: Apr. 24, 2023. [Online]. Available: https://en.wikipedia.org/w/index.php?title=Supercritical_fluid&oldid=1146011676
[47] E. Björklund and C. Sparr-Eskilsson, “EXTRACTION | Supercritical Fluid Extraction,” in *Encyclopedia of Analytical Science (Second Edition)*, P. Worsfold, A. Townshend, and C. Poole, Eds., Oxford: Elsevier, 2005, pp. 597–604. doi: 10.1016/B0-12-369397-7/00691-9.
[48] “Carbon dioxide,” *Wikipedia*. Jun. 11, 2023. Accessed: Jun. 11, 2023. [Online]. Available: https://en.wikipedia.org/w/index.php?title=Carbon_dioxide&oldid=1159552314
[49] “Carbon dioxide | Definition, Formula, Uses, & Facts | Britannica.” Accessed: Jun. 11, 2023. [Online]. Available: https://www.britannica.com/science/carbon-dioxide
[50] BUDAPEST UNIVERSITY OF TECHNOLOGY AND ECONOMICS, “Supercritical Fluids,” Web Archives. Accessed: Apr. 24, 2023. [Online]. Available: https://web.archive.org/web/20160108021936/http://sfe.kkft.bme.hu/en/current-research.html
[51] “Carbon Dioxide,” VEDANTU. Accessed: Jun. 13, 2023. [Online]. Available: https://www.vedantu.com/chemistry/carbon-dioxide
[52] “CO2 Corrosion.” Accessed: Jun. 13, 2023. [Online]. Available: https://www.twi-global.com/what-we-do/research-and-technology/technologies/materials-and-corrosion-management/corrosion-testing/co2-corrosion.aspx
[53] U.S. Department of Energy, “Quadrennial Technology Review 2015 Supercritical Carbon Dioxide Brayton Cycle.” 2015. Accessed: May 26, 2023. [Online]. Available: https://www.energy.gov/sites/prod/files/2016/06/f32/QTR2015-4R-Supercritical-Carbon-Dioxide-Brayton%20Cycle.pdf
[54] Y. Liu, Y. Wang, and D. Huang, “Supercritical CO2 Brayton cycle: A state-of-the-art review,” *Energy*, vol. 189, p. 115900, Dec. 2019, doi: 10.1016/j.energy.2019.115900.

[55] Gary E. Rochau and Jim J. Pasch, “Supercritical CO2 Brayton Cycles.” Aug. 04, 2014. Accessed: Oct. 04, 2023. [Online]. Available: https://www.osti.gov/servlets/purl/1221819

[56] O. Olumayegun, M. Wang, and G. Kelsall, “Closed-cycle gas turbine for power generation: A state-of-the-art review,” *Fuel*, vol. 180, pp. 694–717, Sep. 2016, doi: 10.1016/j.fuel.2016.04.074.

[57] D. Fleming, A. Kruizenga, J. Pasch, T. Conboy, and M. Carlson, “Corrosion and Erosion Behavior in Supercritical CO2 Power Cycles,” in *Volume 3B: Oil and Gas Applications; Organic Rankine Cycle Power Systems; Supercritical CO2 Power Cycles; Wind Energy*, Düsseldorf, Germany: American Society of Mechanical Engineers, Jun. 2014, p. V03BT36A002. doi: 10.1115/GT2014-25136.

[58] “Real gas,” *Wikipedia*. Mar. 26, 2023. Accessed: Jun. 13, 2023. [Online]. Available: https://en.wikipedia.org/w/index.php?title=Real_gas&oldid=1146774292

[59] “Thermodynamic Table - an overview | ScienceDirect Topics.” Accessed: Jun. 21, 2023. [Online]. Available: https://www.sciencedirect.com/topics/engineering/thermodynamic-table

[60] K. Kosowski and M. Piwowarski, “Design Analysis of Micro Gas Turbines in Closed Cycles,” *Energies*, vol. 13, no. 21, Art. no. 21, Jan. 2020, doi: 10.3390/en13215790.

[61] “ML-1,” *Wikipedia*. Aug. 07, 2022. Accessed: May 20, 2023. [Online]. Available: https://en.wikipedia.org/w/index.php?title=ML-1&oldid=1102958179

[62] Sandia National Laboratories, “Supercritical CO2 Brayton Cycle Brochure.” Accessed: May 21, 2023. [Online]. Available: https://energy.sandia.gov/wp-content//gallery/uploads/PaschBrochureFinal_SAND20124480P_rev.pdf

[63] National Renewable Engine Laboratory, “10 MW Supercritical-CO2 Turbine Project.” Apr. 23, 2013. Accessed: May 21, 2023. [Online]. Available: https://www.energy.gov/eere/solar/articles/10-mw-supercritical-co2-turbine-project

[64] S. E. Zitney and E. Liese, “Design and Operation of a 10 MWe Supercritical CO2 Recompression Brayton Power Cycle,” National Energy Technology Laboratory (NETL), Pittsburgh, PA, Morgantown, WV (United States), NETL-PUB-20474, Apr. 2016. Accessed: May 23, 2023. [Online]. Available: https://www.osti.gov/biblio/1507773

[65] S. Patel, “The POWER Interview: Pioneering STEP Supercritical Carbon Dioxide Demonstration Readying for 2022 Commissioning,” POWER Magazine. Accessed: May 23, 2023. [Online]. Available: https://www.powermag.com/the-power-interview-pioneering-step-supercritical-carbon-dioxide-demonstration-readying-for-2022-commissioning/

[66] “STEP Demo pilot plant achieves supercritical CO2 fluid conditions,” Southwest Research Institute. Accessed: May 23, 2023. [Online]. Available: https://www.swri.org/press-release/step-demo-pilot-plant-achieves-supercritical-co2-fluid-conditions

[67] Mollie Rappe, “We’ve got the power,” Sandia LabNews. Accessed: May 20, 2023. [Online]. Available: https://www.sandia.gov/labnews/2022/08/11/weve-got-the-power/

[68] A. Yu, W. Su, X. Lin, and N. Zhou, "Recent trends of supercritical CO2 Brayton cycle: Bibliometric analysis and research review," *Nuclear Engineering and Technology*, vol. 53, no. 3, pp. 699–714, Mar. 2021, doi: 10.1016/j.net.2020.08.005.

[69] B. D. Iverson, T. M. Conboy, J. J. Pasch, and A. M. Kruizenga, "Supercritical CO2 Brayton cycles for solar-thermal energy," *Applied Energy*, vol. 111, pp. 957–970, Nov. 2013, doi: 10.1016/j.apenergy.2013.06.020.

[70] S. Guccione, S. Trevisan, R. Guedez, B. Laumert, S. Maccarini, and A. Traverso, "Techno-Economic Optimization of a Hybrid PV-CSP Plant With Molten Salt Thermal Energy Storage and Supercritical CO2 Brayton Power Cycle," presented at the ASME Turbo Expo 2022: Turbomachinery Technical Conference and Exposition, American Society of Mechanical Engineers Digital Collection, Oct. 2022. doi: 10.1115/GT2022-80376.

[71] D. Luo and D. Huang, "Thermodynamic and exergoeconomic investigation of various SCO2 Brayton cycles for next generation nuclear reactors," *Energy Conversion and Management*, vol. 209, p. 112649, Apr. 2020, doi: 10.1016/j.enconman.2020.112649.

[72] J. Hidalgo-Salaverri, P. Cano-Megias, R. Chacartegui, J. Ayllon-Guerola, and E. Viezzer, "Analysis of supercritical carbon dioxide Brayton cycles for a helium-cooled pebble bed blanket DEMO-like fusion power plant," *Fusion Engineering and Design*, vol. 173, p. 112860, Dec. 2021, doi: 10.1016/j.fusengdes.2021.112860.

[73] D. Thanganadar, F. Asfand, K. Patchigolla, and P. Turner, "Techno-economic analysis of supercritical carbon dioxide cycle integrated with coal-fired power plant," *Energy Conversion and Management*, vol. 242, p. 114294, Aug. 2021, doi: 10.1016/j.enconman.2021.114294.

[74] A. K. Sleiti, W. Al-Ammari, S. Ahmed, and J. Kapat, "Direct-fired oxy-combustion supercritical-CO2 power cycle with novel preheating configurations -thermodynamic and exergoeconomic analyses," *Energy*, vol. 226, p. 120441, Jul. 2021, doi: 10.1016/j.energy.2021.120441.

[75] "Hot Dry Rock - an overview | ScienceDirect Topics." Accessed: Jun. 26, 2023. [Online]. Available: https://www.sciencedirect.com/topics/engineering/hot-dry-rock

[76] E. Ruiz-Casanova, C. Rubio-Maya, J. J. Pacheco-Ibarra, V. M. Ambriz-Díaz, C. E. Romero, and X. Wang, "Thermodynamic analysis and optimization of supercritical carbon dioxide Brayton cycles for use with low-grade geothermal heat sources," *Energy Conversion and Management*, vol. 216, p. 112978, Jul. 2020, doi: 10.1016/j.enconman.2020.112978.

[77] S. I. Schöffer, S. A. Klein, P. V. Aravind, and R. Pecnik, "A solid oxide fuel cell-supercritical carbon dioxide Brayton cycle hybrid system," *Applied Energy*, vol. 283, p. 115748, Feb. 2021, doi: 10.1016/j.apenergy.2020.115748.

[78] D. Alfani, M. Binotti, E. Macchi, P. Silva, and M. Astolfi, "sCO2 power plants for waste heat recovery: design optimization and part-load operation strategies," *Applied Thermal Engineering*, vol. 195, p. 117013, Aug. 2021, doi: 10.1016/j.applthermaleng.2021.117013.

[79] L. Xie and J. Yang, "Performance Modulation of S-CO2 Brayton Cycle for Marine Low-Speed Diesel Engine Flue Gas Waste Heat Recovery Based on MOGA," *Entropy (Basel)*, vol. 24, no. 11, p. 1544, Oct. 2022, doi: 10.3390/e24111544.

[80] S. A. Wright, R. F. Radel, M. E. Vernon, P. S. Pickard, and G. E. Rochau, "Operation and analysis of a supercritical CO2 Brayton cycle.," Sandia National Laboratories (SNL), Albuquerque, NM, and Livermore, CA (United States), SAND2010-0171, Sep. 2010. doi: 10.2172/984129.

[81] E. Morosini, G. Manzolini, G. D. Marcoberardino, C. Invernizzi, and P. Iora, "Investigation of CO2 mixtures to overcome the limits of sCO2 cycles," *E3S Web Conf.*, vol. 312, p. 08010, 2021, doi: 10.1051/e3sconf/202131208010.

[82] S. S. Saravi and S. A. Tassou, "An investigation into sCO2 compressor performance prediction in the supercritical region for power systems," *Energy Procedia*, vol. 161, pp. 403–411, Mar. 2019, doi: 10.1016/j.egypro.2019.02.098.

[83] Y. Du, C. Yang, H. Wang, and C. Hu, "One-dimensional optimisation design and off-design operation strategy of centrifugal compressor for supercritical carbon dioxide Brayton cycle," *Applied Thermal Engineering*, vol. 196, p. 117318, Sep. 2021, doi: 10.1016/j.applthermaleng.2021.117318.

[84] Y. Zhu *et al.*, "Experimental Study on a Supercritical CO2 Centrifugal Compressor Used in a MWe Scale Power Cycle," *Applied Sciences*, vol. 13, no. 1, Art. no. 1, Jan. 2023, doi: 10.3390/app13010385.

[85] G. R. K. Aretis, A. A. Gkountas, D. G. Koubogiannis, and I. E. Sarris, "Preliminary Design and Numerical Investigation of a Centrifugal Compressor for Supercritical Carbon Dioxide Operating in the Vicinity of Its Critical Thermodynamic State," *Computation*, vol. 11, no. 4, Art. no. 4, Apr. 2023, doi: 10.3390/computation11040077.

[86] "PCHE," Alfa Laval. Accessed: Jun. 05, 2023. [Online]. Available: http://www.alfalaval.com/pche/

[87] J. S. Kwon, S. Son, J. Y. Heo, and J. I. Lee, "Compact heat exchangers for supercritical CO2 power cycle application," *Energy Conversion and Management*, vol. 209, p. 112666, Apr. 2020, doi: 10.1016/j.enconman.2020.112666.

[88] H. Seo, J. E. Cha, J. Kim, I. Sah, and Y.-W. Kim, "Design and Performance Analysis of a Supercritical Carbon Dioxide Heat Exchanger," *Applied Sciences*, vol. 10, no. 13, Art. no. 13, Jan. 2020, doi: 10.3390/app10134545.

[89] J. Stepanek, J. Syblik, and S. Entler, "Axial sCO2 high-performance turbines parametric design," *Energy Conversion and Management*, vol. 274, p. 116418, Dec. 2022, doi: 10.1016/j.enconman.2022.116418.

[90] Z. Li, W. Bian, L. Jiang, C. Liu, J. Shi, and N. Hao, "Supercritical Carbon Dioxide Turbine Design and Arrangement Optimization," *Frontiers in Energy Research*, vol. 10, 2022, Accessed: Jun. 04, 2023. [Online]. Available: https://www.frontiersin.org/articles/10.3389/fenrg.2022.922542

[91] D. Zhang, Y. Wang, and Y. Xie, "Investigation into Off-Design Performance of a S-CO2 Turbine Based on Concentrated Solar Power," *Energies*, vol. 11, no. 11, Art. no. 11, Nov. 2018, doi: 10.3390/en11113014.

[92] "EPS100," ECHOGEN Power Systems. Accessed: May 20, 2023. [Online]. Available: https://www.echogen.com/our-solution/product-series/eps100/

[93] M. S. Kim, Y. Ahn, B. Kim, and J. I. Lee, "Study on the supercritical CO2 power cycles for landfill gas firing gas turbine bottoming cycle," *Energy*, vol. 111, pp. 893–909, Sep. 2016, doi: 10.1016/j.energy.2016.06.014.

[94] Timothy J. Held, "Supercritical CO2 Cycles for Gas Turbine Combined Cycle Power Plants," presented at the Power Gen International, Nevada, Dec. 2015.

Accessed: Jul. 03, 2023. [Online]. Available: https://www.echogen.com/_CE/pagecontent/Documents/Papers/Supercritical%20CO2%20Cycles%20for%20Gas%20Turbine%20Combined%20Cycle%20Power%20Plants.pdf

[95] "Regenerative Brayton Cycle - an overview | ScienceDirect Topics." Accessed: Jul. 05, 2023. [Online]. Available: https://www.sciencedirect.com/topics/engineering/regenerative-brayton-cycle

[96] MAN Energy Solutions, "MAN ME-GA." Jul. 2022. Accessed: Jul. 11, 2023. [Online]. Available: https://www.man-es.com/docs/default-source/document-sync/me-ga-eng.pdf?sfvrsn=b8afb1ad_4

[97] "Heat capacity ratio," *Wikipedia*. Jan. 14, 2023. Accessed: Jul. 13, 2023. [Online]. Available: https://en.wikipedia.org/w/index.php?title=Heat_capacity_ratio&oldid=1133488665

[98] Deepak Kumar Sahani, "Boiler Efficiency and Sulphur Dew Points | LinkedIn," LinkedIn. Accessed: Jul. 15, 2023. [Online]. Available: https://www.linkedin.com/pulse/boiler-efficiency-sulphur-dew-points-deepak-kumar-sahani/

[99] N. Weiland and D. Thimsen, "A Practical Look at Assumptions and Constraints for Steady State Modeling of sCO2 Brayton Power Cycles," National Energy Technology Laboratory (NETL), Pittsburgh, PA, Morgantown, WV (United States), NETL-PUB-20271, Mar. 2016. Accessed: Aug. 09, 2023. [Online]. Available: https://www.osti.gov/biblio/1491086

[100] J. J. Dyreby, S. A. Klein, G. F. Nellis, and D. T. Reindl, "Modeling Off-Design and Part-Load Performance of Supercritical Carbon Dioxide Power Cycles," presented at the ASME Turbo Expo 2013: Turbine Technical Conference and Exposition, American Society of Mechanical Engineers Digital Collection, Nov. 2013. doi: 10.1115/GT2013-95824.

[101] H. U. Frutschi, *Closed-cycle Gas Turbines: Operating Experience and Future Potential*. ASME Press, 2005.

[102] M. Akman and S. Ergin, "An investigation of marine waste heat recovery system based on organic Rankine cycle under various engine operating conditions," *Proceedings of the Institution of Mechanical Engineers Part M Journal of Engineering for the Maritime Environment*, vol. 233, pp. 586–601, May 2019, doi: 10.1177/1475090218770947.

[103] The MathWorks, Inc. (2022). MATLAB version: 9.13.0 (R2022b). Accessed: April 18, 2023. Available: https://www.mathworks.com.

[104] MAN Energy Solutions. MAN CEAS engine calculations. Accessed: September 10, 2023. Available: https://www.man-es.com/marine/products/planning-tools-and-downloads/ceas-engine-calculations

[105] I. Bell, J. Wronski, S. Quoilin. Coolprop version: 6.4.1. Accessed: June 10, 2023. Available: http://www.coolprop.org

[106] Digital Scholar. Zotero version: 6.0.27. Accessed: April 2, 2023. Available: https://www.zotero.org

[107] Lyes Kadem. "ENGR 251: Thermodynamics I", YouTube, Sep. 26 2021 [Video Playlist]. Available:

https://www.youtube.com/playlist?list=PLNTRu_uCErYEtCqLyLQ7a_1DZ2cFlOiid (Accessed May 13, 2023).